

# Structural and functional analysis of hybrid proteasome Strukturna i funkcionalna analiza hibridnog proteasoma

---

Belačić, Katarina

Master's thesis / Diplomski rad

2018

Degree Grantor / Ustanova koja je dodijelila akademski / stručni stupanj: **University of Zagreb, Faculty of Science / Sveučilište u Zagrebu, Prirodoslovno-matematički fakultet**

Permanent link / Trajna poveznica: <https://um.nsk.hr/um:nbn:hr:217:182054>

Rights / Prava: [In copyright](#)/[Zaštićeno autorskim pravom.](#)

Download date / Datum preuzimanja: **2025-02-17**



Repository / Repozitorij:

[Repository of the Faculty of Science - University of Zagreb](#)



University of Zagreb  
Faculty of Science  
Department of Biology

Katarina Belačić

**Structural and functional analysis  
of hybrid proteasomes**

Graduation thesis

Zagreb, 2018

This master thesis was produced at the Research Institute of Molecular Pathology in Vienna under guidance of Dr. David Haselbach and Asst. prof. dr. Nenad Malenica. The thesis was submitted for evaluation to the Department of Biology, Faculty of Science, University of Zagreb to acquire the academic title of Master of Molecular Biology.

## ACKNOWLEDGEMENTS

I would first like to thank my thesis advisor Dr. David Haselbach for his patient guidance, enthusiastic encouragement and useful critiques of this thesis. The door to David's office was always open whenever I ran into a trouble spot or had a question about my research or writing. He consistently allowed this thesis to be my own work, but steered me in the right direction whenever he thought I needed it.

A very special thanks to Irina Grishkovskaya and Susanne Kandolf for their constant help in the lab and for all coffee breaks when things went wrong (and right).

I would also like to thank the experts and colleagues who were involved in this research project, the Clausen group, especially Ana, Antonia, Renato, Toni and Juraj and Tom and Harald from Electron microscopy facility. I am gratefully indebted to their passionate contribution to this thesis.

I would also like to acknowledge Assist. Prof. Dr. Nenad Malenica of the Faculty of Science, Department of Biology at University of Zagreb as the second reader of this thesis, and I am thankful for his very valuable comments on this thesis.

I would like to thank my friend Anja for her unconditional friendship and support.

Finally, I must express my very profound gratitude to my parents, Ksenka and Djuro and my siblings, Kristina and Đuro, for providing me with unfailing support and continuous encouragement throughout my years of study and through the process of researching and writing this thesis. This accomplishment would not have been possible without them.

And finally, finally I would like to thank my boyfriend Stjepan, the most special person in my life.

Sveučilište u Zagrebu

Prirodoslovno-matematički fakultet

Biološki odsjek

Diplomski rad

### **Strukturna i funkcionalna analiza hibridnih proteasoma**

Katarina Belačić

Rooseveltov trg 6, 10 000 Zagreb, Hrvatska

Proteasom je proteinski kompleks zadužen za razgradnju proteina unutar stanice te je stoga važan za regulaciju staničnih procesa – diobu i smrt stanice, prijenos signala, imunološki odgovor, metabolizam, provjeru kvalitete proteina i razvoj. Katalitički aktivan dio čini 20S kompleks čija je aktivnost regulirana vezanjem različitih aktivatora poput 19S regulatornog kompleksa (19S RP), PA28 $\alpha\beta$ , PA28 $\gamma$  te PA200. Hibridni proteasom sadrži 19S RP na jednoj i PA28 ili PA200 na drugoj strani istog 20S kompleksa. Hibridni proteasomi mogu biti prisutni u normalnim uvjetima ili njihov nastanak može biti potaknut (npr. stimulacijom interferonom- $\gamma$ ). Međutim, točna funkcija hibridnih proteasoma je još uvijek nepoznata, a struktura nikada nije detaljno istraživana. Strukturna analiza krio-elektronskom mikroskopijom pojedinačnih čestica hibridnih proteasoma izoliranih iz tkiva goveđih testisa i stanica ljudskog rektalnog karcinoma tretiranih interferonom- $\gamma$  pokazala je prisutnost samo hibridnih proteasoma koji sadrže PA200 aktivator. Međutim, zbog preniske rezolucije nisu dobivene pouzdane strukturne informacije. Također, pronađeno je da se u prisutnosti kompleksa 19S-20S-PA28 $\alpha\beta$  ili 19S-20S-PA28 $\gamma$ , uzorak peptidnih fragmenata odabranog proteinskog supstrata razlikuje od uzorka dobivenog u odustnosti PA28 aktivatora. Takav rezultat ukazuje na to da PA28 aktivator alosterički regulira specifičnosti proteolitičkog cijepanja 20S-19S kompleksa.

Rad sadrži: XXVI + 94 stranica, 40 slika, 3 tablice, 107 literaturnih navoda, jezik izvornika: engleski

Rad je pohranjen u Središnjoj biološkoj knjižnici.

**Ključne riječi:** 20S kompleks, 19S regulatorni kompleks, hibridni proteasom, specifičnosti proteolitičkog cijepanja, krio-elektronska mikroskopija

**Voditelj:** Dr. sc. David Haselbach

**Suvoditelj:** Doc. dr. sc. Nenad Malenica,

**Ocjenitelji:** Dr. sc. Nenad Malenica, doc.

Dr. sc. Antun Alegro, prof.

Dr. sc. Marin Ježić, doc.

**Rad prihvaćen:** 31.10.2018.

University of Zagreb

Faculty of Science

Department of Biology

Graduation thesis

**Structural and functional analysis of hybrid proteasomes**

Katarina Belačić

Rooseveltovo trg 6, 10 000 Zagreb, Croatia

Proteasomes perform the majority of proteolysis that occurs in cells, and thereby, perform crucial roles in regulation of cellular processes such as cell division and death, signal transduction, immune response, metabolism and protein quality control. The catalytic heart of proteasome complexes is the 20S core particle (20S CP) which activity is regulated through association with different activators – 19S regulatory particle (19SRP), PA28 $\alpha\beta$ , PA28 $\gamma$  and PA200. The hybrid proteasome complex contains the 19S RP on the one side and PA28 or PA200 on the opposite side of the same 20S CP. The hybrid proteasome complexes can be found under native conditions, or their formation can be induced (e.g., by interferon- $\gamma$  treatment). The exact function of hybrid proteasomes is still unknown and their structures have never been thoroughly investigated. The structural analysis of hybrid proteasome complexes from bovine testes and interferon- $\gamma$  treated human rectal carcinoma cells by single particle cryo-electron microscopy has resulted only in the structures of the PA200 hybrid proteasome complex, however at a too low resolution for reliable structural insights. Meanwhile, the peptide pattern in the presence of 19S-20S-PA28 $\alpha\beta$  or 19S-20S-PA28 $\gamma$  complexes was found to be changed in comparison with the one obtained without PA28 complexes, indicating that PA28 allosterically regulates the cleavage specificities of 19S-20S proteasome complex.

The thesis has: XXVI + 94 pages, 40 figures, 3 tables, 107 references, original in English

Thesis deposited in the Central biological library.

**Key words:** 20S core particle, 19S regulatory particle, hybrid proteasome, cleavage specificities, cryo-electron microscopy

**Supervisor:** Dr. David Haselbach

**Cosupervisor:** Dr. Nenad Malenica, Asst. Prof.

**Reviewers:** Dr. Nenad Malenica, Asst. Prof.

Dr. Antun Alegro, Prof.

Dr. Marin Ježić, Asst. Prof

**Thesis accepted:** 31.10.2018

## Table of Contents

<b>1. Introduction</b>	<b>1</b>
<b>1.1. The ubiquitin-proteasome system</b>	<b>1</b>
<b>1.2. The 20S proteasome core particle (20S CP)</b>	<b>2</b>
1.2.1. Structure of the 20S CP	2
1.2.2. Functions of the 20S CP	4
<b>1.2.3. The immunoproteasome</b>	<b>8</b>
<b>1.3. Regulation of the 20S CP activity</b>	<b>9</b>
1.3.1. The 19S regulatory particle (19S RP)	10
1.3.2. 11S proteasome regulators (PA28 or REG)	14
1.3.3. PA200	18
<b>1.4. The hybrid proteasome</b>	<b>20</b>
<b>1.5. Single-particle electron microscopy</b>	<b>23</b>
<b>1.6. Aim of this thesis</b>	<b>26</b>
<b>2. Materials and methods</b>	<b>27</b>
<b>2.1. Materials</b>	<b>27</b>
2.1.1. Standard chemicals	27
2.1.2. Stains and reagents	27
2.1.3. Standards, enzymes and commercial kits	27
2.1.4. <i>Escherichia coli</i> strains, cell lines and expression plasmids	28
2.1.5. Chromatography columns and magnetic beads	28
2.1.6. Bacterial and cell culture media	28
2.1.7. Buffers	29
2.1.8. Software	31
2.1.9. Equipment	31
<b>2.2. Methods</b>	<b>32</b>
2.2.1. Biochemical methods	32
2.2.2. Single-particle sample preparation	43
2.2.3. Single-particle electron microscopy	44
<b>3. Results</b>	<b>47</b>
<b>3.1. Purification of the bait protein GST-UBL</b>	<b>47</b>
<b>3.2. Affinity purification of proteasome complexes from bovine organs and RKO cells</b>	<b>49</b>
<b>3.3. Semiquantitative analysis of purified proteasome complexes</b>	<b>51</b>
3.3.1. Proteasome complexes from different bovine organs	51
3.3.2. Proteasome complexes from RKO cells	53
<b>3.4. Functional analysis of purified proteasome complexes</b>	<b>55</b>
3.4.1. Generation of proteasome substrate polyUb securin	55
3.4.2. <i>In vitro</i> degradation of polyUb securin	56
3.4.3. Analysis of peptides generated during proteasomal degradation of polyUb securin	58
<b>3.5. Analysis of purified proteasome complexes by negative stain TEM</b>	<b>62</b>
<b>3.6. Structural analysis of the hybrid proteasome by single-particle cryo-EM</b>	<b>64</b>
<b>4. Discussion</b>	<b>71</b>
<b>4.1. Affinity purification of proteasome complexes using an ubiquitin-like domain</b>	<b>71</b>

4.2.	Semiquantitative mass spectrometry as a screening tool for 11S and PA200 proteasome activators .....	73
4.3.	Generation of polyUb proteasome substrate and functional assays .....	75
4.4.	Analysis of the generated pattern of peptide fragments by different proteasome complexes .....	76
4.5.	Inspection of purified proteasome complexes by negative stain TEM and structural analysis of the hybrid proteasome by single-particle cryo-EM.....	79
5.	<i>Conclusions</i> .....	82
6.	<i>Literature</i> .....	84
7.	<i>Supplement informations</i> .....	94
8.	<i>CURRICULUM VITAE</i> .....	XXVI



## LIST OF ABBREVIATIONS AND SYMBOLS

### List of amino acids

Symbol	Amino acid	Symbol	Amino acid
<i>Ala (A)</i>	<i>alanine</i>	<i>Met (M)</i>	<i>methionine</i>
<i>Cys (C)</i>	<i>cysteine</i>	<i>Asn (N)</i>	<i>asparagine</i>
<i>Asp (D)</i>	<i>aspartic acid</i>	<i>Pro (P)</i>	<i>proline</i>
<i>Glu (E)</i>	<i>glutamic acid</i>	<i>Gln (Q)</i>	<i>glutamine</i>
<i>Phe (F)</i>	<i>phenylalanine</i>	<i>Arg (R)</i>	<i>arginine</i>
<i>Gly (G)</i>	<i>glycine</i>	<i>Ser (S)</i>	<i>serine</i>
<i>His (H)</i>	<i>histidine</i>	<i>Thr (T)</i>	<i>threonine</i>
<i>Ile (I)</i>	<i>isoleucine</i>	<i>Val (V)</i>	<i>valine</i>
<i>Lys (K)</i>	<i>lysine</i>	<i>Trp (W)</i>	<i>tryptophan</i>
<i>Leu (L)</i>	<i>leucine</i>	<i>Tyr (Y)</i>	<i>tyrosine</i>

### List of abbreviations

**19S RP:** 19S regulatory particle

**2D:** 2-dimentional

**20S CP:** 20S core particle

**3D:** 3-dimensional

**Å:** Angstrom

**APC/C:** Anaphase promoting complex/cyclosome

**APS:** ammonium persulfate

**cCP:** constitutive proteasome

**DTT:** dithiothreitol

**FCS:** fetal calf serum

**GSH:** reduced L-glutathione

**GST:** glutathione-S-transferase

**iCP:** immunoproteasome

**IFN- $\gamma$ :** interferon- $\gamma$

**kDa:** kilodaltons

**MDa:** megadaltons

**RKO:** human rectal carcinoma

**polyUb:** polyubiquitin(ated)

**SDS-PAGE:** sodium dodecyl sulfate polyacrylamide gel electrophoresis

**(T)EM:** (transmission) electron microscopy

**TEMED:** N,N,N',N'-tetramethylethane-1,2-diamine

**UBL:** Ubiquitin-like (domain)

**UPS:** Ubiquitin-proteasome system

# 1. Introduction

## 1.1. The ubiquitin-proteasome system

The ubiquitin-proteasome system (UPS) is the major ATP-dependent protein degradation system. It is a highly complex, temporally controlled, and tightly regulated process (Ciechanover & Brundin, 2003) which controls almost all basic cellular processes such as progression through cell cycle, signal transduction, cell death, immune responses, metabolism, protein quality control and development (Tanaka, 2009). In this system, proteins are targeted for degradation by covalent ligation to ubiquitin, a highly conserved small protein (Hershko & Ciechanover, 1998). This linkage of the 76-amino acid long ubiquitin protein is executed via an ATP-dependent mechanism by which three enzymes, the ubiquitin-activating enzyme E1, the ubiquitin-conjugating enzyme E2 and the ubiquitin-protein-ligase E3, catalyze the transfer of the carboxy terminus of the Gly76 of ubiquitin to the  $\epsilon$ -amino group of a lysine residue of the selected protein to form an isopeptide bond (Scheffner et al., 1995). Further addition of at least three ubiquitin moieties in line at position Lys11 or Lys48 of ubiquitin to form a K11 or K48 polyubiquitin (polyUb) chain, respectively, destines the protein for degradation (Wolf & Hilt, 2004). Proteins ligated to polyUb chains are usually recognized and degraded by the cell's proteolytic molecular machine called proteasome, into small peptides of about three to 22 amino acids in length (**Figure 1.1**) (Hershko & Ciechanover, 1998).

The proteasome population in cells exists as a collection of complexes that are centered on the 20S proteasome core particle (20S CP), a 700-kDa barrel-shaped complex (Kish-Trier & Hill, 2013). In the eukaryotic cell, proteasome complexes are present in the nucleus and cytosol, and some particles are also found associated with the endoplasmic reticulum and with the cytoskeleton (Coux et al., 1996). In addition to the degradation of polyUb proteins, proteasome complexes can directly degrade proteins damaged by oxidation, misfolded or intrinsically disordered proteins (IDPs) as part of the ubiquitin-independent proteasome system (UIPS) (**Figure 1.1**) (Pickering & Davies, 2012).

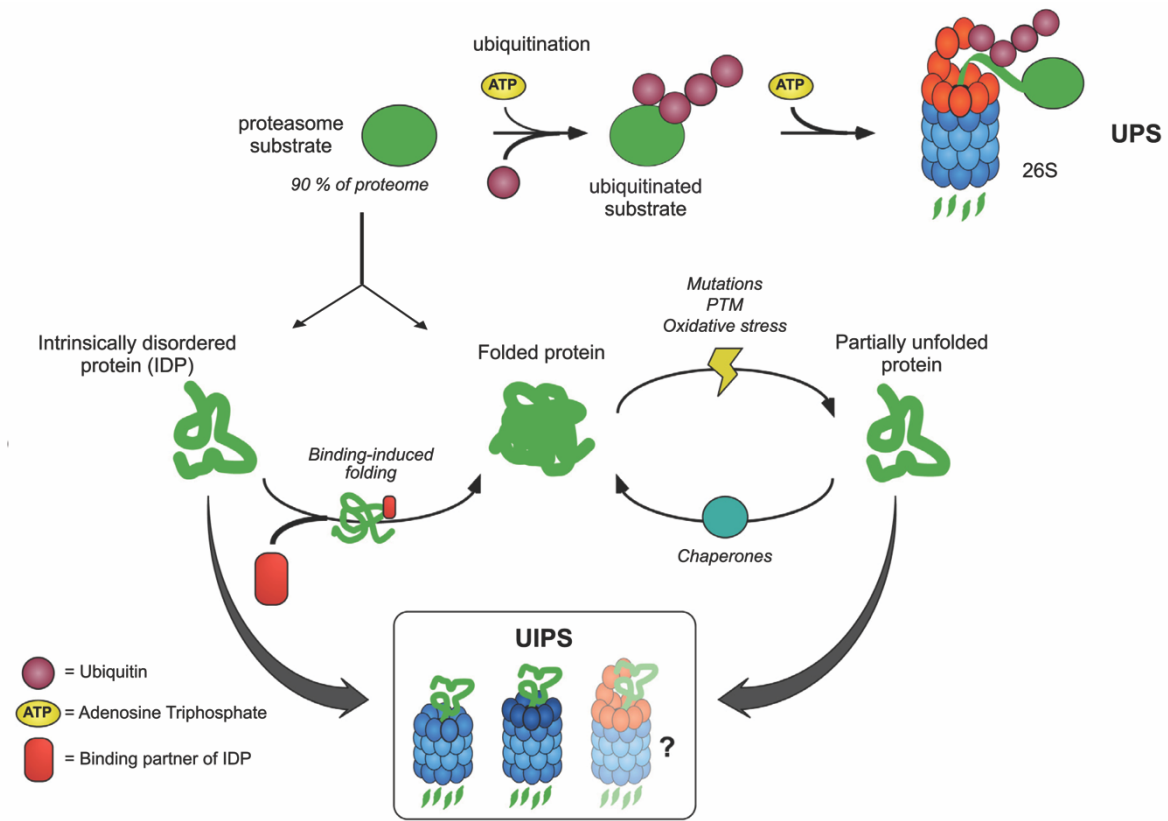


**Figure 1.1. Function and substrate profile of the proteasome degradation pathway.**

The 26S proteasome degrades over 90% of the proteome, by the ubiquitin- and ATP-dependent ubiquitin-proteasome system (UPS). The ubiquitin-independent proteasome system (UIPS) targets substrates independent of ubiquitin conjugation and can effectively degrade intrinsically disordered proteins (IDPs), but not folded proteins due to their 3-dimensional structure. Cellular stresses, including mutations, post-translational modifications (PTMs) and oxidative damage can partially unfold structured proteins making them susceptible to a turnover by the UIPS. Taken and adapted from (Opoku-Nsiah & Gestwicki, 2018).

## 1.2. The 20S proteasome core particle (20S CP)

### 1.2.1. Structure of the 20S CP

The 20S CP structure from various organisms has been widely studied. The first 20S CP structure, derived from the archaeon *Thermoplasma acidophilum*, was elucidated in 1995 by X-ray crystallography at 3.4 Å resolution (Löwe et al., 1995) (**Figure 1.2.A**). In 1997, the crystal structure of the 20S CP from the yeast *Saccharomyces cerevisiae* was determined at 2.4 Å resolution (Groll et al., 1997) (**Figure 1.2.B**) and finally, in 2002 the crystal structure of the mammalian 20S from the bovine liver was reported at 2.75 Å resolution (**Figure 1.2. C**) (Unno et al., 2002).

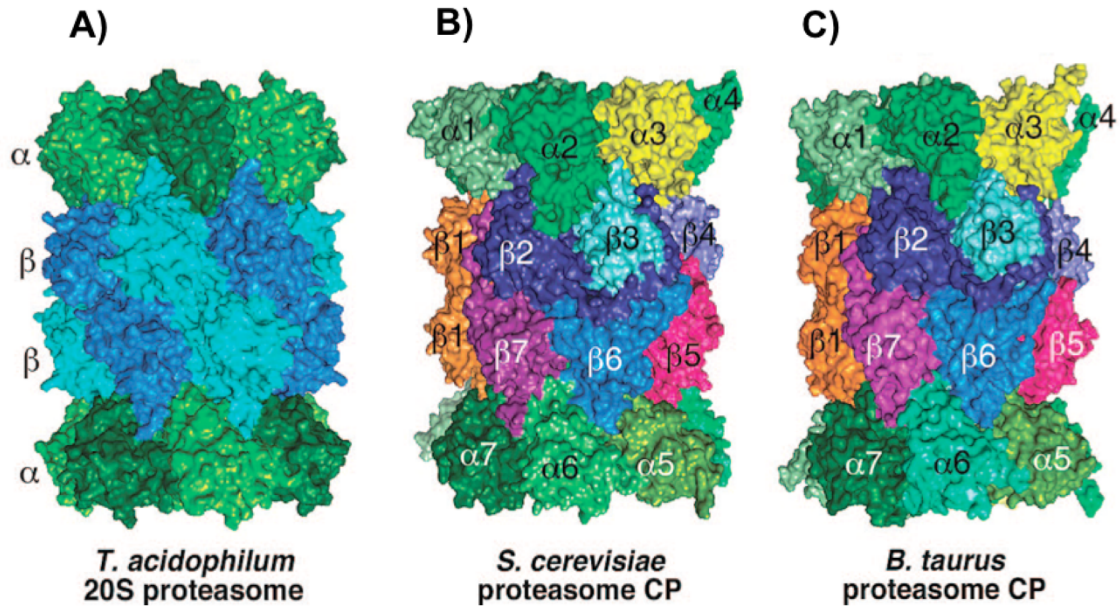


**Figure 1.2.** Structure and complexity of archaeal and eukaryotic 20S core particles.

Surface representation of the crystal structures of 20S CP from A) *T. acidophilum*, B) *S. cerevisiae*, and C) *B. taurus*. The identical  $\alpha$  and  $\beta$  type subunits of the *T. acidophilum* are each shown in two different shades of green and blue, respectively. The 14 individual subunits of the yeast and bovine 20S CPs are displayed in distinct colors. Taken from (Marques et al., 2009).

The overall shape of the archaeal 20S CP is an elongated cylinder of four stacked rings, having a central penetrating channel with three large cavities and four narrow constrictions. The two inner rings consist of seven  $\beta$  subunits each, and the two outer rings consist of seven  $\alpha$  subunits each ( $\alpha_7\beta_7\beta_7\alpha_7$ ). The core of the  $\alpha$  subunit is a sandwich of two five-stranded antiparallel  $\beta$  sheets. The  $\beta$  sandwich is open at one side where only the N terminal  $\alpha$  helix H0 is, but at the opposite side, the  $\beta$  sandwich is closed by four hairpin loops connecting  $\beta$  strands. The  $\beta$  sandwich is flanked by the three  $\alpha$  helices on top and two  $\alpha$  helices at the bottom. The structure of the  $\beta$  subunits is strikingly similar to that of the  $\alpha$  subunits but deviates predominantly at the N terminal where it starts with strand S1. The absence of  $\alpha$  helix H0 in the  $\beta$  subunits provides access to the interior of the  $\beta$  sandwich (Löwe et al., 1995).

The composition of the eukaryotic 20S CP is more complex than that of the archeal complex because the number of distinct subunits increased during evolution: seven distinct  $\alpha$  and  $\beta$  subunits are present in yeast, while mammals have seven different  $\alpha$  and 10 different  $\beta$  proteasome subunit genes. (Groll et al., 1997, Unno et al., 2002, Harshbarger et al., 2015). Each  $\alpha$  and  $\beta$  subunits occupy unique positions in the respective rings of eukaryotic 20S CP, resulting in asymmetric structures with only approximate seven-fold symmetry (Stadtmueller & Hill, 2011). The molecular mass of different subunits are in the range of 22-30 kDa and thus sum up to a molecular mass of about 700 kDa and a sedimentation coefficient of 20 S (Dahlmann,

2016). Differences among the eukaryotic  $\alpha$  and  $\beta$  subunits appear in turns, which vary in length by one or two residues, in long insertions connecting secondary structural elements, and in the N terminal and especially C terminal regions (Groll et al., 1997). The approximate length and diameter of mammalian 20S CP are 150 and 115 Å, respectively (Unno et al., 2002).

### 1.2.2. Functions of the 20S CP

Although the  $\alpha$  and  $\beta$  subunits share sequence and structural similarity, there are functionally important differences associated with their distinct N termini. The  $\beta$  rings contain the proteolytic active sites, while the outer  $\alpha$  rings define a gated channel leading into the internal proteolytic chamber.

The gated channel isolates proteolytic compartment from the cellular components, preventing unwanted degradation of endogenous proteins and probably favoring processive degradation of substrates by restricting dissociation of partially digested polypeptides. At the same time, it also imposes strong constraints on the access of substrates into the proteolytic chamber and on the release of degradation products (Bajorek & Glickman, 2004).

The first obstacle for substrate entry into the proteolytic chamber is a narrow channel known as the  $\alpha$  annulus formed by loops in the  $\alpha$  subunits and is located slightly below the surface of the  $\alpha$  ring (**Figure 1.3.A**) (Stadtmueller & Hill, 2011). The  $\alpha$  annulus appears to be a fixed opening of 13 Å diameter and it ensures that substrates are substantially unfolded before they can enter the proteasome. Additionally, the crystal structure of the 20S CP reveals that the center of the  $\alpha$  ring is completely closed in the eukaryotic 20S CP, thus presenting another obstacle for protein penetration into the inner chamber of the  $\beta$  ring. (Groll & Huber, 2003, Tanaka, 2009). The complete seal of the entrance to the proteolytic channel is formed by N-terminus of the  $\alpha$  subunits that point towards the center of the ring (**Figure 1.3.B**).

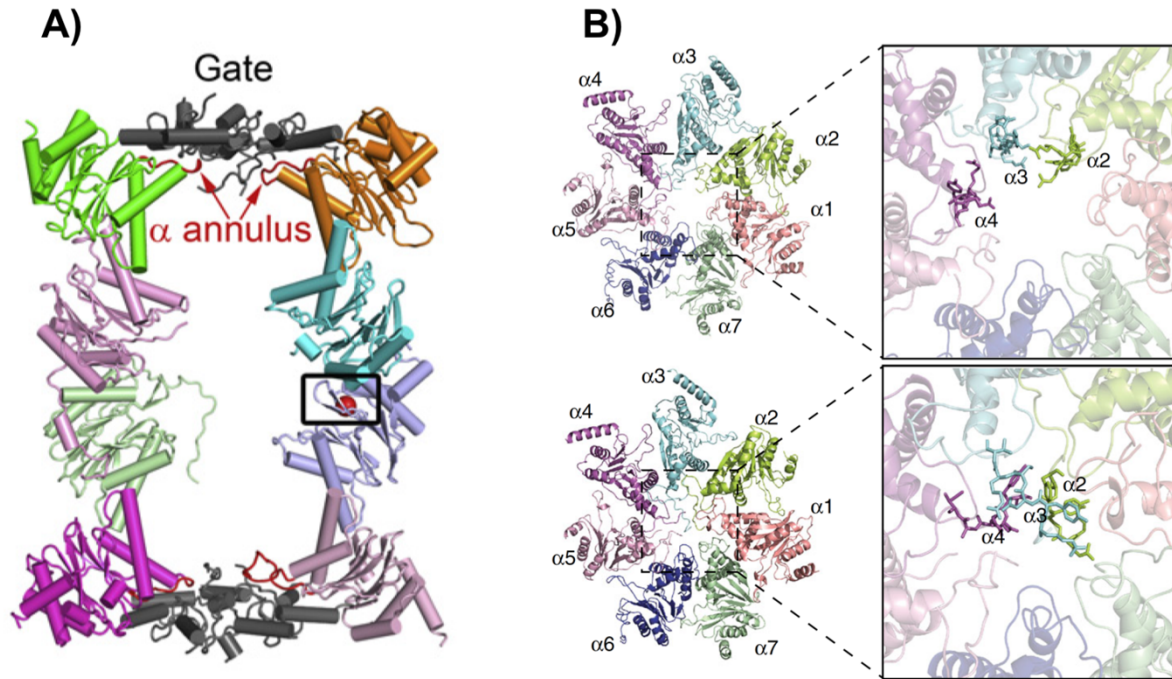


**Figure 1.3. Gated channel formed by  $\alpha$  subunits of the 20S CP**

**A)** Cartoon representation of the 20S CP. The closed gate region is colored gray. The  $\alpha$  annulus, just interior from the gate, is an opening formed by loops (red) in the  $\alpha$  subunits. **B)** The atomic models of two different conformations of  $\alpha$  rings of the 20S CP (left). Close-up views of the central parts of the  $\alpha$  rings, showing the open gate conformation (upper right) and closed gate conformation (lower right). Taken from (Stadtmueller & Hill, 2011, Zhu et al., 2018).

Interestingly, in eukaryotes, the paralogous  $\alpha$  subunits show structural and sequence similarities over the bulk of the protein, but diverge at their N terminal region in both sequence and relative length which associates with their unique conformation at the center of the ring forming closed gate conformation (Tanaka, 2009). The only sequence conserved from one  $\alpha$  tail to another is Tyr8-Asp9-Arg10 (YDR motif) (Groll & Huber, 2003). The side chains of YDR residues participate in the stabilization of the closed state of the channel (Bajorek & Glickman, 2004). Moreover, among all  $\alpha$  subunits, the tail of  $\alpha 3$  is somewhat distinct from the others in that it points directly across the surface of the  $\alpha$  ring towards the center, maintaining close contacts to every other  $\alpha$  subunit suggesting that this subunit has a pivotal role in formation of the closed gate conformation (Bajorek & Glickman, 2004).

The closed state of the channel seen in the crystal structure of the wild-type CP is predominant in solution (Bajorek & Glickman, 2004) and represents a latent state, in which substrate entry is the rate-limiting step for hydrolysis and also possibly regulates selectivity as well by requiring complete or partial unfolding over the whole length of the protein substrate (Groll & Huber, 2003). Nevertheless, it was observed that some proteins with hydrophobic or

unfolded patches can enter the wild-type 20S CP regardless of the closed gate conformation (Bajorek & Glickman, 2004).

As already mentioned, the N terminus of  $\beta$  subunits contributes to the proteolytic active sites, which belong to the N-terminal nucleophile (Ntn) hydrolase family (Marques et al., 2009). Ntn-hydrolases are synthesized as inactive precursors, which upon autocatalytic cleavage, expose N terminal amino acid residue with a nucleophilic side chain (threonine, serine or cysteine). Catalytically active  $\beta$  subunits of the proteasome use a threonine side chain (Thr1) as the attacking nucleophile and the free N-terminal amine to activate an ordered water molecule that is incorporated into the product during hydrolysis (Stadtmueller & Hill, 2011). During proteolysis, a polypeptide substrate docks at the Thr1 site, probably via hydrogen bonds, the hydroxyl group of the side chain of Thr1 produces a nucleophilic attack on the carbonyl of the peptide bond, leading to the formation of an acyl-enzyme intermediate in which a peptide fragment remains attached to the proteasome by an ester link. During formation of an acyl-enzyme intermediate, a water molecule present in the neighborhood of the active site is thought to mediate proton transfer between Thr1O $\gamma$  and Thr1N. Another water molecule present in the chamber rapidly hydrolyzes this acyl-enzyme intermediate thereby releasing a peptide fragment that is then transferred back into the cytosol and regenerates Thr1O $\gamma$  for another reaction (**Figure 1.4**). (Marques et al., 2009, Vigneron & Van den Eynde, 2014).

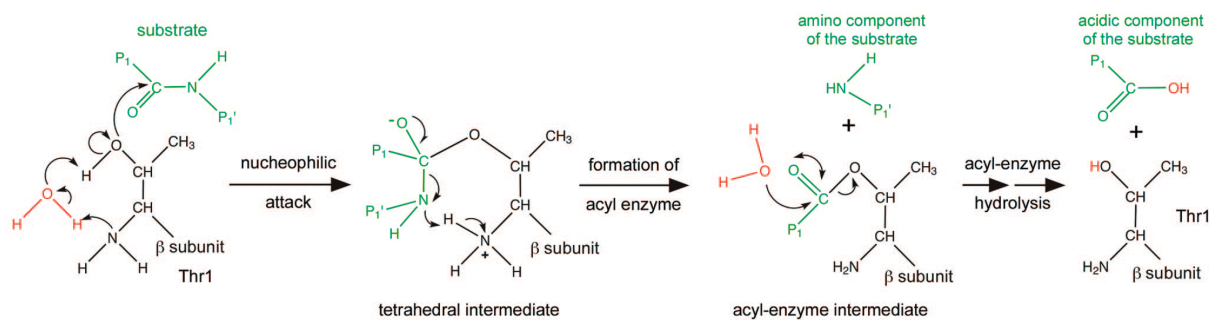


**Figure 1.4. Proteolytic mechanism of the 20S CP.**

The mechanism leading to substrate peptide bond hydrolysis by the N-terminal Thr residue of a proteasomal active  $\beta$  subunit is shown. The substrate is shown in green; the  $\beta$  subunit in black; a water molecule in red. Taken from (Marques et al., 2009).

In contrast to archaeal proteasome which contains 14 identical proteolytic active sites, in eukaryotic CPs only subunits  $\beta$ 1,  $\beta$ 2 and  $\beta$ 5 harbor the nucleophilic Thr1O $\gamma$ , whereas the remaining  $\beta$  subunits are inactive (Groll & Huber, 2003, Groll & Huber, 2004). Two pairs of these three active sites face the interior of the cylinder and reside in a chamber formed by the centers of the abutting  $\beta$  rings (Tanaka, 2009). The  $\beta$ 1,  $\beta$ 2 and  $\beta$ 5 subunits are associated with caspase-like/PGPH (peptidylglutamyl-peptide hydrolyzing), trypsin-like (TL) and

chymotrypsin-like activities (ChTL), respectively, which confer the ability to cleave peptide bonds at the C terminal side of acidic, basic and hydrophobic amino acid residues, respectively, as determined by the cleavage of fluorogenic substrates (Tanaka, 2009, Marques et al., 2009).

For the description of the substrate binding pockets in the proteasome, the following terminology is used: the substrate binding pocket names,  $S_n$  or  $S_n'$ , refer to the binding sites of substrate amino acid residues either before ( $P_n$ ) or after ( $P_n'$ ) the peptide bond to be cleaved. The number  $n$  defines the distance to the cleavage site (**Figure 1.5**) (Marques et al., 2009).

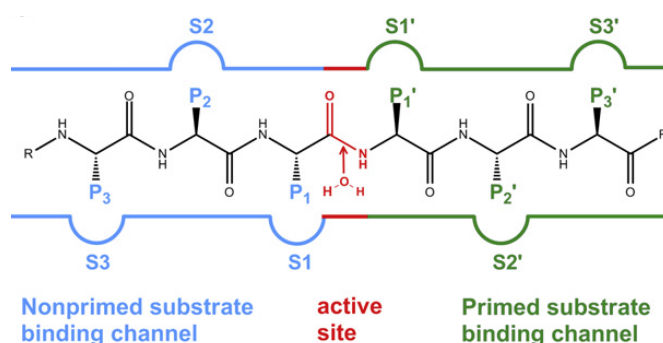


**Figure 1.5. Illustration of the substrate-specificity pockets of the three proteasomal activities and the S/P nomenclature.**

The unprimed (S) pockets, localized N-terminally of the scissile bond (red), and the corresponding substrate residues (P) are colored in blue. The primed (S') pockets and the respective parts of the ligand (P') are highlighted in green. The active site and the nucleophilic water molecule that is incorporated into the cleavage products during hydrolysis are shown in red. Taken from (Huber et al., 2012).

The cleavage pattern of the proteasome degradation of proteins indicates that the active sites are specific with regard to the recognition of certain amino acid residues in the P1 position (Nussbaum et al., 1998). However, substrate residues other than those at P1 are of relevance as well for the complex cleavage patterns of protein substrates. In fact, a stretch of amino acid residues flanking the cleavage point, ranging from P5 up to P5', appears to be important for the selection of the cleavage site by the specific  $\beta$  subunit (Nussbaum et al., 1998).

Generally, the major residue responsible for the formation of each S1 specificity pocket is located at the position 45 (Groll & Huber, 2004). Structural analysis revealed that the  $\beta$ 1 subunit has Arg at the location 45 that preferentially interacts with glutamate P1 residue which restricts the PGPH-activity of the CP to this subunit (Groll & Huber, 2004).  $\beta$ 1 has also limited the branched chain amino acid-preferring (BrAAP) activity. In the  $\beta$ 2 subunit, Gly is situated at the position 45 therefore the S1 pocket of  $\beta$ 2 subunit is very spacious and can accommodate very large P1 residues and together with Glu53 at the bottom of S1 pocket which shows a preference for basic P1 residues confers the trypsin-like activity of this subunit. Finally, in subunit  $\beta$ 5 there is Met residue at the location 45 which confers chymotrypsin-like activity to



this subunit. However, the mutational analysis also confers BrAAP activity and small neutral amino acid-preferring (SNAAP) activity to  $\beta 5$  subunit (Groll & Huber, 2004). Adjacent non-catalytic subunits in the  $\beta$  rings also contribute to the S1 pockets and significantly influence their selectivity.

### 1.2.3. The immunoproteasome

In lymphoid cells or after exposure to the inflammatory cytokines, interferon- $\gamma$  (IFN- $\gamma$ ) or tumor necrosis factor  $\alpha$  (TNF- $\alpha$ ), the alternative catalytic subunits, named  $\beta 1i$ ,  $\beta 2i$  and  $\beta 5i$ , are expressed and incorporated into the proteasome in place of their constitutive counterparts,  $\beta 1c$ ,  $\beta 2c$  and  $\beta 5c$  (constitutive proteasomes, cCP), to form another particle called the immunoproteasome (iCP) (Huber et al., 2012, Vigneron & Van den Eynde, 2014). Apart from cytokine induction, the formation of immunoproteasomes can also be induced by less specific physiological triggers for instance aging and environmental stress factors like heat shock (Dahlmann, 2016). However, the replacement of three standard subunits by immuno subunits doesn't have to be complete and proteasomes containing both subunit types are termed intermediate or mixed type proteasomes called  $\beta 5i$  ( $\beta 1c$ ,  $\beta 2c$ ,  $\beta 5i$ ) and  $\beta 1i$ - $\beta 5i$  ( $\beta 1i$ ,  $\beta 2c$ ,  $\beta 5i$ ) (Fabre et al., 2013). Nevertheless, the quaternary structures of the cCP and iCP differ only in the substitution of the c subunits with their i counterparts. The superposition of the  $\alpha$  rings, as well as for the inactive  $\beta$  subunits, from the cCP and iCP, reveals high structural similarity which is important for the aspect of regulation of gating mechanism by activator complexes (Huber et al., 2012).

From the functional point of view, as a result of their different subunit composition, the cCPs and the iCPs are endowed with different cleavage specificities. The substrate-binding channel of subunit  $\beta 2i$  was found to be identical with that of  $\beta 2c$ , except for the substitution of Asp53 ( $\beta 2c$ ) with Glu ( $\beta 2i$ ) (Huber et al., 2012). In contrast to the consistent character of subunits  $\beta 2c$  and  $\beta 2i$ , upon the comparison of  $\beta 1c$  and  $\beta 1i$  several important structural distinctions were observed. The hydrophobicity of S1 pocket of the  $\beta 1i$  subunit is increased and the size is decreased which has for consequence that peptide bond hydrolysis preferentially occurs after small, hydrophobic and branched residues such as Ile, Leu and Val. Additionally, comparing subunits  $\beta 1c$  and  $\beta 1i$ , the latter prefers smaller and more polar amino acids in P3. As for the  $\beta 5$  subunit, the S1 pocket of subunit  $\beta 5i$  is more spacious, the S2 pocket is more shallow and the S3 pocket is more hydrophilic in contrast to the S1, S2 and S3 pocket of the  $\beta 5c$  subunit, respectively (Huber et al., 2012).

Having a different cleavage specificities, the immunoproteasome plays a pivotal role in the generation of major histocompatibility complex (MHC) class I ligands. The vast majority of these ligands (known as antigenic peptides or epitopes) are generated during the degradation of mature proteins or defective ribosomal products (DRiPs) by the ubiquitin-proteasome system (UPS). These peptides are then translocated through transporters associated with antigen processing (TAPs) to the endoplasmic reticulum (ER) (Cascio, 2014). Inside the ER, those peptides will be further trimmed by ER-resident proteases, and peptides of appropriate size (8-10 amino acids) and sequence will then associate with class I molecules of the MHC (Vigneron & Van den Eynde, 2014). Peptide-MHC complexes are finally displayed at the cell surface for potential recognition by cytotoxic T-lymphocytes (CTLs). Apart from their role in antigen generation, the immunoproteasomes are important for the efficient cytokine production and have been implicated in a number of pathological disorders such as cancer, neurodegenerative and autoimmune diseases (Cascio, 2014).

### **1.3. Regulation of the 20S CP activity**

Several structural features of the 20S CP, especially sequestration of catalytic sites within the catalytic chamber and closed gate conformation formed by  $\alpha$  subunits, raise the questions towards how the 20S CP degrades proteins under physiological conditions (DeMartino & Slaughter, 1999). To overcome the structural features mentioned above, the activity of the 20S CP is primarily regulated through association with proteasome activator complexes. The best-known activator is PA700 (proteasome activator MW 700, also known as 19S or regulatory particle (RP)) which has been highly conserved from yeast to humans (Rechsteiner & Hill, 2005). The 19S RP can occupy one or both ends of the 20S core particle thus forming 26S or 30S proteasome, respectively (Schmidt et al., 2005). Two other evolutionary conserved proteasome activator families are PA28 (also known as 11S or REG) and PA200 (Blm10 in yeast) (Rechsteiner & Hill, 2005). Higher eukaryotes express three 11S isoforms called PA28 $\alpha$ , PA28 $\beta$  and PA28 $\gamma$  (aka, REG $\alpha$ , REG $\beta$ , REG $\gamma$ ) (Stadtmueller & Hill, 2011). These proteasome activators can bind to one or both sides of the 20S particle or form hybrid proteasomes where the 20S CP binds two different regulators (Rechsteiner & Hill, 2005).

### 1.3.1. The 19S regulatory particle (19S RP)

#### 1.3.1.1. Structure of the 19S RP

The general architecture of the 19S RP is described in terms of two subcomplexes termed the “base” and the “lid” (Glickman et al., 1998). The base is comprised of six ATPase subunits that belong to the family of ATPases-associated-with-different-cellular-activities (AAA+ ATPase family) (Rpt1-6) and three non-ATPase subunits – the two largest, structurally related subunits Rpn1 and Rpn2 and shuttle ubiquitin receptor Rpn13. The lid comprises at least nine non-ATPase subunits (Rpn3, Rpn5-9, Rpn11, Rpn12 and Rpn15), of which just one, the deubiquitylase Rpn11, displays enzymatic activity (Kish-Trier & Hill, 2013). An additional ubiquitin-receptor subunit of the 19S RP, the Rpn10 is not considered part of the base or lid per se, but instead bridges both subcomplexes in the assembled RP (**Figure 1.6**) (Bard et al., 2018).

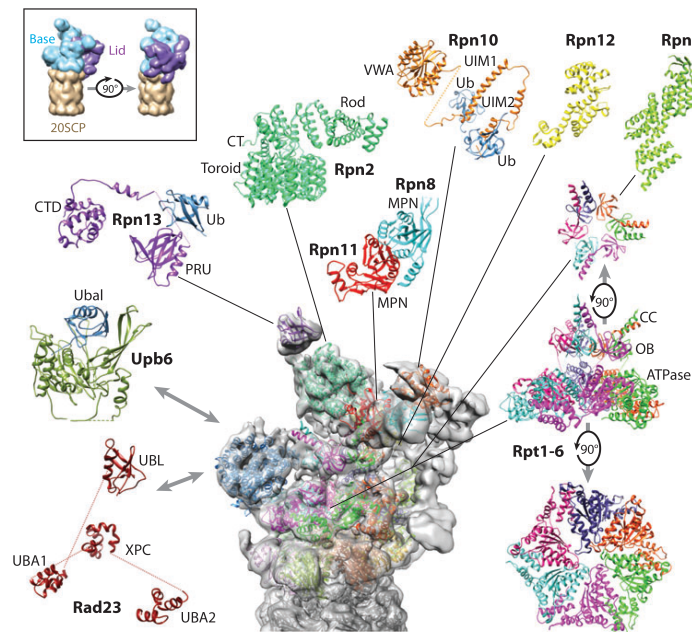


**Figure 1.6.** The 19S regulatory particle from *S. cerevisiae*.

**Box at the top left:** two side views of a schematic depiction of the 26S proteasome electron micrograph structures showing the 20S CP, base, and lid. **Main figure:** the protein subunits of the 19S RP and their protein interactors. (Taken from Kish-Trier & Hill, 2013).

Each Rpt subunit consists of an N-terminal coiled-coil, an oligonucleotide and oligosaccharide-binding domain (OB-fold) and an AAA+ domain which is comprised of large and small AAA+ subdomains (Schweitzer et al., 2016). Protein-protein interactions between the different ATPases occur via the N terminal coiled-coil region of each Rpt subunit and those

interactions have been characterized as pairs: Rpt2 binds to Rpt1, Rpt3 binds to Rpt6 and Rpt5 binds to Rpt4 (Ferrell et al., 2000).

Rpn2 has an N terminal rod-like domain of 17 stacked helices, a central domain composed of 11 proteasome/cyclosome (PC) repeats and a globular C terminal domain  $\beta$  structure. Rpn2 contains the binding site for the ubiquitin receptor Rpn13 and also serves as a lid-binding scaffold (He et al., 2012, Schweitzer et al., 2016). Rpn1 shares similar architecture as Rpn2 with some reorientation of the rod domain. Rpn1 is also a binding module for the shuttle ubiquitin receptors, Rad23 and Dsk2, and the deubiquitinating enzyme (DUB) Ubp6/USP14. These proteins bind through their N terminal ubiquitin-like (UBL) domains to Rpn1 (He et al., 2012). Rpn13 consists of an N terminal pleckstrin like receptor of ubiquitin (PRU) domain, which binds ubiquitin, and a C-terminal extension containing a nine-helix bundle that binds the deubiquitinating enzymes Uch37 and UchL5 (DUBs) (Huang et al., 2016).

Each of six Rpn subunits (Rpn 3, 5, 6, 7, 9 and 12) contain a solenoid fold followed by a proteasome-CSN-eIF3 (PCI) domain of varying length that is assumed to have scaffolding functions in the lid and allow inter-subunit contacts (Lander et al., 2012). Rpn8 and Rpn11 each have a Mpr1-Pad1-N terminal (MPN) domain. Rpn10 contains multiple ubiquitin-interacting motifs at its C termini and a von Willebrand factor A (VWA) domain at its N terminus. Finally, Rpn15 is a small acidic protein with neither PCI nor MPN domains (Tomko & Hochstrasser, 2013).

#### 1.3.1.2. The 26S proteasome

The 26S proteasome is involved in an ATP-dependent degradation of polyUb protein substrates as part of the ubiquitin-proteasome pathway (UPS) (Matthews et al., 1989). During that process the 19S RP has to perform a set of functions: 1) it has to recognize and bind selectively the protein substrates designated to degradation by ubiquitin chains; 2) these substrates have to be unfolded; 3) the ubiquitin chains have to be cleaved of the polyUb proteins; 4) the gates formed by the  $\alpha$  subunits have to be opened; and 5) the unfolded substrates have to be driven into the proteolytic chamber of the 20S CP for degradation (Wolf & Hilt, 2004).

The selection of proteasomal substrates by the 19S RP occurs via the recognition of polyUb chains bound to proteins that are destined to be degraded (Wolf & Hilt, 2004). The binding of ubiquitinated substrates to the 26S proteasome is facilitated through intrinsic ubiquitin receptors Rpn1, Rpn10 and Rpn13 (shuttle receptor in mammals) (Wang et al., 2017).

Rpn10 and Rpn13 are localized in the apical region of the RP near the periphery, whereas Rpn1 associates with Rpt1/Rpt2. Rpn10 binds ubiquitin chains and UBL domains of substrates strongly through its ubiquitin-interacting motifs (UIMs) at the C terminus. Rpn1 contains two binding sites (T1 and T2) within its first toroidal region. UBL-UBA (ubiquitin-associated) proteins and ubiquitin chains bind to the T1 site, whereas the UBL domain of Ubp6/USP14 DUB binds to the T2 site. Rpn13 binds ubiquitin via its N terminal PRU domain, while via its C terminal region directly interacts with the Uch37/UchL5 DUB (Jiang et al., 2018).

In addition to the intrinsic ubiquitin receptors, there are several extrinsic UBL-UBA ubiquitin receptors: Rad23, Dsk2 and Ddi1 (Tanaka, 2009). These proteins bind the polyUb chains on the substrates via their UBA domains and shuttle them to the proteasome by interacting with the Rpn10 subunit via their UBL domains (Tomko & Hochstrasser, 2013).

Once the polyUb substrates are bound to the 26S proteasome in order to achieve efficient substrate unfolding and translocation into the proteolytic core, the attached ubiquitin chains have to be removed (Worden et al., 2017). The removal of polyUb chains occurs through the action of the intrinsic DUB Rpn11, a Zn<sup>2+</sup> metalloproteinase of the JAB1/Mpr1-Pad1 N terminal (MPN)/MOV34 (JAMM)/MPN DUB family (Wang et al., 2017). The Rpn11 active site is positioned directly above the entrance to the central processing pore of the AAA+ motor and forms a heterodimer with the non-catalytic MPN domain of another lid subunit, Rpn8. Rpn11 cleaves the polyUb chain at a proximal site by hydrolyzing the isopeptide bond at the very base of the chain, between the substrate lysine and the C terminus of the first ubiquitin (**Figure 1.7.A and B**) (Worden et al., 2017). The remaining polyUb chain is further cleaved into the monomeric ubiquitin proteins by other DUBs. In addition, DUBs associated with the base complex, Ubp6/USP14 and Uch37/UchL5, cleave the ubiquitin moiety at a distal site (Tanaka, 2009).

Surprisingly, it was established that ubiquitination alone is not sufficient for the efficient engagement and degradation in case of tightly folded proteins. These proteins require an unstructured initiation region for engagement of a substrate with the proteasomal ATPases (Prakash et al., 2004). Further, this unstructured initiation region has an important role in committing substrates to proteasomal processing once the substrate is threaded through the ATPase (Bard et al., 2018) and the rate of substrate degradation afterwards greatly depends on the sequence composition of this region. For example, small side chains as in serine or glycine in this region result with less efficient degradation, and flexible, hydrophobic or charged side chains result in more efficient degradation of substrates (Bard et al., 2018).

After engagement, the translocation of a substrate into the proteolytic chamber of the 20S CP is thought to be coordinated by the Rpn1-Rpn2 through their asymmetrical solenoid

structure due to the physical separation between the initial binding site and the entry pore into the 20S CP (Rosenzweig & Glickman, 2008). The hexameric Rpt ring, driven by ATP binding and hydrolysis, unfolds substrate by pulling the polypeptide through an axial channel and translocates it into the proteolytic chamber of the 20S CP for degradation (Wehmer et al., 2017). The substrate unfolding is probably induced by threading the substrate polypeptide chain through the N ring formed by OB-fold domains above the AAA+ domains of the Rpt subunits (Bard et al., 2018). The AAA+ ATPase ring is lined by pore-1 and glycine-rich pore-2 loops, which directly contact the polypeptide chain. The pore 1 loops have the characteristic aromatic-hydrophobic-glycine motif (Ar- $\Phi$ -G), of which the aromatic residue is the one that engages the substrate polypeptide directly (**Figure 1.7.C**) (Huang et al., 2016, Schweitzer et al., 2016). Simultaneously, mechanical translocation of a still ubiquitinated substrate is thought to accelerate the ubiquitin cleavage by Rpn11 and also position polyUb substrates for cleavage of ubiquitin chain (Worden et al., 2017).

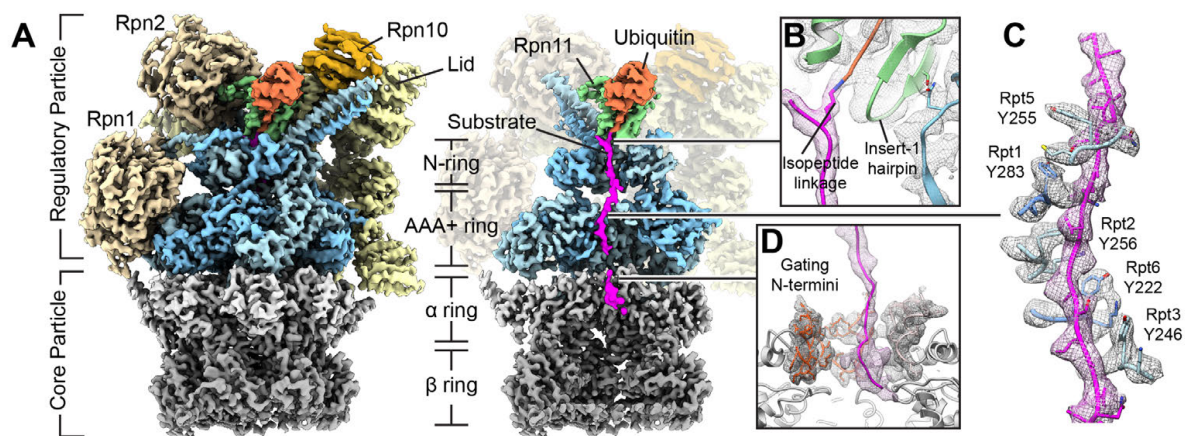


**Figure 1.7. High-resolution structure of the substrate-engaged 26S proteasome**

**A)** Exterior (left) and cutaway (right) views of the substrate-engaged proteasome. The substrate (magenta) is shown extending from the ubiquitin moiety (orange), through the central pore formed by the N-ring and the AAA+ motor (blue), into the gate of the 20S CP (gray). **B)** The isopeptide bond between the lysine and the C terminus of the ubiquitin moiety is bound in the catalytic groove of Rpn11 (green). **C)** The substrate polypeptide is encircled by a spiral-staircase of pore-1-loop tyrosines projecting from the Rpt subunits. **D)** Substrate enters the open gate of the 20S CP. Taken from (de la Pena et al., 2018).

According to different steps during protein degradation by the 26S proteasome, several conformational states were identified for the human proteasome termed  $S_A$ ,  $S_B$ ,  $S_C$  and  $S_D$  (Bard et al., 2018).  $S_A$  is considered to be ground, substrate accepting, state as it is most populated.  $S_B$  and  $S_C$  represent intermediates between  $S_A$  and  $S_D$  state whereas  $S_D$  represents the translocating or fully engaged state of the proteasome. Progressing from  $S_A$  to  $S_D$  state, the orientation of the lid and the base relative to each other and to the 20S CP changes dramatically,

whereas general structure of the core particle remains virtually unchanged, except for  $S_D$  state where gate formed by N termini of the 20S CP  $\alpha$  subunits opens to allow substrate translocation into the proteolytic chamber (**Figure 1.7.D**), and most likely for degradation products to exit the 20S CP (Chen et al., 2016). The gate opening necessitates breaking the interactions that anchor N terminal tails in closed gate conformation while at the same time competing interactions form which stabilize them in an open conformation (Bajorek & Glickman, 2004). Three Rpt subunits, Rpt2, Rpt3 and Rpt5, contain hydrophobic-tyrosine-X (HbYX) motifs located at C terminus. These tails insert into pockets between neighboring  $\alpha$  subunits (Finley et al., 2016). In the  $S_A$  state the HbYX motifs of Rpt3 and Rpt5 are inserted into the  $\alpha_1$ - $\alpha_2$  and  $\alpha_5$ - $\alpha_6$  pockets, respectively and in the  $S_D$  state, the C terminal tails of Rpt1, Rpt2 and Rpt6 are also inserted into the  $\alpha_4$ - $\alpha_5$ ,  $\alpha_3$ - $\alpha_4$  and  $\alpha_2$ - $\alpha_3$  pockets respectively (Chen et al., 2016). According to those observations it was evident that the simple RP-CP association is not enough to achieve gate opening but rather a series of coordinated, stepwise remodeling events around the RP-CP interface is required to open the CP channel.

### 1.3.2. 11S proteasome regulators (PA28 or REG)

The proteasome activator PA28 family consists of three members: PA28 $\alpha$ , PA28 $\beta$  and PA28 $\gamma$  (also known as Ki antigen) (Tanahashi et al., 1997). The PA28 $\alpha$  and PA28 $\beta$  have a molecular mass of 28 kDa and are 50% identical in primary structure (DeMartino & Slaughter, 1999). The PA28 $\gamma$  has a slightly greater molecular mass of 31 kDa and shares ~30% sequence identity with PA28 $\alpha$  and PA28 $\beta$  homologs (Tanahashi et al., 1997). The PA28 $\gamma$  is found in both invertebrates and vertebrates, whereas PA28 $\alpha$  and PA28 $\beta$  are found only in vertebrates (Li et al., 2006). The intracellular distribution of PA28 $\alpha$ , PA28 $\beta$  and PA28 $\gamma$  also differs. The PA28 $\alpha$  and PA28 $\beta$  are mainly cytoplasmic, whereas PA28 $\gamma$  is confined to the nucleus (Rechsteiner & Hill, 2005). For the 11S proteasome activators was shown that they do not promote the degradation of intact proteins like 19S RP but rather activate peptidase activities of the 20S CP (Li & Rechsteiner, 2001). However, there are some indications that PA28 and PA200 (discussed later in the text) proteasome activators are mediating resistance to higher levels of oxidative stress by increasing the ability of 20S CP to selectively degrade oxidized proteins (Pickering & Davies, 2012). For different 11S regulators, the pattern of proteasomal activation is different. The PA28 $\alpha$  and PA28 $\beta$  in combination or alone, direct cleavage specificity after basic, acidic and hydrophobic residues and PA28 $\gamma$  after only basic residues in the P1 position (Li & Rechsteiner, 2001).

The proposed mechanism by which 11S regulators activate the 20S CP is through the opening of the channel at the terminal  $\alpha$  ring, thereby increasing access of substrates to the catalytic sites and/or by allosteric activation of the catalytic sites (DeMartino & Slaughter, 1999). This mechanism was elucidated by solving a crystal structure of the *Trypanosoma brucei* 11S homolog PA26 in complex with yeast 20S CP (Whitby et al., 2000). The PA26 homoheptamer complex binds the 20S CP by inserting the C terminus of each subunit into pockets located between the proteasome  $\alpha$  subunits (**Figure 1.8.A**). Upon binding, the PA26 pore aligns with the roughly seven-fold axis of the 20S CP and the  $\alpha$  subunit N terminal sequences extend into the PA26 pore where they pass close to the activation loop in the PA26 subunits (**Figure 1.8.B**). The N terminal strands of  $\alpha 2$ ,  $\alpha 3$ ,  $\alpha 4$  and partially  $\alpha 5$  subunit that provide a tight seal of the 20S CP, are rearranged to open the axial pore to allow the substrate entrance/exit (Whitby et al., 2000).

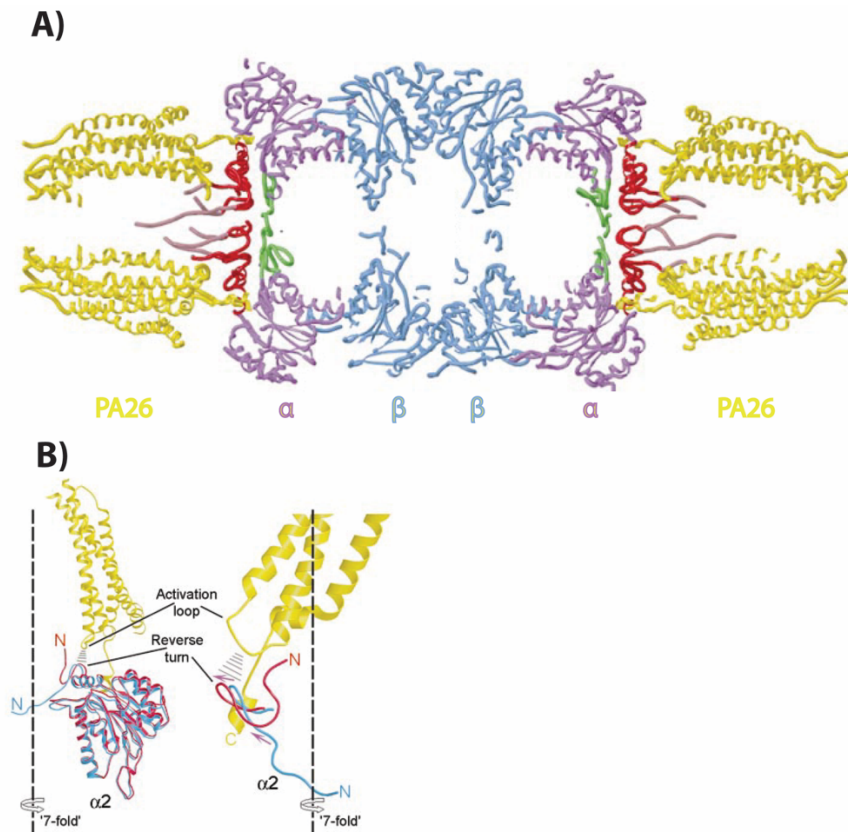


**Figure 1.8. Structural basis for the activation of 20S proteasomes by 11S regulators**

**A)** The trypanosome PA26 in complex with yeast 20S CP complex. Residues of the  $\alpha$ -annulus are green; ordered N terminal residues of  $\alpha$  subunits that do not have counterparts in  $\beta$  subunits are red; and disordered N terminal residues of  $\alpha$  subunits are pink. **B)** The PA26 C terminal helix (yellow) is visible behind  $\alpha 2$ . Rotation by  $90^\circ$  about the vertical axis shows the displacement of the  $\alpha 2$  N terminus reverse turn. Taken from (Whitby et al., 2000).



The structure of PA26 resembles that of a human PA28 $\alpha$ , despite sharing only 14% sequence identity and likewise, C termini of the mammalian 11S regulators have also been implicated in binding of the 20S CP, but not in the activation of specific proteasome catalytic subunits. (Li et al., 2000, Whitby et al., 2000). Due to the fact that 11S proteasome regulators lack the HbYX-motif, most probably, as seen for PA26, the gate opening by PA28 complexes is not promoted by insertion of the C-termini but rather via internal loop structure, the activation loops, that form contacts with the  $\alpha$  subunits and promote opening of the gate (Schmidt & Finley, 2014).

### 1.3.2.1. The PA28 $\alpha$ /PA28 $\beta$ complex

PA28 $\alpha$  and PA28 $\beta$  subunits can assemble into homoheptamers referred as the PA28 $\alpha_7$  and PA28 $\beta_7$ , respectively or into heteroheptamers containing both, PA28 $\alpha$  and PA28 $\beta$  subunits. The formation of PA28 $\alpha\beta$  heteroheptamers is favored. The quaternary structure of the PA28 $\alpha\beta$  heteroheptameric complex consists of an alternating arrangement of four  $\alpha$  and three  $\beta$  subunits (PA28 $\alpha_4\beta_3$ ) (**Figure 1.9**) (Huber & Groll, 2017). The PA28 $\alpha\beta$  complex stimulates proteasome activity more efficiently than the homooligomeric PA28 $\alpha$  or PA28 $\beta$  complexes (Huber & Groll, 2017). The electron microscopy images show that PA28 $\alpha\beta$  forms a cap on the end of the 20S CP which is about 10-11 nm wide at the base, where it attaches to proteasome  $\alpha$  subunits, and 7-8 nm long from the base to the tip (Cascio, 2014).

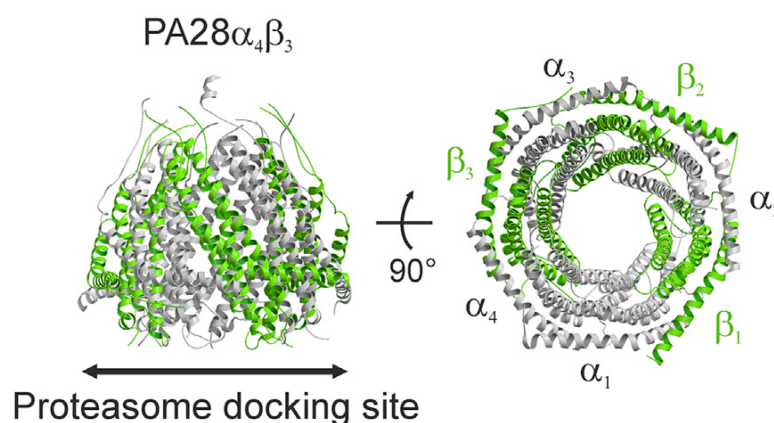


**Figure 1.9.** Side and bottom view of the PA28 $\alpha_4\beta_3$  crystal structure. The  $\alpha$  subunits are colored in gray and the  $\beta$  subunits are colored in green. Taken from (Huber & Groll, 2017).

The PA28 $\alpha\beta$  complex is present at a basal level in all tissues or can be induced by IFN- $\gamma$  and is thought to be involved in the MHC class I antigen presentation in association with

immunoproteasomes (Yang et al., 1995). Since intact antigenic proteins cannot be degraded by the 20S-PA28 $\alpha\beta$  complex, it has been suggested that antigens are initially cleaved by the 26S proteasome and that the fragments are subsequently pruned by the 20S-PA28 $\alpha\beta$  proteasome to fit with the specificities of the TAP transporters and MHC class I where PA28 could play three potential functions namely specifying, lengthening or channeling proteasomal cleavage products (Rechsteiner & Hill, 2005). The study by Raule et al (2014) demonstrated that several individual peptides with a length of 8 to 23 residues are released in much higher amounts by 20S-PA28 $\alpha\beta$  than by 20S or 26S immunoproteasomes. Moreover, the products longer than seven residues whose generation is strongly enhanced in the presence of PA28 $\alpha\beta$  were, on average, more hydrophilic than those preferentially released by the 20S alone (Raule et al. 2014). These findings suggest that PA28 $\alpha\beta$  might act as a selective smart “sieve” that strictly controls the exit of products from proteasome on the basis of size and, presumably, sequence.

Moreover, apart from the production of peptides that present the correct hydrophobic or basic C-terminal anchor residue required for association with the MHC class I groove, the PA28 $\alpha\beta$  was found to induce a generation of a certain number of peptides with an acidic C terminus which cannot bind efficiently to MHC class I molecules (Raule et al., 2014). Taking that into account it is also possible that PA28 $\alpha\beta$  might exert a regulatory function by blunting excessive cytotoxic responses against antigens of self-origin, thus preventing the risk of potentially harmful autoimmune reactions. In addition to being involved in antigen processing and immune recognition, the PA28 $\alpha\beta$  proteasomes play a role in cellular adaptation to altered redox homeostasis because PA28 $\alpha\beta$  can stimulate the 20S CP to degrade oxidized and misfolded proteins independently of ubiquitylation (Jiang et al., 2018).

#### 1.3.2.2. PA28 $\gamma$ complex

PA28 $\gamma$  forms a homoheptamer complex that has a molecular mass of approximately 210 kDa. PA28 $\gamma$  was recovered in yeast two-hybrid library screening using the mitogen-activated protein (MAP) kinase kinase (MEKK3) as bait (Hagemann et al., 2003). MEKK3 is an upstream activator of c-Jun N terminal kinases (JNKs), which have long been implicated in apoptosis. Furthermore, two-hybrid screens show that three proteins implicated in the JNK-mediated apoptosis namely Daxx, RanBPM and PIAS, and the pro-apoptotic protein FLASH interact with PA28 $\gamma$  (Rechsteiner & Hill, 2005). The studies with PA28 $\gamma^{-/-}$  mutant cell lines and mice indicate that PA28 $\gamma$  functions in cell-cycle progression and as an anti-apoptotic factor (Murata et al., 1999). However, it is still unclear how the PA28 $\gamma$  might affect apoptosis and several hypotheses have been proposed: recruitment of the 26S proteasome to specific

promoters, promotion of proteolysis of specific pro-apoptotic components or binding to pro-apoptotic factors thus preventing their action (Rechsteiner & Hill, 2005).

In association with the 20S CP, the PA28 $\gamma$  is involved in degradation of short peptides and intact unstructured or naturally unfolded intracellular proteins in an ubiquitin-independent manner (Mao et al., 2008, Nie et al., 2010, Suzuki et al., 2009). To date, many substrates of the 20S-PA28 $\gamma$  proteasome pathway have been identified, including steroid receptor activator-3 (SRC-3/AIB1) involved in estrogen and growth-factor signaling pathways (Li et al., 2006), p21<sup>Waf/Cip1</sup>, p16 and p14, the cyclin-dependent kinase inhibitors (Chen et al., 2007, Li et al., 2007) and the ubiquitin ligase Smad ubiquitination regulatory factor 1 (Smurf1) which targets many proteins for ubiquitin-dependent proteasomal degradation (Nie et al., 2010). The PA28 $\gamma$  was shown to be involved in the translocation and retention of the hepatitis C virus (HCV) core protein into the nucleus and its proteolysis (Moriishi et al., 2003, Suzuki et al., 2009). Moreover, the PA28 $\gamma$  is also potentially associated with regulation of metabolism because it mediates ubiquitin-independent degradation of glycogen synthase kinase (GSK3)-phosphorylated MAFA, which regulates insulin gene expression and degradation of silent mating type information regulation 2 homolog 1 (SIRT1) which regulates brown remodeling of white adipose tissue (Jiang et al., 2018).

### 1.3.3. PA200

The PA200 was originally identified as a component of a slow migrating, activated form of the 20S CP in rabbit reticulocyte lysate (Hoffman et al., 1992). Mammalian PA200 orthologs can be found in yeast (Blm10), nematodes and plants (Jiang et al., 2018). Bound to the 20S CP as a single, 200 kDa polypeptide chain, the PA200 has an asymmetric, hollow, dome-like structure (Ortega et al., 2005, Iwanczyk et al., 2006). The tertiary structure of Blm10/PA200 proteins is characterized by an array of HEAT repeats, which form an elongated solenoid (Sadre-Bazzaz et. al. 2010). The repeats make extensive contacts with the  $\alpha$  ring surface and lead to the partially open gate conformation of the 20S CP (Iwanczyk et al., 2006). The Blm10-CP association is mediated by the HbYX motif in the Blm10 C-terminus, as observed for the proteasomal ATPases (**Figure 1.10. A and B**) (Sadre – Bazzaz, et. al. 2010).

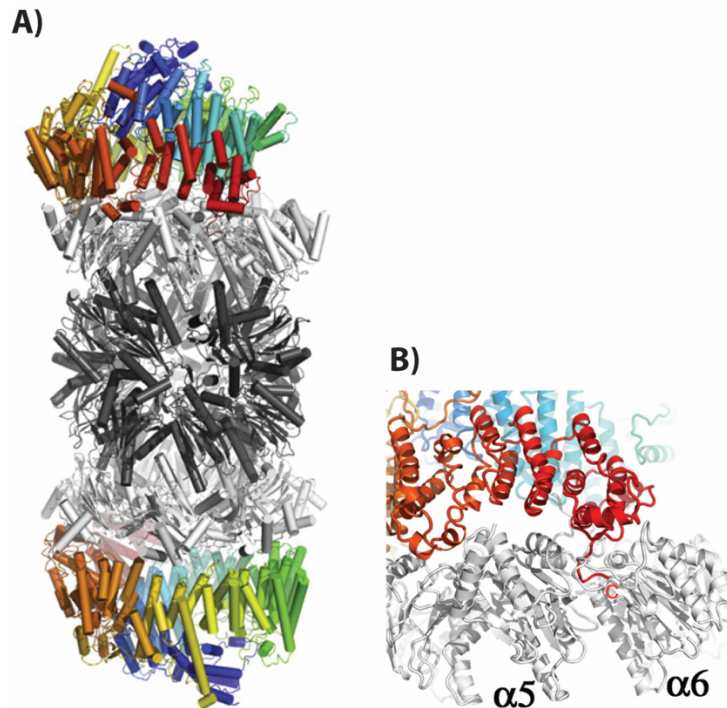


**Figure 1.10. Crystal structure of a 20S CP-Blm10 complex and mechanism for proteasome gate opening.**  
**A) Cartoon of the Blm10 – proteasome complex, side view. Proteasome  $\alpha$  subunits (white) and  $\beta$  subunits (gray); Blm10 rainbow from N terminus (blue) to C terminus (red). B) Enlarged side view with Blm10 C terminus labeled ‘C’. Taken from (Sadre – Bazzaz, et. al. 2010).**

The PA200 activates the 20S CP against peptide substrates in the absence of nucleotides. It stimulates proteasomal hydrolysis of the LLE- $\beta$ NA and IETD-MCA peptide substrates for caspase-like active site almost three times more than the hydrolysis of fluorogenic peptides diagnostic for the chymotrypsin-like and trypsin-like active sites (Ustrell et al., 2002). The preferential hydrolysis of peptides with acidic residues at P1 could be due to PA200 generating a channel into the proteasome that facilitates entry of negatively charged peptides or PA200 could induce activating conformational changes preferentially in the caspase-like catalytic subunit (Ustrell et al., 2002).

Since it was shown that Blm10 binds both, the proteasome and Sir4p, component of DNA repair machinery, it is hypothesized that the Blm10 serves as an adapter between the proteasome and chromatin proteins involved in DNA repair. Likewise, several properties of mammalian PA200 also implicate the protein in DNA repair: the PA200 mRNA and the protein are abundant in testes, where double-strand breaks occur at high frequency during meiotic recombination (Rechsteiner & Hill, 2005), the PA200 is present within the nucleus and, as with several DNA-repair components in mammalian cells, forms foci after  $\gamma$ -irradiation (Ustrell et

al., 2002). However, it is not known whether PA200 enhances or suppresses proteolysis following DNA damage.

In testes, the PA200-containing proteasomes are specialized into the spermatoproteasomes with a testis-specific subunit,  $\alpha 4s$ , and promote degradation of the core histones during spermatogenesis (Qian et al., 2013). Deletion of PA200 in mice causes severe defects in spermatogenesis and reduces fertility in male mice (Khor et al., 2006). Double deletion of PA200 and PA28 $\gamma$  in mice causes complete infertility in males with noteworthy defects in sperm motility due to decreased proteasome activity of the mutant sperm (Huang et al., 2016). Thus, PA200 plays a vital role in spermatogenesis.

#### 1.4. The hybrid proteasome

The immunoprecipitation experiments with HeLa cell extracts performed by Hendil et al. (1998) showed that antibodies against PA28 precipitated some of the components of 19S RP. Conversely, antibodies against 19S subunits precipitated not only 26S proteasomes but also PA28 $\alpha$ ,  $\beta$  and  $\gamma$  subunits. Those results indicated that 20S CP can simultaneously bind both, the 19S RP and PA28 regulatory complex (Hendil et al., 1998). Similar experiments with murine embryonic fibroblasts (MEFs) showed that after immunoprecipitation washes with the S4 antibody against 19S RP, PA200 was completely removed from the sample, but only  $\approx 50\%$  of PA28 regulators was removed indicating that the majority of PA200 is bound in 19S-20S-PA200 complexes while PA28 $\alpha\beta$  and PA28 $\gamma$  have much greater flexibility and may be found in 19S-20S-PA28 $\alpha\beta$ /PA28 $\gamma$  complexes or 20S-PA28 $\alpha\beta$ /PA28 $\gamma$  complexes in this cell line (Pickering & Davies, 2012).

The type of proteasome complex that contains the 19S RP on the one end and PA28 or PA200 complex on the other end of the same 20S CP is called hybrid proteasome. The electron microscopic analysis of hybrid proteasomes that were obtained by *in vitro* reconstitution from purified components, revealed a cork-screw-shaped complex that is 38 nm long as measured along the axis of the 20S CP (**Figure 1.11**) (Kopp et al., 2001).

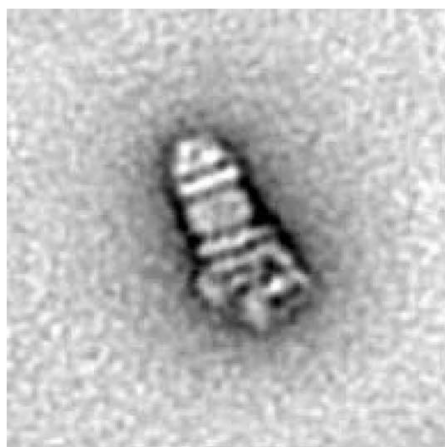


**Figure 1.11.** Average image of the negatively stained hybrid proteasome complex (PA28 $\alpha\beta$ -20S-19S) based on 266 particles. Taken from (Cascio & Goldberg, 2005).

Functional studies of hybrid proteasome complexes were performed with 19S-20S-PA28 $\alpha\beta$  complex by adding the PA28 $\alpha\beta$  complex in the 26S proteasome sample and comparing with the sample containing only 26S proteasomes (Cascio et al., 2002, Cascio & Goldberg, 2005). PA28 $\alpha\beta$  was found to increase 3- to 4-fold the activity of the 26S proteasome against the model fluorescently labeled peptide substrates of the chymotrypsin-like (Suc-LLVY-Amc), the trypsin-like (Boc-LLR-Amc) and the caspase-like active site (Z-YVAD-Amc) (Cascio et al., 2002). A similar approach was used to investigate the protein breakdown by hybrid complexes using the denatured proteins of different sizes (insulin-like growth factor (IGF-1), casein and ovalbumin) which are degraded by the 26S proteasomes in a linear and an ATP-dependent manner. In contrast to the increased peptidase activity of the 26S proteasome, the association of PA28 $\alpha\beta$  with the 26S proteasomes did not alter the rate of protein hydrolysis significantly and the size distributions of peptides released from the 26S proteasome were indistinguishable in the presence or absence of PA28 $\alpha\beta$  (Cascio & Goldberg, 2005). However, PA28 $\alpha\beta$  was found to alter the pattern of peptides generated by the 26S proteasomes (Cascio & Goldberg, 2005).

The observation that the 11S and the 19S regulators can bind simultaneously to each end of the same 20S CP suggests that the *in-vivo* function of 11S regulators may be to open the product exit gate at the opposite end of the proteasome from the 19S RP. This model suggests a function for the 11S regulators in accelerating substrate throughput (**Figure 1.12**) (Withby et al., 2000). The other possibility is that PA28 or PA200 might function as adaptors in these hybrid proteasomes by, for example, recruiting proteasomes to specific intracellular locations (**Figure 1.12**) (Rechsteiner & Hill, 2005). For example, PA200, as a component of the 26S proteasome, could recruit the large ATP-dependent protease to sites of DNA damage. Once

there, the 26S proteasome could degrade chromatin proteins in order to expose DNA to the requisite repair enzymes (Ustrell et al., 2002). The other example is that PA28 $\alpha\beta$  in the PA28 $\alpha\beta$ -20S-19S RP complex couples the hybrid proteasome to the peptide loading complex where ubiquitinated substrates could be transferred into the proteasome for degradation with the peptide products being passed directly into the endoplasmic reticulum (ER) through a continuous channel formed by the PA28 $\alpha\beta$  heptamer bound to the TAP complex. This would prevent accidental destruction of class I epitopes by cytosolic peptidases (Rechsteiner et al., 2001).

The PA28 $\alpha\beta$  can form hybrid proteasomes that include the immunoproteasome 20S CP (Pickering & Davies, 2012). Simultaneous binding of PA28 $\alpha\beta$  and 19S RP to the same immunoproteasome 20S CP suggests that intact proteins, usually after ubiquitinylation, are recognized by the 19S RP, unfolded, and fed into the 20S CP inner chamber for cleavage. The PA28 $\alpha\beta$  complex at the other end of the same 20S CP might then, together with the IFN- $\gamma$  induced subunits in the 20S CP itself, change the cleavage specificity to provide a spectrum of peptides that are more efficiently presented on MHC than the fragments generated by the 26S proteasome alone (Hendil et al., 1998). Other possibility, based on the degradation studies with PA28 $\alpha\beta$ -20S and PA28 $\alpha\beta$ -20S-19S complexes (Cascio & Goldberg, 2005, Raule et al., 2014), is that in hybrid proteasomes (as in 26S proteasomes), the main route of exit of peptides from the inner proteolytic chamber is regulated by the 19S RP, whereas PA28 $\alpha\beta$  might exert its major effect by allowing preferential sorting, through its central channel, of selected products that are more suitable for MHC class I antigen presentation (**Figure 1.12**). The role in MHC class I antigen production by this type of hybrid proteasome is strongly supported by the fact that IFN- $\gamma$  treatment induces expression of the PA28 $\alpha\beta$ , enhances the formation of immunoproteasomes and also the hybrid proteasomes containing PA28 $\alpha\beta$  complex (Tanahashi et al., 2000).

Some more recent studies indicate that the inhibition of proteasome activity induces the formation of hybrid proteasome complexes (Shibatani et al., 2006, Welk et al., 2016). The treatment with MG132, a potent proteasome inhibitor that blocks all three catalytic  $\beta$  subunit activities, was reported to stimulate the PA28 binding to 20S and 26S proteasomes *in vitro* (Shibatani et al., 2006) whereas Welk et al. (2016) observed that upon proteasome inhibition with bortezomib, the preexisting PA28 $\gamma$  and PA200 are recruited to the 26S proteasomes. Moreover, specific inhibition of 26S proteasome activity via siRNA-mediated knockdown of the 19S RP subunit Rpn6, induced recruitment of PA200 only, which included transcriptional activation of the activator (Welk et al., 2016). The recruitment of PA28 $\gamma$  and PA200 directly

correlated with the extent of catalytic inhibition with inhibition of the  $\beta 5$  active site being sufficient for recruitment (Welk et al., 2016). Those results suggested that a decrease in catalytic activity allosterically regulates the association of the 20S/26S CP with those activators. The underlying mechanism for recruitment may involve the accumulation of substrates, dynamic posttranslational modifications, competing binding partners, and cofactors in a complex cellular environment. Once formed alternative, hybrid proteasome complexes might serve as part of a protective cellular stress response to imbalanced protein homeostasis upon proteasome inhibition (Figure 1.12). Noteworthy, the same effect of hybrid proteasome formation upon proteasome inhibition *in vitro*, was not observed (Welk et al., 2016).

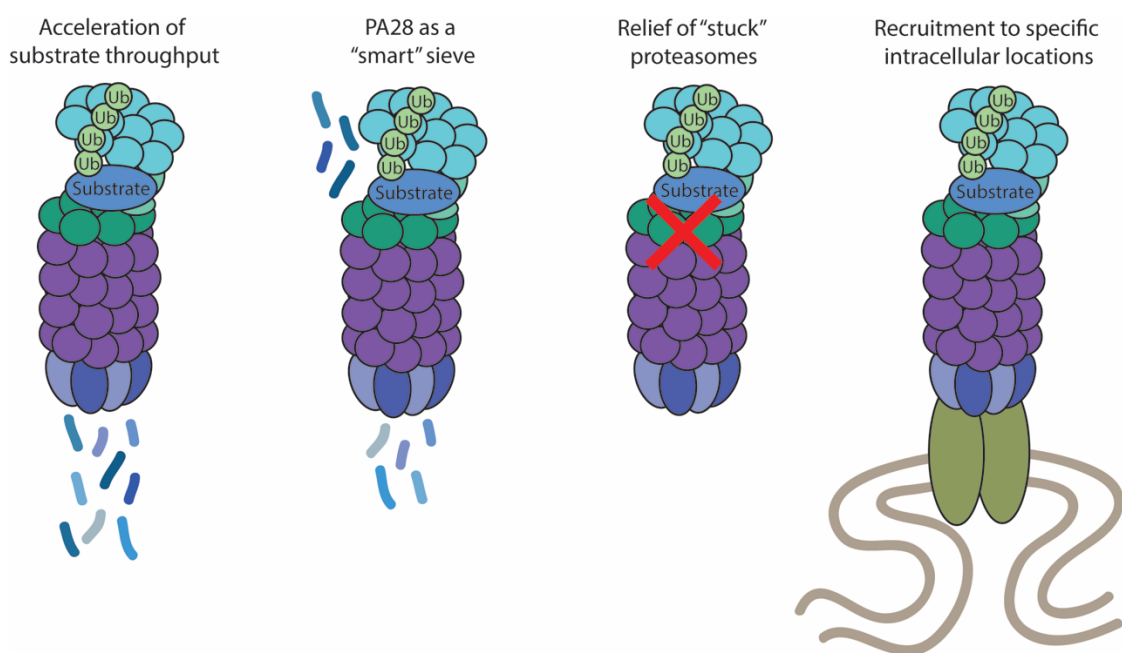


**Figure 1.12. Possible roles of hybrid proteasome complexes.**

The additional activator (11S or PA200) on the 26S proteasome is so far thought to either accelerate the substrate throughput, allow the production of the peptide fragments with a unique sequence by serving as a “smart” sieve, help relief the 26S proteasome when it’s stuck by for example substrates that require more complex unfolding or the additional activator might recruit the 26S proteasome to specific intracellular locations.

### 1.5. Single-particle electron microscopy

A variety of molecular assemblies of different shapes, sizes and biochemical states can be studied by single-particle electron microscopy (single-particle EM). The general idea behind single-particle EM is that for the samples that contain isolated complexes with many identical single particles present on an EM grid, many views of the same molecule can be obtained and from those views a 3D structure of the molecule can be calculated. In general, the single-



particle approach is widely applicable to homogenous preparations of single particles with any symmetry and molecular masses in the range of 0.05-100 MDa (Orlova & Saibil, 2011).

The simplest method for examining a solution of isolated particles such as macromolecular complexes is negative staining, in which a droplet of a suspension of the particles is spread on a support film fixed to an EM grid and then embedded in a heavy metal salt solution, typically uranyl acetate, blotted to a thin film and allowed to dry (**Figure 1.13**). The method is called negative staining because the macromolecular shape is seen by exclusion rather than binding of the electron dense stain (Ohi et al., 2004). The advantage of negative staining is simple and quick sample preparation but the disadvantage is that the fragile assemblies can collapse or disintegrate during staining and drying. In general, under the sample preparation conditions the 3D structure might become flattened to a greater or lesser degree, and the stain may not cover the entire molecule resulting in the distorted or completely missing parts of the structure in the image data (Orlova & Saibil, 2011).

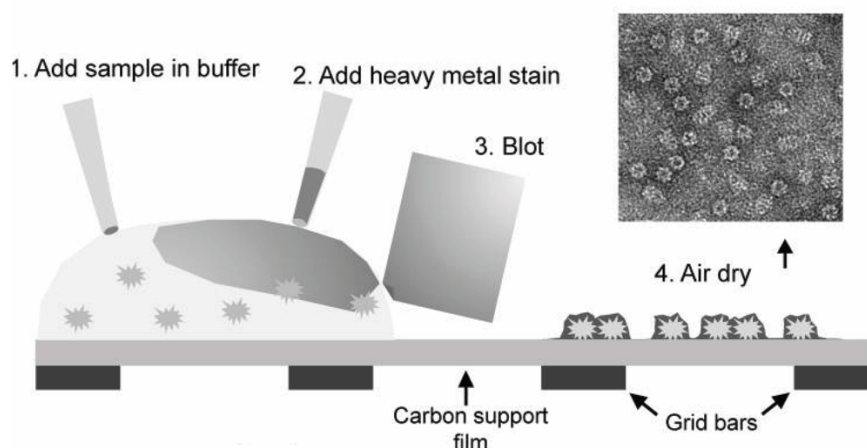


**Figure 1.13. Negative stain sample preparation.**

Schematic view of sample deposition, staining and drying with an example negative stain image. Taken from (Orlova & Saibil, 2011)

A second powerful single-particle EM technique, that doesn't suffer the disadvantages of negative stain EM is single-particle cryo-electron microscopy (cryo-EM). Importantly, cryo-EM is an extremely useful and complementary method in the field of structural biology because it enables visualization of molecular assemblies which are often too large and flexible to be amenable to X-ray crystallography or nuclear magnetic resonance (NMR) (Bai et al., 2015).

In this technique, the specimens consist of randomly dispersed, unstained biological macromolecules embedded in a thin film of non-crystalline, vitreous ice (amorphous solid form

of water), thus preserving the structure of macromolecules in a near-native state (Agard et al., 2014). The basic technique for the sample preparation in cryo-EM involves an apparatus that plunges the EM grid on which the specimen is suspended within a thin water layer into liquid ethane, the EM grid is held at the tip of tweezers, which are in turn mounted on a rod that is held in a position to fall under gravity. The thickness of the water layer is controlled by blotting with a filter paper. As the rod is released, the grid is rapidly plunged into a bath of liquid ethane at about  $-180^{\circ}\text{C}$  cooled by liquid nitrogen (Figure 1.14). Owing to the rapid decrease in temperature, the water turns into vitreous ice and, in the perfect case, the formation of crystals and consequently the disruption of the molecules is avoided (Frank, 2002).

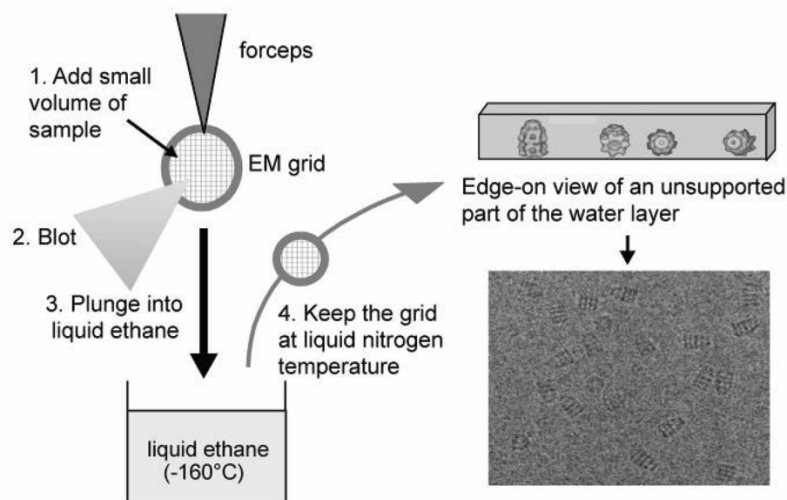


**Figure 1.14. Cryo-EM sample preparation.**

**Schematic of plunge freezing and of a vitrified layer, and an example cryo-EM image. Taken from (Orlova & Saibil, 2011)**

Once the cryo grids of a specimen of interest are prepared, transmission electron microscopy images of a large number of particles (100000-10000000) are recorded at a very low dose to minimize the radiation damage. With the introduction of “direct” electron-detection camera technology that can “count” electrons without thick scintillator layers, the electron exposure used to record high-resolution images is fractionated into 20 or more sequential subexposures, called movie frames. The improved signal-to-noise ratio (SNR) provided by this type of camera is sufficient to allow whole frames, or even small parts of whole frames, to be aligned with one another in order to produce final images. For obtaining a 3D model from the micrographs that represent projection images, the particle images extracted from these micrographs must be aligned translationally and assigned to three Euler angles (corresponding to their 3D orientations with respect to one another). Moreover, systematic

optical errors, such as spherical aberration, defocusing and astigmatism must be quantified and corrected in the final reconstruction (Agard et al., 2014).

## 1.6. Aim of this thesis

Proteolytic activity of the 20S proteasome core particle is regulated by activators that govern substrate movement into and out of the catalytic chamber. The best-known activator is the 19S RP which binds the 20S CP to form the 26S proteasome. Two other protein families in mammals, the 11S and PA200, have also been shown to bind and activate the 20S CP. However, the 19S RP and the 11S/PA200 can simultaneously bind to the same 20S CP and form a complex called hybrid proteasome. While the structure and function of the mammalian 20S core particle and 26S proteasome holoenzyme are well characterized (Unno, 2002, Haselbach, 2017), structural and functional insights into the hybrid proteasome complexes are very obscure. Thus, the aim of this thesis is to perform the analysis of hybrid proteasome complexes in order to gain insights into the structural and functional information about these proteasome complexes.

During this thesis, hybrid proteasome complexes were obtained by two approaches. The first approach was a purification of native hybrid proteasome complexes from bovine testes, and the second was a purification of induced hybrid proteasome complexes from IFN- $\gamma$  treated human rectal carcinoma (RKO) cells. Following purification, the negative stain TEM was used to verify the purity of proteasome samples and to evaluate the relative amount of hybrid proteasome complexes in the overall proteasome population after the purification. Samples that contained the highest amount of hybrid proteasome complexes were used for structural analysis by single-particle cryo-EM in order to obtain a 3D model of hybrid proteasome complexes. Furthermore, purified proteasome complexes were functionally characterized by an *in vitro* degradation assay with the polyUb substrate. The analysis of the generated pattern of peptides was performed in order to investigate the cleavage specificities of different hybrid proteasome complexes.

## 2. Materials and methods

### 2.1. Materials

#### 2.1.1. Standard chemicals

Acetic acid (*VWR Chemicals*), acetonitrile (ACN) (*Sigma Aldrich*), acrylamide (*Roth*), adenosine 5'-triphosphate disodium salt (ATP) (*Roth*), agar (*Sigma Aldrich*), ammonium persulfate (APS) (*Sigma Aldrich*), bis(2-hydroxyethyl)aminotris(hydroxymethyl)methane (BisTris) (*Sigma Aldrich*), beta-cyclodextrin (*Sigma Aldrich*), bovine serum albumin (BSA) (*Sigma Aldrich*), capzimin (kindly provided by Seth M. Cohen, Department of Chemistry and Biochemistry, University of California San Diego, La Jolla, California, USA), dimethyl sulfoxide (DMSO) (*Sigma Aldrich*), dithiothreitol (DTT) (*Sigma Aldrich*), ethanol (*VWR Chemicals*), glycerol (*Sigma Aldrich*), isopropanol (*VWR Chemicals*), kanamycin (Km) (*Sigma Aldrich*), L-glutathione reduced (GSH) (*Roth*), magnesium chloride (*Sigma Aldrich*), magnesium sulfate (*Sigma Aldrich*), MG132 (*APEX BIO*), ortho-phosphoric acid (*Merck*), phenylmethylsulfonyl fluoride (PMSF), phosphor(enol)pyruvic acid monopotassium salt (PEP) (*Sigma Aldrich*), polyethylene glycol (PEG) (*Sigma Aldrich*), potassium chloride (*Sigma Aldrich*), sodium acetate (NaOAc) (*Sigma Aldrich*), sodium chloride (*Sigma Aldrich*), sodium dodecyl sulfate (SDS) (*Sigma Aldrich*), Sterile Mono Q (*Molecular biology service*, IMP), sucrose (*Sigma Aldrich*), N,N,N',N'-tetramethylethane-1,2-diamine (TEMED) (*Sigma Aldrich*), trifluoroacetic acid (TFA) (*Sigma Aldrich*), tris-(hydroxymethyl)-amino-methane (Tris) (*Sigma Aldrich*), Tween 20 (*Sigma Aldrich*).

#### 2.1.2. Stains and reagents

Amido black (*Sigma Aldrich*), bromphenol blue (*Sigma Aldrich*), Coomassie Brilliant Blue G-250 (CBB G-250) (*Fluka*), Protein Assay Dye Reagent Concentrate 5x (Bio-Rad).

#### 2.1.3. Standards, enzymes and commercial kits

PageRuler prestained protein ladder 180 kDa (*Thermo Scientific*), PageRuler unstained protein ladder 200 kDa (*Thermo Scientific*), Precision plus protein standards 250 kDa (*BioRad*), benzonase nuclease (*Sigma Aldrich*), pyruvate kinase type III from rabbit muscle (*Sigma Aldrich*), MiniPEX kit (*Molecular biology service*, IMP), iST Sample Preparation kit (*Preomics*).

#### 2.1.4. *Escherichia coli* strains, cell lines and expression plasmids

BL21 (DE3) (B<sup>-</sup> F<sup>-</sup> ompT gal dcm lon hsdSB(rB<sup>-</sup>mB<sup>-</sup>) λ (DE3 [lacI lacUV5-T7p07 ind1 sam7 nin5]) [malB<sup>+</sup>]<sub>K-12</sub>(λ<sup>S</sup>, *Invitrogen*): strain used for the overexpression of proteins. DE3 lysogen contains T7 polymerase under the control of an inducible promoter *lacUV5*. This strain is deficient of *lon* and *omp-t* proteases and is therefore suitable for expression of non-toxic genes.

DH5α (supE44 ΔlacU169 (Φ80 lacZ) ΔM15) hsdR17 recA1 endA1 gyrA96 thi1 relA1, *Invitrogen*): strain used for the amplification of a plasmid DNA because of the deletion of the *endA1* (endonuclease I) which prevents the unspecific DNA degradation.

RKO (ATCC CRL-2577, *ATCC*®) – a poorly differentiated colon carcinoma cell line. RKO cells contain wild-type p53 but lack endogenous human thyroid receptor nuclear receptor (h-TRbeta1).

pDEST15 (*Invitrogen*) – a gateway-adapted destination vector that allows production of native, N-terminal glutathione-S-transferase (GST) tagged recombinant proteins. The vector also contains a T7 promoter for high-level, T7 RNA polymerase regulated expression of the gene of interest and two recombinant sites, *attR1* and *attR2*, downstream of the T7 promoter for recombinant cloning of the gene of interest.

#### 2.1.5. Chromatography columns and magnetic beads

GSTrap™ FF 5 mL (*GE Healthcare Life Sciences*), Superdex™ 75 16/60 (*GE Healthcare Life Sciences*), Superdex 75' Increase 3.2/300 (*GE Healthcare Life Sciences*), MagneGST™ Glutathione Particles (*Promega*), Sep-Pak C18 columns (*Waters*).

#### 2.1.6. Bacterial and cell culture media

Medium	Component
Autoinduction medium	ZY medium (10 g/L tryptone, 5 g/L yeast extract) P (25 mmol/L (NH <sub>4</sub> ) <sub>2</sub> SO <sub>4</sub> , 100 mmol/L KH <sub>2</sub> PO <sub>4</sub> , 100 mmol/L Na <sub>2</sub> HPO <sub>4</sub> )

	5052 (0.5% (v/v) glycerol, 0.05% (w/v) glucose, 0.2% (w/v) $\alpha$ -lactose) 1 mmol/L MgSO <sub>4</sub> 0.05 mg/L Km
Lysogeny broth (LB) liquid and solid medium ( <i>Molecular biology service, IMP</i> )	5 g/L yeast extract 10 g/L tryptone 10 g/L NaCl 0.05 mg/mL Km (+ 15 g/L agar for solid LB medium)
Super optimal broth (SOC) ( <i>Molecular biology service, IMP</i> )	5 g/L yeast extract 20 g/L tryptone 10 mmol/L NaCl 2.5 mmol/L KCl 10 mmol/L MgCl <sub>2</sub> 10 mmol/L MgSO <sub>4</sub> 20 mmol/L glucose.
Cell culture medium for human rectal carcinoma (RKO) cells	RPMI medium ( <i>Gibco</i> ) 1% (v/v) penicillin-streptomycin 10% (v/v) FCS 2 mmol/L L-glutamine 0.5% (v/v) nonessential amino acids 1 mol/L sodium pyruvate.

#### 2.1.7. Buffers

Buffer	Component
GSH binding buffer (GBB)	1xPBS 10 mmol/L MgCl <sub>2</sub> 1 mmol/L DTT
GST elution buffer (GEB)	1xPBS 1 mmol/L DTT 10 mmol/L GSH, pH 7.3
Size Exclusion Chromatography buffer (SECB)	25 mmol/L BisTris 50 mmol/L KCl

	5 mmol/L MgCl <sub>2</sub> 1 mmol/L DTT 10% (v/v) glycerol
10x Working buffer (10x WB)	25 mmol/L BisTris 50 mmol/L KCl 5 mmol/L MgCl <sub>2</sub>
SDS-PAGE running buffer (10x)	30% (w/v) Tris base 14.4% (w/v) glycine 1% (w/v) SDS
SDS-PAGE resolving gel	375 mmol/L Tris-HCl pH 8.8 0.1% (w/v) SDS 12% (w/v) acrylamide/bisacrylamide 37.5:1 0.05% (w/v) APS 0.1% (v/v) TEMED
SDS-PAGE stacking gel	125 mmol/L Tris-HCl pH 6.8 0.1% (w/v) SDS 4.5% (w/v) acrylamide/bisacrylamide 37.5:1 0.05% (w/v) APS 0.1% (v/v) TEMED
SDS sample buffer (5x)	250 mmol/L Tris-HCl pH 6.8 10% (w/v) SDS 50% (w/v) glycerol 0.5 mol/L DTT 0.25% (w/v) bromphenol blue
Safe Blue gel stain	8.5% (w/v) Coomassie Brilliant Blue G-250 6.6% (v/v) EtOH 4% (v/v) ortho-phosphoric acid 0.55% (w/v) beta-cyclodextrin
Destain buffer	25% (v/v) isopropanole 10% (v/v) acetic acid
Amido black solution	0.1% (w/v) amidoblack 10% (v/v) acetic acid

### 2.1.8. Software

Software	Source
Cow	<a href="https://www.cow-em.de/">https://www.cow-em.de/</a>
cryoSparc	Punjani et al., 2017
EPU	FEI
Gautomatch	<a href="http://www.mrc-lmb.cam.ac.uk/kzhang/">http://www.mrc-lmb.cam.ac.uk/kzhang/</a>
gCTF	Zhang, 2016
EMAN2	Tang et al., 2007
MotionCor2	Zheng, 2017
RELION	Zivanov, 2018
Serial EM	Mastronarde, 2005
UCSF Chimera	Pettersen et al., 2014

### 2.1.9. Equipment

ÄKTA Pure (GE Healthcare Life Sciences), BioPhotometer plus (*eppendorf*), cheesecloth (*Regency Naturals*), ChemiDoc MP Imaging System (*Bio-Rad*), DR201-95, device for measuring sucrose concentration (*KRUSS*), DS-11 FX + Spectrophotometer (*DeNovix*), EMD Milipore™ Amicon™ Ultra-0.5 Centrifugal Filter units (*Fisher Scientific*), Eppendorf™ 5424 Microcentrifuge (*eppendorf*), FEI Tecnai G<sup>2</sup> 20 (*FEI*), FEI Titan Krios (*FEI*), Gradient master 108 (*Biocomp*), HAAKE DC10, Infors HT Triple Stack Incubator (*American laboratory Trading*), Leica EM GP grid plunger (*Leica Microsystems*), magnetic stirrer (*IKA® WERKE*), miracloth (*Merck Milipore*), nitrocellulose membrane (*Amersham*), Optima XE-90 Ultracentrifuge, rotors 45Ti, 70Ti and SW60Ti (*Beckman Coulter*), PowerPac Basic Power Supply (*Bio-Rad*), Quantifoil® R 3.5/1 (*Electron Microscopy Sciences*), RCTbasic, rotating platform (*Denley*), SCD 005 Sputter Coater ver 1.4 (*Bal-Tec*), Sigma 4-16K5 centrifuge (*SciQuip*), Slide-A-Lyzer MINI Dialysis Units (*Thermo Scientific*), Sorvall LYNX 6000 centrifuge, rotors F9-6x1000 LEX, F20-12x50 LEXn (*Thermo Scientific*), Sorvall RC 12BP+ Centrifuge, rotor H -12 000 (*Thermo Scientific*), Spiramix 5, SW60 tubes (*Seton*), syringe and needle (*BBraun/BD*), waterbath (*Thermo Scientific*), Whatmann nr. 1 filter paper (*Sigma Aldrich*), ThermoMixer C (*eppendorf*), Zeba™ Spin Desalting columns, 7K MWCO, 0.5 mL (*Thermo Scientific*), 4-15% Criterion TGX Stain-free Precast gel (*Bio-Rad*), 96-(deep)-well-plate (*Biocompare*).



## 2.2. Methods

### 2.2.1. Biochemical methods

#### 2.2.1.1. Sodium dodecyl sulfate polyacrylamide gel electrophoresis (SDS-PAGE)

SDS-PAGE is an electrophoretic technique used for protein separation. In SDS-PAGE, the electrophoretic mobility of a single kind of protein is only affected by its molecular mass in the porous polyacrylamide gel. The correlation of electrophoretic mobility with a protein's molecular mass is achieved due to the use of discontinuous buffer systems where the sample and gel running buffers differ in composition (Tris-HCl/Tris-glycine) and pH (6.8/8.8) and also due to the use of detergent sodium dodecyl sulfate (SDS) and reducing agents to denature proteins. SDS binds strongly to proteins at an approximate ratio of one SDS molecule per two amino acid residues. Therefore, the negative charge/unit mass ratio when SDS is bound to the polypeptide chain is similar for all proteins.

In this thesis, SDS-PAGE was used to determine the purity of protein samples. Samples for SDS-PAGE were prepared by mixing the protein sample with appropriate volume of 5x SDS sample buffer and denatured at 95°C for 5 minutes. Subsequently, samples were loaded either onto a 4-15% precast gel (Criterion TGX Stain-free Precast gel, *Bio-Rad*) or onto a self-cast polyacrylamide gel prepared using acrylamide/bisacrylamide 37.5:1, TEMED, APS, Tris-HCl buffer and SDS. The self-cast gel has two phases: 4.5% (w/v) stacking gel and 12% (w/v) resolving gel. The stacking gel concentrates the protein molecules while the resolving gel separates the proteins on the basis of molecular mass. The markers used were PageRuler prestained protein ladder (180 kDa) for self-cast gel and PageRuler unstained protein ladder 200 kDa for precast gel. SDS running buffer (1x) was added to both anode and cathode chamber. The pre-cast gel was running at 200 V for 40 minutes and the self-cast gel was running at 180V for 75 minutes using the PowerPac Basic Power Supply (*Bio-Rad*). The gels were stained in Safe Blue gel stain on a shaker for 2 hours and destained by MiliPore water until the background was blank. After destaining, the gels were imaged in a ChemiDoc MP Imaging System (*Bio-Rad*).

#### 2.2.1.2. Detection of proteins on blot membranes by dot blot

A dot blot is a technique used to detect proteins. The protein sample is applied directly on a membrane in a single spot and the membrane can be stained with any of the general protein stains. In this thesis, a dot blot was used for the detection of a relative protein content in

fractions after density sucrose gradient ultracentrifugation. From each fraction, a 2  $\mu\text{L}$  volume was spotted on the nitrocellulose membrane (*Amersham*). The membrane was stained using the Amido black solution for 2 minutes and destained in the destaining buffer for 1 hour.

#### 2.2.1.3. Determination of protein concentration

In this thesis, two different methods were used for measuring protein concentration: the Bradford assay and absorbance at 280 nm. The Bradford assay is a colorimetric assay based on the interaction between Coomassie brilliant blue and the arginine and aromatic residues in protein molecules. When the dye binds to these residues, its maximum absorption shifts from 470 to 595 nm. Samples for the Bradford assay were prepared by mixing 1 mL of Protein Assay Dye Reagent Concentrate 1x (*Bio-Rad*) and certain volume (2 – 10  $\mu\text{l}$ ) of a sample. The absorbance of the sample was measured at 595 nm on the BioPhotometer plus (*Eppendorf*). In order to calculate the protein concentration, first, the absorbance of a series of known concentrations (2 – 16  $\mu\text{g/mL}$ ) of a protein standard, bovine serum albumin (BSA), was measured and plotted to create a standard curve. Subsequently, that standard curve was used to calculate the concentration of protein sample based on its absorbance.

The second method for measuring protein concentration, absorbance at 280 nm, is based on the fact that aromatic residues, like tyrosine and tryptophan, absorb UV light at 280 nm. If the molar extinction coefficient ( $\epsilon$  [ $\text{L mol}^{-1} \text{cm}^{-1}$ ]) for the protein of interest is known and the absorbance of a protein sample is measured in a UV/Vis spectrometer, the concentration of protein can be calculated using the Beer-Lambert's law ( $A=\epsilon lc$ ) where  $l$  is the length of the light path through cuvette. For determining the mass concentration, the absorbance ( $A_{280}$ ) for 1% (=1 g/L) protein sample was measured with DS-11 FX + Spectrophotometer (*DeNovix*) and the percent extinction coefficient ( $\epsilon^{1\%}$  [ $\text{L g}^{-1} \text{cm}^{-1}$ ]) was estimated based on the sequence using Exspasy's ProtParam tool (Gasteiger et al., 2005). The relationship between molar extinction coefficient ( $\epsilon_{\text{molar}}$ ) and percent extinction coefficient ( $\epsilon^{1\%}$ ) is  $(\epsilon_{\text{molar}})*10 = (\epsilon^{1\%}) \times (\text{molecular mass of protein})$ . Given the percent extinction coefficient, the spectrophotometer determines protein concentration (mg/mL) by using the Beer-Lambert relation.

#### 2.2.1.4. Protein/peptide identification by mass spectrometry

##### Protein identification

The aim of protein identification was to identify constitutive proteasome subunits, proteasome interacting proteins and proteasome activators that are present before and after affinity purification of proteasomes from bovine organ extracts. Protein samples for protein identification by mass spectrometry were prepared with iST Sample Preparation Kit (*Preomics*). All steps were performed at room temperature. The protocol was following: 50  $\mu$ l LYSE was added to the protein sample and placed in a heating block pre-heated at 95°C for 10 minutes in order to denature, reduce and alkylate proteins. The sample was centrifuged at 300 $\times$ g for 30 sec. The cartridge was placed in a waste tube with the adaptor. The sample was transferred to the cartridge and cooled down to room temperature. The digestion mixture was prepared by adding 210  $\mu$ l RESUSPEND protease reconstitution buffer for enzyme into the DIGEST tube that contains trypsin/lysC mix for protein digestion and incubated on a shaker at room temperature for 10 minutes at 500 rpm. Subsequently, 50  $\mu$ l of the prepared RESUSPEND+DIGEST mixture was added to the sample and the cartridge was placed in a preheated ThermoMixer C (*Eppendorf*) at 37°C for 2 hours at 500 rpm. To stop the enzymatic reaction, 100  $\mu$ l of STOP solution was added to the sample and the cartridge was incubated at 500 rpm for 1 min. The cartridge was centrifuged in a table-top microcentrifuge (5424 Microcentrifuge, *Eppendorf*) at 3 800 $\times$ g for 3 minutes. The column was washed with 200  $\mu$ l of WASH1 that removes hydrophobic contaminants from peptides followed by a wash with 200  $\mu$ l of WASH2 that removes hydrophilic contaminants from peptides. After washing, the cartridge was placed in a fresh collection tube. To elute digested protein fragments from the cartridge, 2 $\times$ 100  $\mu$ l of ELUTE was added on the cartridge and passed through by centrifuging at 3 800 $\times$ g for 3 minutes. The sample was completely dried in Speed-Vac at 45°C and then dissolved in LC-LOAD solution so that final peptide concentration is 1 g/L.

##### Peptide fragment identification

For the peptide fragment identification after *in vitro* degradation by proteasome complexes, the silica-based, reverse-phase Sep-Pak C18 columns (Waters) were used for the purification of peptide fragments. Before applying the sample, the columns were equilibrated with 3  $\times$  0.5 mL methanol, 3  $\times$  0.5 mL 70% acetonitrile (ACN) in 0.1% (w/v) trifluoroacetic acid (TFA) and 3  $\times$  0.5 mL 0.1% (w/v) TFA. Prior to sample loading, samples were acidified with 10  $\mu$ l 10% (w/v) TFA. Once the whole sample volume passed through, the columns were

washed  $6 \times 0.5$  mL 0.1% (w/v) TFA. Peptide fragments were eluted from the columns in two steps: in the first step with  $3 \times 150$   $\mu$ L 30% (v/v) ACN in 0.1% (w/v) TFA and in the second step with  $3 \times 150$   $\mu$ L 40% (v/v) ACN in 0.1% (w/v) TFA or with  $3 \times 150$   $\mu$ L 50% (v/v) ACN in 0.1% (w/v) TFA and in the second step with  $3 \times 150$   $\mu$ L 70% (v/v) ACN in 0.1% (w/v) TFA. Elutions with the same percentage of ACN were collected in the same tube, samples were dried in Speed-Vac at 45°C and dissolved in the buffer for LC-MS analysis.

Subsequent mass spectrometry experiments and data analysis were done in collaboration with Karl Mechtler lab (*Protein Chemistry facility, IMBA, Vienna Austria*)

#### 2.2.1.5. Purification of GST-UBL

##### Chemical transformation of *E. coli* DH5 $\alpha$ and Mini Prep

The plasmid vector (pDEST15-UBL-hHR23B-GST) for the overexpression of glutathione-S-transferase (GST) - tagged ubiquitin-like domain of a human RAD23B (GST-UBL) was provided from Besche & Goldberg (2012). In order to prepare a larger amount of GST-UBL encoding plasmid vector, 50  $\mu$ L of *E. coli* cells (strain DH5 $\alpha$ ) was mixed with 1  $\mu$ L plasmid vector and incubated on ice for 30 minutes. Cells were transformed by heat-shock for 1 minute at 42°C and 800 rpm followed by immediate transfer of cells back on the ice. Subsequently, 250  $\mu$ L of the SOC medium was added and cells were incubated at 37°C and 1600 rpm for 1 hour after which 100  $\mu$ L of the cell suspension was spread on the agar plate (LB solid medium, *Molecular biology service, IMP*). Cells were grown on the plate overnight at 37°C. Grown colonies were inoculated in two 5 mL LB liquid media (*Molecular biology service, IMP*) containing 0.05 mg/mL Km. Cells were grown overnight at 37°C and 300 rpm.

Plasmid Mini-Prep was prepared using the MiniPex 3 in 1 kit (*Molecular biology service, IMP*). Ten mL of overnight cell culture was centrifuged at  $3\ 877\times g$  and 4°C for 10 minutes to pellet the cells (Sigma 4-16K5 centrifuge, *SciQuip*). The supernatant was discarded and the pellet was resuspended in 250  $\mu$ L of Buffer R1 and transferred to the 1.5 mL microcentrifuge tube (*Eppendorf*). For the cell lysis, 250  $\mu$ L of Buffer L2 was added and the tube was inverted 6 times until the solution became clear. To stop the lysis reaction, 350  $\mu$ L Buffer N3 was added and the tube was immediately inverted 6 times to mix the solution. The lysed cell solution was centrifuged at  $21\ 130\times g$  and 4°C for 10 minutes in a table-top microcentrifuge (5424 Microcentrifuge, *Eppendorf*). The supernatant that contains the plasmid DNA was transferred to the spin column provided in the kit followed by centrifugation at

21 130×g and 4°C for 60 seconds. The flowthrough was discarded and 0.75 mL of Buffer W was added on the spin column and centrifuged at 21 130×g and 4°C for 60 seconds. The flowthrough was discarded and the column centrifuged at 21 130×g and 4°C for 60 seconds to remove residual wash buffer. The spin column was transferred in the clean 1.5 mL microcentrifuge tube. To elute bound plasmid DNA from the column, 30 µL of Sterile MonoQ (*Molecular biology service, IMP*) was added on the center of the spin column, incubated for 1 minute and centrifuged at 21 130×g and 4°C for 60 seconds. The concentration of the plasmid vector was measured with DS-11 FX + Spectrophotometer (*DeNovix*).

#### Chemical transformation of *E. coli* BL21 (DE3) and protein overexpression

For the overexpression of GST-UBL, 50 µL of *E. coli* cells (strain BL21 (DE3)) was mixed with 1 µL of the plasmid vector and incubated on ice for 30 minutes. Cells were transformed by heat-shock for 1 minute at 42°C and 800 rpm followed by immediate transfer of cells back on the ice. Subsequently, 250 µL of SOC medium was added and cells were incubated at 1600 rpm and 37°C for 1 hour after which 100 µL of the cell suspension was spread on the agar plate (LB solid medium, *Molecular biology service, IMP*). Cells were grown on the plate overnight at 37°C. Grown colonies were inoculated in 25 mL of LB liquid media (*Molecular biology service, IMP*) containing 0.05 mg/mL Km. Cells were grown overnight at 300 rpm and 37°C. The overnight culture was inoculated in 4 L of autoinduction media and cells were incubated at 180 rpm and 37°C for 5 hours after which the temperature was decreased to 18°C and cells were incubated in a shaker overnight. The cell culture was centrifuged at 4 000 rpm and 4°C for 15 minutes (Sorvall RC 12BP+ Centrifuge, rotor H -12 000 (*Thermo Scientific*)). The supernatant was discarded and the pellet (45 mL) that contains cells with overexpressed GST-UBL was resuspended in 150 mL of GSH binding buffer (GBB) plus 30 µl benzonase. Cells were lysed with the French press by applying 1.4 kbar pressure. The cell lysate was centrifuged at 15 000×g and 4°C for 35 minutes. The supernatant was collected.

#### Affinity chromatography and size exclusion chromatography

Purification of the GST-UBL was performed using the fast protein liquid chromatography in two steps: the affinity chromatography on a GSTrap™ FF 5 mL (*GE Healthcare Life Sciences*) and size exclusion chromatography on a Superdex™ 75 16/60 (*GE Healthcare Life Sciences*).

Affinity chromatography makes use of specific binding interactions between molecules. A particular ligand is chemically immobilized or “coupled” to a solid support so that when a complex mixture is passed over the column, those molecules having a specific binding affinity to the ligand become bound. After other sample components are washed away, the bound molecule is stripped from the support. For the purification of GST-UBL by affinity chromatography, a 5 mL GSTrap™ FF column was equilibrated with 5 column volumes (CVs) of GSH binding buffer (GBB) and the supernatant containing soluble GST-UBL was loaded on the column at 0.5 mL/min flow rate. The column was washed with 20 CV of GBB at 0.5 mL/min flow rate. Bound GST-UBL was eluted from the column with a gradient of 0-10 mmol/L reduced GSH in GST elution buffer (GEB). The eluate was collected with a fraction collector with fraction volume of 1.5 mL. For each fraction, a UV/Vis spectrum was recorded. Fractions showing a peak at UV280 contained the protein of interest and those fractions were collected, pooled together and analyzed by SDS-PAGE. Pooled fractions were concentrated using the EMD Millipore™ Amicon™ Ultra-0.5 Centrifugal Filter units (*Fisher Scientific*) at 4 800×g and 4°C (Sigma 4-16K5 centrifuge, *SciQuip*) to the final volume of 5 mL.

Second purification step was the size exclusion chromatography (SEC) that separates molecules on the basis of differences in size as they pass through a SEC medium packed in a column. SEC media consists of spherical particles with pores of different sizes where molecules small enough to enter the pores are retarded as compared to larger molecules. In the SEC, samples are eluted isocratically (single buffer, no gradient). In this thesis, a 120 mL Superdex™ 75 16/600 column was used to separate the GST-UBL from the glutathione used in the previous purification step. The SEC purification step was necessary because glutathione would interfere with the further use of the GST-UBL as a bait protein. The column was equilibrated with 2 CVs of Size Exclusion Chromatography buffer (SECB). The concentrated sample from a GSTrap™ FF column was loaded on the Superdex™ 75 column at 0.5 mL/min flow rate. The sample was run through the column with 1 CV of SECB at 0.5 mL/min flow rate. For each fraction, a UV/Vis spectrum was recorded. Fractions showing a peak at UV280 contained the protein of interest and those fractions were collected and pooled together. The protein concentration was measured with DS-11 FX + Spectrophotometer (*DeNovix*).

#### 2.2.1.6. Purification of proteasome complexes

Bovine organs were mechanically homogenized in 1× working buffer (WB) with freshly added 10% (v/v) glycerol, 4 mmol/L ATP, 1 mmol/L DTT, 0.1% (v/v) Tween20 and 0.1 mmol/L PMSF. The crude cell extract was centrifuged at 16 000×g and 4°C for 30 minutes

to remove remaining tissue pieces (Sorvall LYNX 6000 centrifuge, F20-12x50 LEXn rotor, *Thermo Scientific*). The supernatant was filtered through a miracloth and ultracentrifuged at 100 000×g and 4°C for 1 hour (Optima XE-90 Ultracentrifuge, 45Ti rotor, *Beckman Coulter*) to remove cellular organelles, membrane fragments, and ribosomes. After ultracentrifugation, the supernatant was filtered once more through miracloth. The extract was additionally clarified using a two-step PEG precipitation from 4% to 20% PEG with 50% PEG 8 000. PEG was slowly added to the final concentration of 4% while stirring on the magnetic stirrer. After 15 minutes incubation, the extract was centrifuged at 16 000×g and 4°C for 15 minutes (Sorvall LYNX 6000 centrifuge, F9-6x1000 LEX rotor, *Thermo Scientific*). The supernatant was again transferred in a beaker and 50% PEG 8 000 was slowly added to the final concentration of 20% while stirring on the magnetic stirrer. After 15 minutes incubation, the extract was centrifuged at 12 000×g and 4°C for 15 minutes (Sorvall LYNX 6000 centrifuge, F9-6x1000 LEX rotor, *Thermo Scientific*). The supernatant was removed, and the pellet was dissolved in 1×WB plus freshly added 10% (v/v) glycerol, 4 mmol/L ATP and 1 mmol/L DTT.

RKO cells were lysed in the same buffer as bovine organs by freezing and thawing followed by additional cell disruption by douncing. The crude cell extract was ultracentrifuged at 100 000×g and 4°C for 1 hour (Optima XE-90 Ultracentrifuge, 70Ti rotor, *Beckman Coulter*) to remove cellular organelles, membrane fragments, and ribosomes. After the ultracentrifugation, the supernatant (cell extract) was clear enough and a two-step PEG precipitation wasn't necessary. The cell extracts from RKO cells were prepared from two batches of RKO cells where one batch (~10<sup>8</sup> cells) was treated with IFN- $\gamma$  (500 U/mL, 72 h) and the other batch (~10<sup>8</sup> cells) was untreated (control) (kindly provided from Gijs Versteeg Lab, *MFPL, Vienna Austria*). The IFN- $\gamma$  treatment was used in order to induce the formation of hybrid proteasome complexes that contain the PA28 $\alpha\beta$  and proteasomes from untreated cells were necessary as a control for the effect of IFN- $\gamma$  treatment in terms of the relative amount of PA28 $\alpha\beta$  and  $\beta$ i immunoproteasome subunits and their effect on the proteolytic activity of purified proteasome complexes.

In this thesis, the purification of proteasome complexes was done by a single-step affinity purification described in Besche & Goldberg (2012). This purification approach uses the ubiquitin-like domain of a human RAD23B as an affinity bait, which allows rapid and gentle isolation of proteasomes. A large amount of recombinant GST-tagged UBL and the corresponding amount of GSH coated magnetic beads (1 mL of settled particles for 10 mg of the bait protein) were added to cell extracts prepared from bovine organs and RKO cells. Purified bait protein, the GST-UBL, serves as a middle binder between the Rpn10 subunit of

the 19S RP and glutathione covered magnetic beads. Extracts were incubated overnight on the rotating platform at 4°C to allow binding of the GST to the magnetic beads and UBL to the Rpn10 subunit. The following day, magnetic beads with bound proteasome complexes were captured with a magnet and the supernatant (flowthrough) was collected. Beads were washed with 1×WB with freshly added 10% (v/v) glycerol, 4 mmol/L ATP, 1 mmol/L DTT until the supernatant (wash) became clean. After the final wash, proteasome complexes were eluted corresponding to two CVs of particles with 25 mmol/L reduced L-glutathione (GSH) prepared in 1×WB with freshly added 10% (v/v) glycerol, 4 mmol/L ATP and 1 mmol/L DTT, pH 6.5 at 12°C, for 10 minutes at 300 rpm. The flowthrough, the wash and elution fractions were analyzed by SDS-PAGE in order to establish the amount and purity of purified proteasome complexes. The elution fractions containing proteasome complexes were combined and the protein content was concentrated using the EMD Millipore™ Amicon™ Ultra-0.5 Centrifugal Filter units (*Fisher Scientific*) at 4 800×g and 4°C (Sigma 4-16K5 centrifuge, *SciQuip*) to the final volume of 200 µL – 800 µL. The final volume depended on the amount of purified proteasome complexes that was detected by SDS-PAGE.

Subsequently, the concentrated protein sample was subjected to a sucrose density gradient ultracentrifugation to remove the excess of the GST-UBL. A 10-30% (w/v) sucrose gradient in the 1×WB with freshly added 4 mmol/L ATP and 1 mmol/L DTT was prepared in the SW60 tubes (*Seton*) using the Gradient master 108 (*Biocomp*). The top 200 µL from the top of the total volume of 4.2 mL were substituted by the same amount of the sample. Eventually, the gradient tubes were centrifuged at 100 000×g and 4°C for 16 hours (Optima XE-90 Ultracentrifuge, SW60Ti rotor, *Beckman Coulter*). During sucrose density gradient ultracentrifugation different proteins and protein complexes travel through the gradient until they reach the point in the gradient at which their density matches that of the surrounding sucrose. The gradients were manually fractionated into 200 µL portions in the 96-(deep)-well-plate (*Biocompare*). The individual gradient fractions were analyzed by *dot blot* on the nitrocellulose membrane to visualize their relative protein content.

The fractions containing proteasome complexes were buffer exchanged to the 1×WB plus 4 mmol/L ATP and 1 mmol/L DTT without any sucrose using a Zeba™ Spin Desalting columns, 7K MWCO, 0.5 mL (*Thermo Scientific*). The storage buffer was removed by centrifugation at 1 500×g and 4°C for 1 minute. Columns were equilibrated in 4×300 µL of 1×WB plus 4 mmol/L ATP and 1 mmol/L DTT by centrifugation at 1 500×g and 4°C for 1 minute. Columns were placed in a clean 1.5 mL collection tube, the sample (100 µL) was



added on the top of the column and passed through by centrifugation at 1 500×g and 4°C for 2 minutes.

#### 2.2.1.7. Preparation of proteasome substrates

##### Ubiquitination reaction

In order to be recognized and degraded by the 26S proteasome, a protein substrate has to be post-translationally modified by polyUb chains. The formation of ubiquitin chains is carried out by an enzymatic cascade. It is initiated by the generation of a thioester between the carboxyl terminus of ubiquitin and a cysteine in the ubiquitin-activating enzymes (E1). This ubiquitin is transferred to the active site of ubiquitin-conjugating enzymes (E2), which delivers it to ubiquitin ligases (E3) (Jin, 2008). A RING-E3s simultaneously bind to E2s and substrate and facilitate ubiquitin transfer directly from the E2. Subsequent ubiquitin molecules are linked to the lysine residue at position 11 (K11), 48 (K48) and/or 63 (K63) in substrate-bound ubiquitin (Jin, 2008). One example of RING-E3 ligase is the anaphase-promoting complex/cyclosome (APC/C) that forms ubiquitin chains in order to trigger protein degradation to control cell-cycle progression, quiescence, and differentiation. The APC/C can assemble K11, K48 and K63- ubiquitin chains on substrates, rapidly and with high processivity (Brown, 2016). One of the APC/C substrates is a regulatory protein securin. Securin is an inhibitor of anaphase because it prevents the proteolysis of the cohesin complex by separase and the subsequent segregation of the chromosome. At the onset of anaphase, it is ubiquitinated and degraded by the 26S proteasome (Hagting et al., 2002). Securin can be ubiquitinated *in vitro* by (APC/C) (Hagting et al., 2002). The APC/C has two E2 partners, UBE2C and UBE2S that catalyze the polyubiquitination of securin with ubiquitin activated by the Uba1 E1 enzyme (Brown, 2016).

To be able to test the ATP- and ubiquitin-dependent degradation activity of proteasome complexes, the fluorescently labeled polyUb securin was generated in a multistep ubiquitination reaction catalyzed by four distinct enzymes: the Uba1, the UBE2C, the UBE2S and the APC/C in the presence of certain cofactors (**Table 2.1**). For this type of reaction, it was important to have a large excess (at least 10x) of ubiquitin over the substrate. The polyubiquitylation reaction was performed at room temperature for 1.5 hours and the reaction was stopped with 50 mmol/L DTT. The effectiveness of the formation of polyUb chains was inspected by SDS-PAGE.

**Table 2.1. Reaction components for the preparation of polyUb proteasome substrate. All components used in this assay were kindly provided by Nicholas Gene Brown, UNC School of Medicine, North Carolina, USA.**

Component	Concentration	Role
Uba1 (E1)	1 $\mu$ mol/L	Ubiquitin activation
Ubch10 (E2)	1 $\mu$ mol/L	Ubiquitin-conjugation
UBE2S (E2)	1 $\mu$ mol/L	Ubiquitin-conjugation
APC/C (E3)	100 nmol/L	Ubiquitin ligation
CDH1	1 $\mu$ mol/L	APC/C coactivator
Ubiquitin	120 $\mu$ mol/L	Signal for proteasome degradation
ATP-MgCl <sub>2</sub>	5 mmol/L	Cofactor for the E1, E2 and E3
Securin	10.2 $\mu$ mol/L	Fluorescein labeled substrate protein
HEPES, NaCl	20 mmol/L, 200 mmol/L	Buffer

#### Purification of the polyUb substrate by SEC

In order to separate the polyUb substrate from the rest of the components used in the ubiquitination reaction, the reaction was acidified with 50 mmol/L NaOAc, pH 4.3. This step that separates the polyUb substrate from other components, mainly the APC/C E3 ligase, is necessary because they would probably interfere with *in vitro* substrate degradation by the proteasome. While ubiquitin is tolerant to extreme pH changes and maintains its native structure allowing the solubility of the polyUb substrate after the acidification, other components in the reaction are denatured and form aggregates. The reaction was incubated 20 minutes on ice and centrifuged at 21 130 $\times$ g and 4°C for 15 minutes. After centrifugation, only the polyUb substrate and if any remained free ubiquitin were in the soluble fraction while other reaction components were pelleted to the bottom of a microcentrifuge tube. The supernatant that contained the soluble proteasome substrate was applied on a Superdex 75' Increase 3.2/300 (*GE Healthcare Life Sciences*) equilibrated with 1 CV (2.4 mL) of SECB. The sample was run through the column with 1 CV of SECB at 0.035 mL/min flow rate and 100  $\mu$ L fractions were collected. Collected fractions were analyzed by SDS-PAGE and imaging of the fluorescein fluorescence on a ChemiDoc MP Imaging System (*Bio-Rad*). Fractions that contained fluorescent signal were pooled, protein concentration was measured using the absorbance at 280 nm using the DS-11 FX + Spectrophotometer (*DeNovix*) and, accordingly, the sample was concentrated to a final protein concentration of 0.6 mg/mL. The concentrated protein sample was dialyzed overnight in 500 mL 1 $\times$ WB plus 10% (v/v) glycerol using the Slide-A-Lyzer MINI Dialysis Units (*Thermo Scientific*) at 4°C on a magnetic stirrer.

#### 2.2.1.8. *In vitro* degradation assay

##### Activity assay

The degradation activity of purified proteasome complexes was tested using an *in vitro* degradation assay with a fluorescein-labeled polyUb substrate. To maintain the ATP-dependent activity of the proteasome, an ATP-regenerating system was used in the reaction. Following each cycle of ATP hydrolysis, the regeneration system consisting of phosphoenolpyruvate (PEP) and pyruvate kinase converts one molecule of PEP to pyruvate when the ADP is converted back to the ATP.

Purified proteasomes (0.2  $\mu\text{mol/L}$ ) were mixed with the substrate (20  $\mu\text{mol/L}$ ), pyruvate kinase (37 U/mL), PEP (2 mmol/L), ATP (4 mmol/L) and DTT (1 mmol/L) in 1 $\times$ WB plus 10% (v/v) glycerol. The final volume of the reaction was 150  $\mu\text{L}$ . The assay was performed at 37°C and 300 rpm for 24 h. 16  $\mu\text{L}$  aliquots were taken at several time points: 0, 1, 2, 3, 4, 5 and 24 hours. The reaction was quenched with 4  $\mu\text{L}$  of 5x SDS sample buffer. The quenched aliquots were analyzed by SDS-PAGE and imaging of fluorescence on ChemiDoc MP Imaging System (*Bio-Rad*). The loss of the fluorescence was indicator of substrate degradation.

##### *In vitro* degradation assay for analysis of peptides generated during proteasomal degradation

For analysis of peptides generated during proteasomal degradation, two different experimental setups were used. One was identical to the experimental setup for the activity assay described in the previous section but without the aliquoting. The second was an *in vitro* degradation assay similar to described activity assay but without pyruvate kinase and PEP because the reaction was performed for only 2 hours at 37°C and 300 rpm.

Since several publications indicate that the formation of the hybrid complex might affect either the peptide pattern, promote the generation of certain peptides or alter the mean size or the number of peptides generated by the 26S proteasome (Casio & Goldberg, 2005, Hendil et al., 1998, Raule et al., 2014), a 2-hour *in vitro* degradation assay without pyruvate kinase and PEP and with polyUb securin was performed with the 26S proteasome in the presence or absence of 11S regulators. For this analysis, proteasomes purified from bovine heart were used since in bovine heart none of the 11S isoforms were found to be expressed (**Table S1**). The recombinant PA28 $\alpha\beta$  and PA28 $\gamma$  proteasome activator complexes used in this analysis were purified and provided by Irina Grishkovskaya (Haselbach group, *IMP, Vienna Austria*). Three reactions were performed: reaction containing only 26S proteasomes, 26S proteasomes and PA28 $\alpha\beta$  or 26S proteasomes and PA28 $\gamma$ . The 11S regulators were added in 10x molar excess over the 26S proteasomes and incubated 30 minutes prior to the addition of

substrate. The conditions of *in vitro* degradation assay (e.g. a large excess of protein substrate) ensured that different peptide products are generated at similar linear rates and are not cleaved further again by the 26S proteasomes after their release from the 20S CP. Importantly, since polyUb substrate was used, the degradation was performed only by the proteasome complexes containing 19S RP – the 26S proteasome or the *in vitro* reconstituted hybrid proteasome (19S-20S-PA28 $\alpha\beta$  or 19S-20S-PA28 $\gamma$ ) because the 11S regulators bound to free 20S (11S-20S or 11S-20S-11S) are not involved in the ATP- and ubiquitin-dependent degradation.

## 2.2.2. Single-particle sample preparation

### 2.2.2.1. Negative stain grid preparation

To validate sample quality and quantity, or to record micrographs of negative stained hybrid proteasome complexes, the samples were stained with 0.75% (w/v) uranyl acetate (Booth, 2011). Carbon-coated grids were glow-discharged using SCD 005 Sputter Coater (*Bal-Tec*) for 60 seconds at ~20 mA on a glass slide. 4  $\mu$ L of the proteasome sample was applied on the glow-discharged grid and incubated for 1 minute. The sample was blotted off using a filter paper. The grid was washed three times by gentle placing of the grid surface on a water drop and then blot off the water using a filter paper. 4  $\mu$ L of the 0.75% uranyl acetate (stain) was applied on the grid with adsorbed sample and incubated for 1 minute. The stain was blotted off using a filter paper. The grids were air-dried before micrograph recording.

### 2.2.2.2. Cryo grid preparation

For the structural analysis of hybrid proteasome complexes by cryo-EM, fractions from a sucrose gradient that, according to negative stain micrographs, contained the majority of hybrid proteasome complexes were used for the preparation of cryo grids. The particles were adsorbed on a continuous carbon film attached to a Quantifoil R3.5/1 grid glow-discharged for 60 seconds at ~20 mA using SCD 005 Sputter Coater (*Bal-Tec*). 4  $\mu$ L of ddH<sub>2</sub>O was added on the grid and sample was blotted for 2 seconds with a Whatman No. 1 filter paper in a chamber precooled at 4°C and with 80% humidity. Grids were plunge-frozen in liquid ethane using a Leica EM GP grid plunger (*Leica Microsystems*).

### 2.2.3. Single-particle electron microscopy

#### 2.2.3.1. Image acquisition

For negative stain image acquisition, an FEI Tecnai G<sup>2</sup> 20 (*FEI*) electron microscope was used at an acceleration voltage of 200 kV. This microscope has an Eagle 4k HS camera, a LaB<sub>6</sub> filament emitter as an electron source and a dual-axis tomography holder that enables tilting of samples. Images were taken at a magnification of 62k $\times$  (1.85 Å/pixel).

All cryo-EM data were acquired using an FEI Titan Krios (*FEI*) cryo-electron microscope at Max Planck Institute for Biophysical Chemistry, Göttingen, Germany. The microscope was operated at an acceleration voltage of 300 kV. Images were taken with an FEI Falcon III direct electron detector with a nominal magnification of 75k $\times$  (1.1 Å/pixel). The total dose of 45 electrons per Å<sup>2</sup> was fractionated on 20 frames to obtain “movies” of specimens.

#### 2.2.3.2. 2D image processing

##### Image preprocessing and sorting

Due to low exposure (2.25 electrons per Å<sup>2</sup>), the acquired individual movie frames have low signal-to-noise (SNR) ratio. Moreover, because of the accumulation of radiation damage, most of the high-resolution information is present in the first few frames while the last few frames contain mostly the low-resolution information. In addition, two effects, beam-induced motion of specimens and charging of the surface of vitrified ice after exposure to the electron beam lead to the blurring of an image. Those effects can be corrected by registering identical features in the single frames, followed by summing the registered frames to produce a motion-corrected image. In order to extract information from images of single particles and reduce the effects of drift and charging, the raw movie frames were aligned and weighted using the software MotionCor2 (Zheng, 2017).

The cryo-EM image of a vitrified specimen is also modulated by contrast transfer function (CTF) that mathematically describes the physical processes in a transmission electron microscope. The CTF can be described by equation (1), with wavelength  $\lambda$ , defocus  $\Delta z$ , spherical aberration coefficient  $C_s$ , and spatial frequency  $f$  (Wade, 1992). The significant factors that affect the CTF of cryo-EM image formation are the defocus and aberrations of the lens. Original information of the images must be corrected using accurate CTF parameters in order to obtain a reliable 3D reconstruction. The CTF parameters of aligned, unweighted micrographs were estimated using the software Gctf (Zhang, 2016). One of the outputs of Gctf

contains a STAR file which contains all the determined CTF parameters that can be directly used for further 2D or 3D processing.

$$CTF = -2 \cdot \sin \left[ \pi \left( \Delta z \cdot \lambda \cdot f^2 - \frac{c_s \cdot \lambda^3 \cdot f^4}{2} \right) \right] \quad (1)$$

After image preprocessing with MotionCor2 and Gctf, a micrograph sorting was performed using the software Cow Micrograph Quality Checker. In this step, micrographs that contained broken or dry ice, were contaminated, blurred or empty - were discarded.

### Particle picking and 2D classification

2D image processing was performed using the software RELION ver. 3.0 (Zivanov, 2018) and CryoSPARC ver. 0.6.5 (Punjani et al., 2017). RELION (for REgularised Likelihood Optimisation) employs an empirical Bayesian approach to refinement of (multiple) 3D reconstructions or 2D class averages in cryo-EM. In the corresponding Bayesian framework, many parameters of a statistical model are estimated from the data, which leads to objective and high-quality results (Scheres, 2012). CryoSPARC (cryo-EM single-particle *ab initio* reconstruction and classification) combines two algorithms: the stochastic gradient descent (SGD) for *ab initio* reconstruction of protein structure by random initialization from a set of particles, without any initial models or starting structures and second, the branch-and-bound maximum likelihood optimization algorithm for refinement of 3D maps to high resolution (Punjani et al., 2017).

Manual particle picking, particle extraction, and reference-free 2D classification were performed in RELION to generate 2D class averages that were used as templates for the automatic particle picking in the software Gautomatch. Results of the automatic particle picking were inspected in RELION and once the picking was optimized (almost every particle in the micrograph was picked and particles were centered) particles were extracted from the micrographs. The following reference-free 2D classification of extracted particles was performed using CryoSPARC to facilitate stack cleaning and removal of junk particles. The resulting 2D class averages were visually inspected and particles belonging to class averages that clearly showed ice contamination, charging, drift or false-positive images (such as carbon edges) or that did not show clear particle views were discarded.

#### 2.2.3.3. 3D processing

Particles belonging to best class averages were used to generate an initial 3D model using the *ab-initio* reconstruction in CryoSPARC. Once obtained, the initial 3D model was refined using the homogenous refinement in CryoSPARC to eliminate the false structural features and to improve the resolution. The initial 3D model was used as a reference in a 3D classification and 3D refinement in RELION. The generated 3D class averages were visually inspected using the software UCSF Chimera (Pettersen et al., 2014).

For separation of particles that contain or don't contain PA28 or PA200 on the free end of the 26S proteasome, a mask (hybrid mask) was created using the software CowEyes and RELION for 3D volume on the side of the 26S proteasome where PA28 or PA200 should be to form the hybrid proteasome. The hybrid mask focuses the 3D classification on that part of the complex. After separation, 3D class averages representing hybrid proteasome complexes, were combined and particles belonging to those 3D class averages were subjected to two more rounds of 3D refinement: in the first refinement the same reference and hybrid mask as in the previous refinement were used and the second and final refinement was performed using the result 3D model from latest refinement as a reference and a new mask for the whole complex created in RELION to yield the final structure.

The resolution of the final structures was estimated using a method called Fourier shell correlation (FSC). The 3D FSC was introduced by Harauz & van Heel (1986). It measures the normalized cross-correlation coefficient between two independently refined 3D volumes obtained from subsets of the dataset over corresponding shells in Fourier space, i.e., as a function of spatial frequency. Finally, a threshold of 0.143, which represents a signal-to-noise ratio of 1, is used to determine the resolution.

## 3. Results

### 3.1. Purification of the bait protein GST-UBL

For the affinity purification of proteasome complexes, the bait protein, GST-UBL, which contains the glutathione-S-transferase (GST)-tagged UBL domain from a human Rad23B, which binds the Rpn10 subunit of the 19S RP, had to be purified. The purification protocol for the bait protein was adapted from Besche & Goldberg (2012). The first purification step was the affinity purification on a glutathione sepharose resin (**Figure 3.1**).

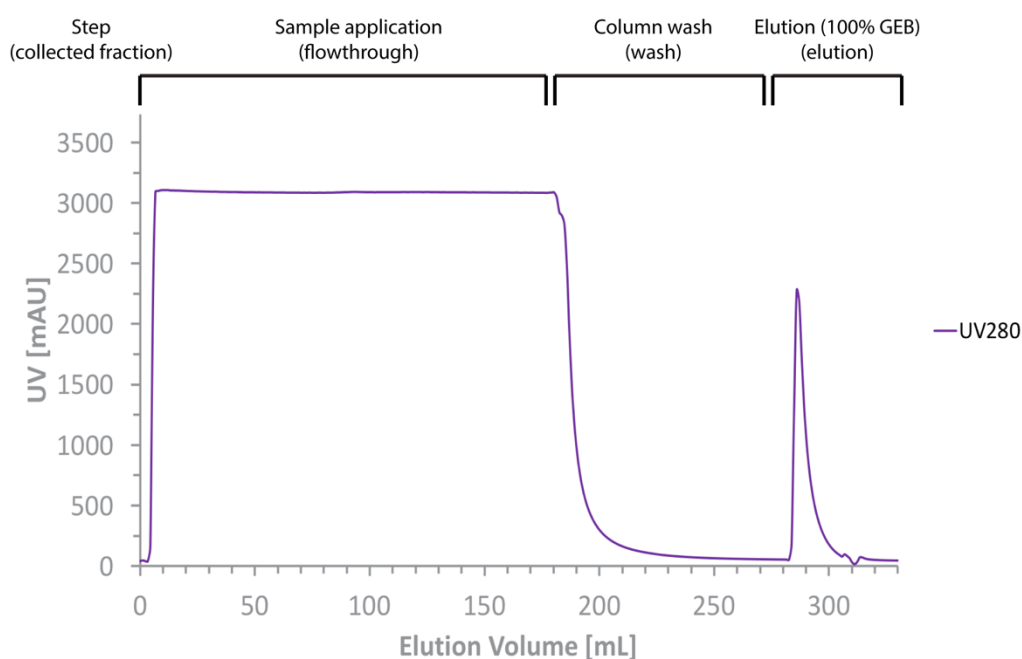


**Figure 3.1.** Affinity chromatography FPLC chromatogram of the GST-UBL.

The sample application, column wash and elution of the GST-UBL with a gradient of 0-10 mmol/L reduced GSH were monitored via absorbance at 280 nm; the peak at UV280 during the elution shows GST-UBL that was eluted from the column. GEB – GST elution buffer.

Collected fractions from the GST-UBL affinity purification were analyzed via SDS-PAGE (**Figure 3.2**). The protein band visualized at ~38 kDa represents overexpressed GST-UBL.



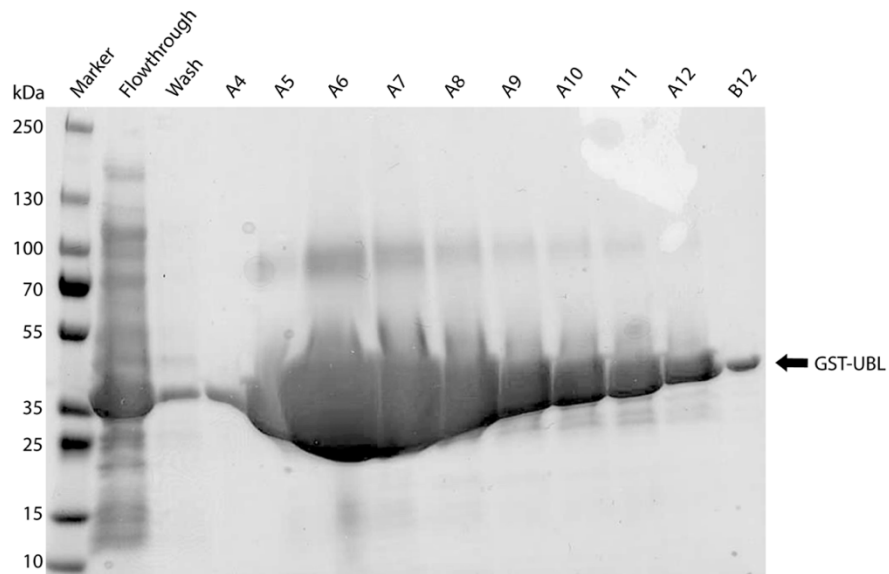


**Figure 3.2. Analysis of GST-UBL via SDS-PAGE.**

**Marker – Precision Plus protein ladder 250 kDa, A4-A12 and B12 – elution fractions corresponding to the peak at UV280. On the right the expected band of GST-UBL is marked; the molecular mass of GST-UBL is ~38 kDa.**

The second purification step for GST-UBL was the size exclusion chromatography (**Figure 3.3**). Following SEC, the fractions that contained GST-UBL were concentrated and measured protein concentration was 4.6 mg/mL ( $\epsilon^{1\%}(\text{GST-UBL}) = 13.2$ ). On average, an amount of approximately 60 mg could be obtained from only 4 L of cell culture.

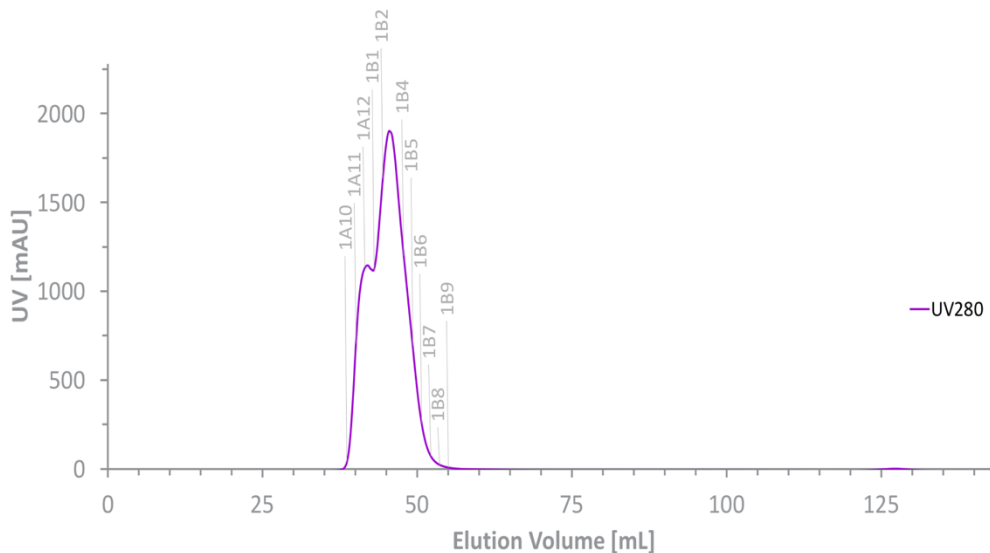


**Figure 3.3. Size exclusion chromatography FPLC chromatogram of the GST-UBL.**

**Fractions showing absorbance at 280 nm (A10-A12 and B1-B7) contain the GST-UBL that is separated from the GSH which ran out of the column at the elution volume of 125-130 mL.**

### 3.2. Affinity purification of proteasome complexes from bovine organs and RKO cells.

Six different bovine organs, pancreas, testes, heart, brain, spleen and liver, were used as source materials to obtain mammalian proteasome complexes in order to identify organs in which the 11S and PA200 proteasome activators are expressed. Fractions collected during a single-step affinity purification of proteasome complexes by using the bait protein GST-UBL were analyzed via SDS-PAGE (**Figure 3.4**) to confirm the presence of all proteasome subunits: the 20S CP subunits and the 19S RP subunits. The efficiency of affinity purifications was comparable among different bovine organs except the spleen where the efficiency of affinity purification was a notably lower and the amount of purified proteasome complexes was lower in comparison with other organs from the same amount of extract.

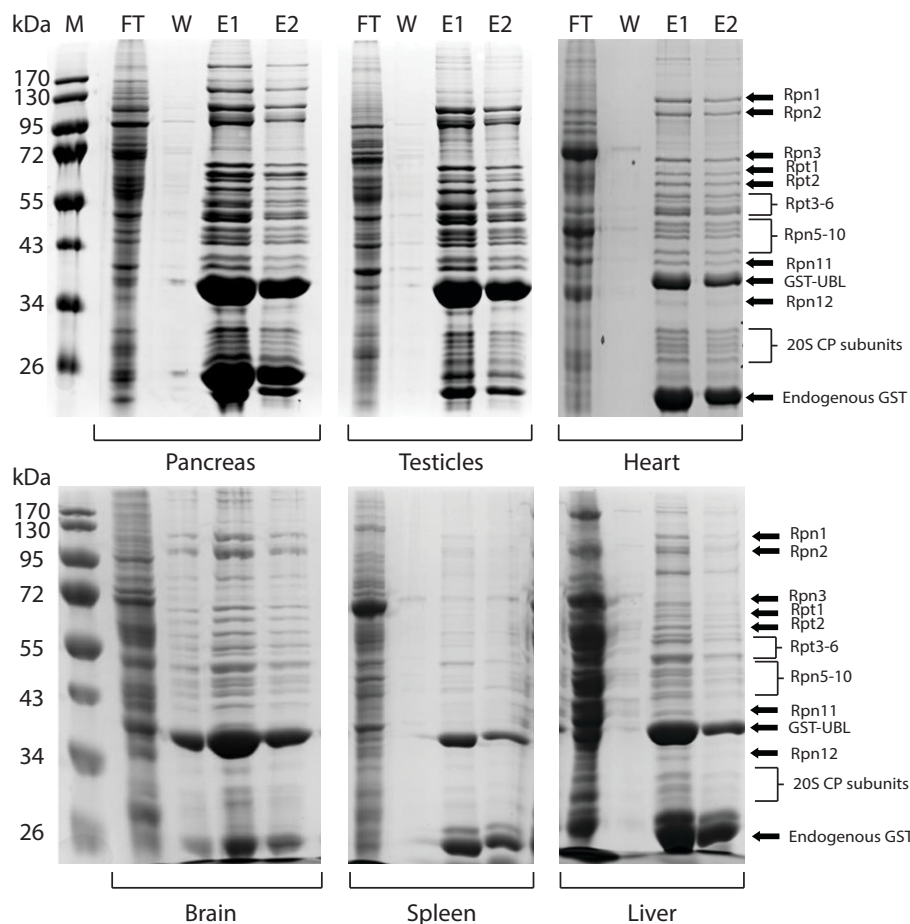


**Figure 3.4. SDS-PAGE analysis of affinity purification of proteasome complexes from different bovine organs.**

**M – marker, PageRuler prestained protein ladder 180 kDa; F – flowthrough, W – wash, E1 and E2 – two separate elution fractions. On the right the bands corresponding to individual subunits of the 26S proteasome and band corresponding to the bait protein GST-UBL are marked. A small amount of the endogenous GST protein was present in the elution.**

The protein concentration of the elution fraction E1 from each organ was determined using the Bradford assay. The protein concentrations were: 0.7 mg/mL for pancreas and liver, 0.6 mg/mL for brain and testes, 0.3 mg/mL for spleen and 0.1 mg/mL for heart. Importantly, the measured concentration does not reflect the concentration of purified proteasome complexes due to the presence of bait protein GST-UBL, endogenous GST and copurified proteasome interacting proteins (PIPs).

The same protocol was used for the purification of proteasome complexes from RKO cells. Two batches of RKO cells were used as source material: RKO cells that were treated with IFN- $\gamma$  and untreated RKO cells. As for the purification from bovine organs, the same single-step affinity purification with GST-UBL was used and collected fractions were analyzed via SDS-PAGE (**Figure 3.5**). The amount of purified proteasome complexes was comparably successful from both, IFN- $\gamma$  treated and untreated RKO cells.

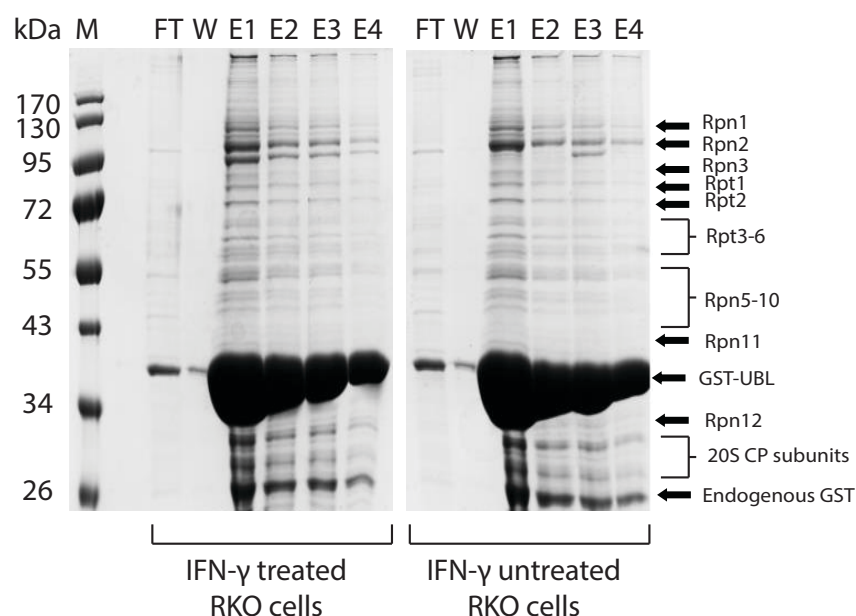


**Figure 3.5. SDS-PAGE analysis of affinity purification of proteasome complexes from RKO cells.**

**M** – marker, PageRuler prestained protein ladder 180 kDa; **F** – flowthrough, **W** – wash, **E1**, **E2**, **E3** and **E4** – four separate elution fractions. On the right the bands corresponding to individual subunits of the 26S proteasome and band corresponding to the bait protein GST-UBL are marked. A small amount of the endogenous GST protein was present in the elution.

The protein concentration of the elution fraction E1 from both, IFN- $\gamma$  treated and untreated RKO cells, was determined with Bradford assay. The protein concentrations were: 0.4 mg/mL for IFN- $\gamma$  treated RKO cells and 0.6 mg/mL for untreated RKO cells.

Before any further analysis of purified proteasome complexes, the excess of GST-UBL was removed by density gradient ultracentrifugation on a 10-30% sucrose gradient. 200  $\mu$ L gradient fractions were analyzed via *dot blot* on the nitrocellulose membrane stained in amido black solution (**Figure 3.6**).

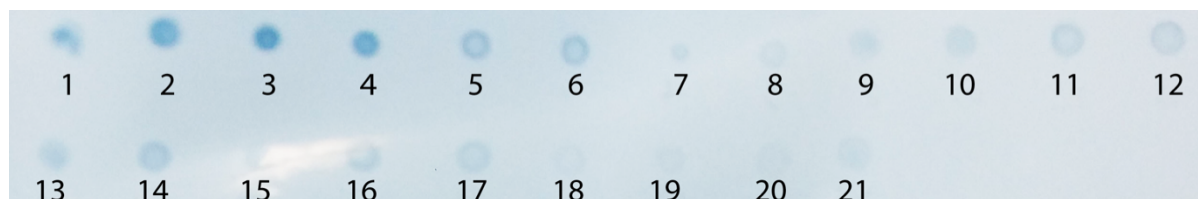


**Figure 3.6.** Example of a *dot blot* on the nitrocellulose membrane.

2  $\mu$ L of the sucrose gradient fraction (1-21) was applied on the nitrocellulose membrane. After staining with amido black and destaining in the destaining buffer, the relative protein amount in each fraction was detected by the appearance of blue color. The fractions with more intense blue color contain more proteins.

The bait protein GST-UBL has the molecular mass of 38 kDa and proteasome complexes have the molecular mass in a range of 1.5 – 2.5 MDa, hence they can be effectively separated in the sucrose gradient. According to the intensity of amido black staining, the fractions at the beginning of a gradient were the most enriched in protein content, the middle fraction somewhat less and then again after eleventh fraction the protein content increases. Hence, the corresponding distribution of protein components was the following: the most abundant protein in the sample, the GST-UBL, was mainly present in first few fractions (1-6) while proteasome complexes traveled much further and were mainly present in fractions 12 – 17.

### 3.3. Semiquantitative analysis of purified proteasome complexes

#### 3.3.1. Proteasome complexes from different bovine organs

The extract and elution samples were analyzed semiquantitatively by mass spectrometry in order to find the optimal bovine organ that could be used as a source material to purify hybrid proteasome complexes. Apart from the constitutive 26S proteasome subunits, most prominent identified proteins included PIPs like UCHL5 and Usp14 DUBs, Rad23A, Rad23B and proteasome assembly chaperones. 11S and PA200 proteasome activators were found in all organs, except heart. (**Table S1**).

Moreover, to semiquantify the mass spectrometry protein identification results, the detected normalized area corresponding to a specific proteasome activator was normalized to detected normalized area corresponding to the  $\alpha$ 1 subunit of the 20S CP and thus represents

the relative amount of each regulator per proteasome complex in the individual sample. The relative amounts of PA28 $\alpha$ , PA28 $\beta$ , PA28 $\gamma$  and PA200 were calculated and compared between the corresponding extract and elution samples from each bovine organ used in purification (Figure 3.7, Table S2).

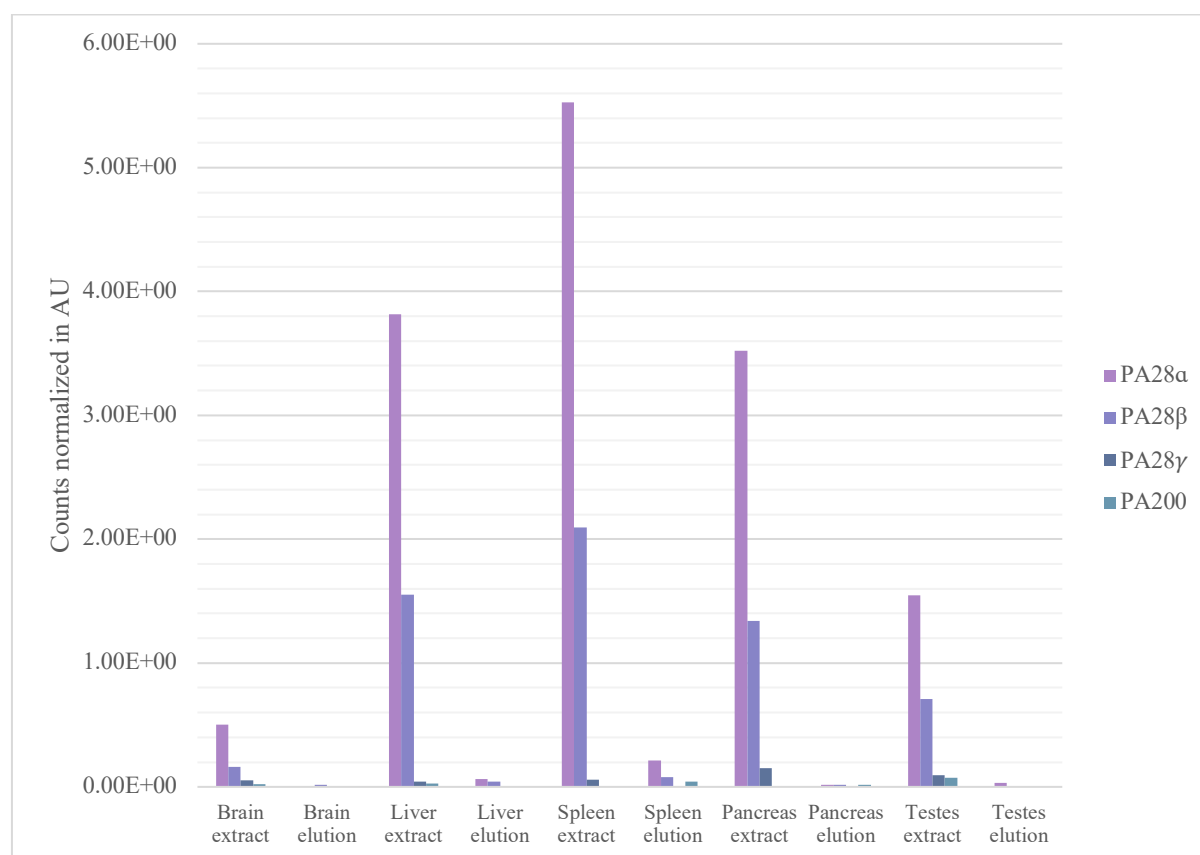


**Figure 3.7. Relative amounts of PA28 $\alpha$ , PA28 $\beta$ , PA28 $\gamma$  and PA200 present before (extract) and after (elution) affinity purification of proteasome complexes from different bovine organs.**

**The relative amount of individual proteasome activator is normalized to the relative amount of proteasome  $\alpha$ 1 subunit in the corresponding extract/elution; the relative amount of individual proteasome activators in extract or elution within the same organ are comparable but they are neither comparable between different organs nor between extracts and elutions from the same organ.**

The relative amount of PA28 $\alpha$  is by far the highest in all extracts, followed by the PA28 $\beta$  with more than half as less in the relative amount than PA28 $\alpha$ . The PA28 $\gamma$  complex and PA200 have the lowest relative amounts in all organs. Meanwhile, in elution samples, all proteasome activators have similarly low relative amounts with the only exception being the PA28 $\alpha$  in elution from bovine spleen.

### 3.3.2. Proteasome complexes from RKO cells

The same semiquantitative analysis of mass spectrometry protein identification results was performed with extracts and elutions after affinity purification of proteasome complexes from IFN- $\gamma$  treated and untreated RKO cells. As for the bovine organs, all subunits of the 26S proteasome were identified as well as several PIPs, proteasome assembly chaperons and proteasome activators PA28 $\alpha$ , PA28 $\beta$ , PA28 $\gamma$  and PA200 (**Table S1**). The relative amounts of PA28 $\alpha$ , PA28 $\beta$ , PA28 $\gamma$  and PA200 were calculated and compared between the IFN- $\gamma$  treated and untreated RKO cells (**Figure 3.8, Table S2**).

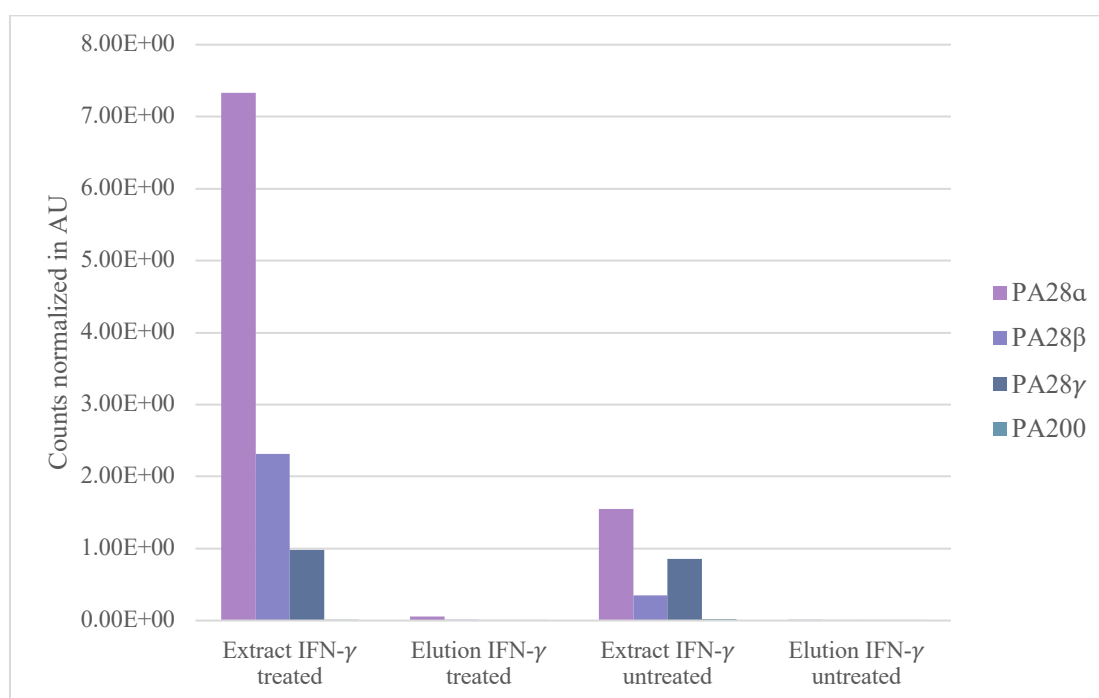


**Figure 3.8. Relative amounts of PA28 $\alpha$ , PA28 $\beta$ , PA28 $\gamma$  and PA200 present in IFN- $\gamma$  treated and untreated RKO cells before (extract) and after (elution) affinity purification of proteasome complexes.**

**The relative amount of individual proteasome activator is normalized to the relative amount of proteasome  $\alpha$ 1 subunit in the corresponding extract/elution; the relative amount of individual proteasome activators in extract or elution from the same type of RKO cells (IFN- $\gamma$  treated or untreated) are comparable but they are neither comparable between different types of RKO cells nor between extracts and elutions from the same type of RKO cells.**

The IFN- $\gamma$  treatment resulted in a different pattern of relative amounts of distinct proteasome activators in cell extracts: the relative amount of PA28 $\alpha$  upon IFN- $\gamma$  induction remained the highest, however, the relative amount of PA28 $\beta$  rose above the relative amount of PA28 $\gamma$  whereas in untreated cells is below. The relative amount of PA200 was the lowest in both extracts. The relative amounts of proteasome activators in elutions from either IFN- $\gamma$

treated or untreated cells are comparable with only slightly higher relative amount of PA28 $\alpha$  in comparison to other proteasome regulators in elution from IFN- $\gamma$  treated cells.

An additional search was performed to verify the effect of IFN- $\gamma$  treatment of RKO cells. This search aimed to identify the IFN- $\gamma$  inducible catalytic proteasome subunits  $\beta$ 1i,  $\beta$ 2i and  $\beta$ 5i in extracts and elutions. However, only  $\beta$ 2i and  $\beta$ 5i were detected (**Table S1**) and their relative amounts were calculated (**Figure 3.9, Table S2**).

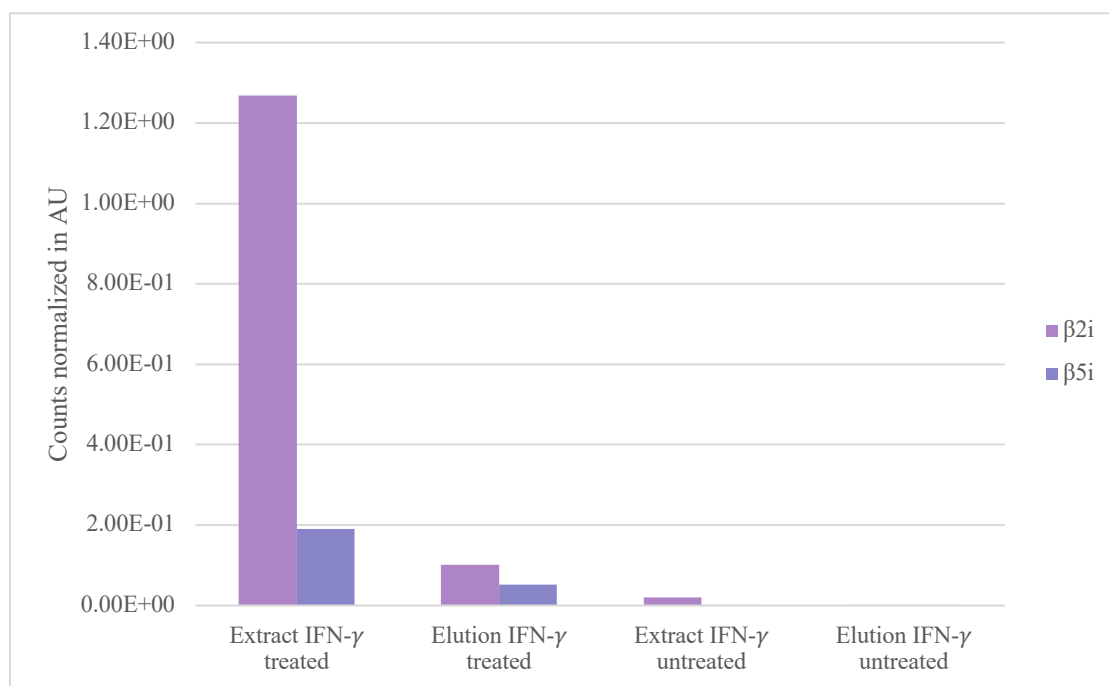


**Figure 3.9. Relative amounts of  $\beta$ 2i and  $\beta$ 5i present in IFN- $\gamma$  treated and untreated RKO cells before (extract) and after (elution) affinity purification of proteasome complexes.**

**The relative amount of individual  $\beta$  subunits is normalized to the relative amount of proteasome  $\alpha$ 1 subunit in the corresponding extract/elution; the relative amount of individual  $\beta$  subunits in extract or elution from the same type of RKO cells (IFN- $\gamma$  treated or untreated) are comparable but they are neither comparable between different types of RKO cells nor between extracts and elutions from the same type of RKO cells.**

The IFN- $\gamma$  inducible catalytic proteasome subunits  $\beta$ 2i and  $\beta$ 5i seem to be constitutively expressed in untreated RKO cells since low relative amounts were detected in samples from untreated cells. The IFN- $\gamma$  treatment clearly induced the expression of  $\beta$ 2i subunit since the relative amount of  $\beta$ 2i in the extract from treated cells was almost a 6-fold higher than the relative amount of  $\beta$ 5i while in the extract from untreated cells is only slightly higher. The  $\beta$ 1i subunit was not detected at all.

### 3.4. Functional analysis of purified proteasome complexes

#### 3.4.1. Generation of proteasome substrate polyUb securin

In order to perform functional assays with purified proteasome complexes, a native proteasome substrate, polyUb securin was produced in reaction catalyzed via Uba1, UBE2C, UBE2S and APC/C<sup>Cdh1</sup>. The aliquots during polyUb reaction were taken at different time-points during the reaction and analyzed via SDS PAGE (**Figure 3.10**).

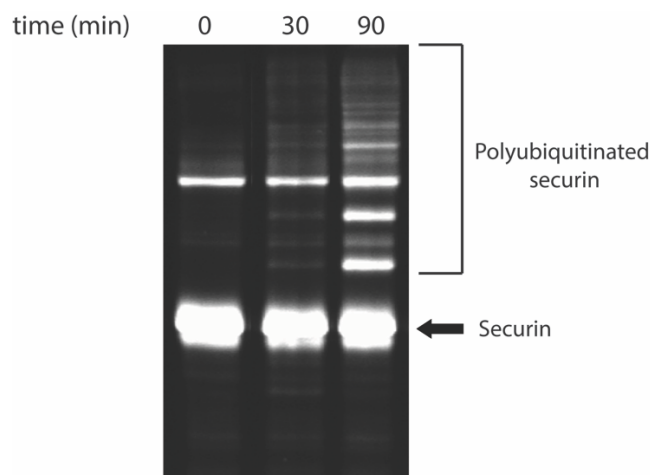


**Figure 3.10.** Analysis of ubiquitination reaction via SDS-PAGE.

The aliquots were taken at three different time points (0, 30 and 90 minutes); the substrate molecules were detected by imaging of fluorescence of the fluorescein label. On the right the band of securin is marked (~22 kDa); the fluorescent bands with higher molecular mass after 90 minutes represent the polyUb securin with a different number of attached ubiquitins.

To ensure the complete purity of the substrate and to remove any remained free ubiquitin, the sample was acidified and passed through a size exclusion column (**Figure 3.11**).

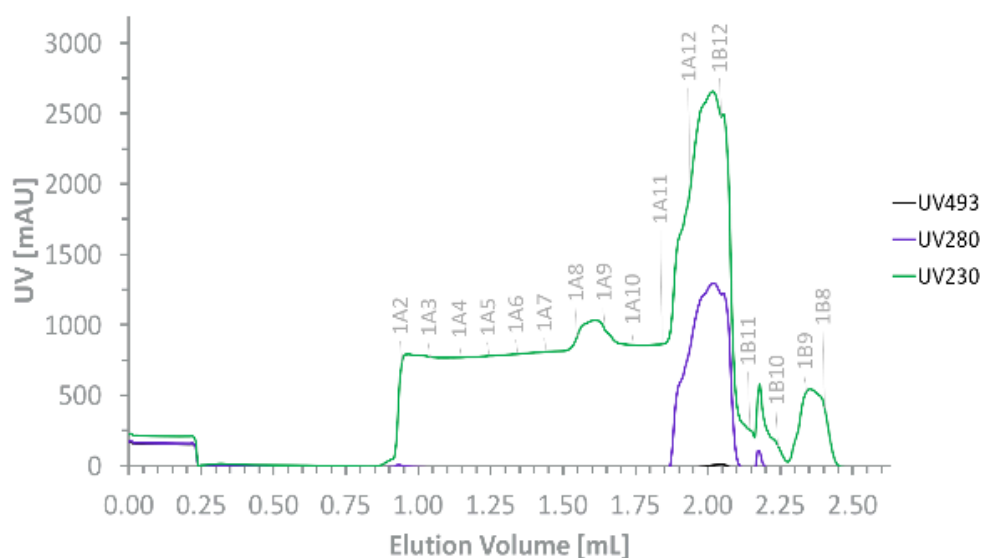




**Figure 3.11. Size exclusion chromatography FPLC chromatogram of polyUb securin.**

Fractions showing absorbance at 280 nm (1A11, 1A12, 1B12, 1B10) contain polyUb securin; the fluorescein excitation maximum is at 493 nm hence the absorbance at 493 nm was also monitored.

Each step of the generation of polyUb securin, the ubiquitination reaction, the pellet and the supernatant after acidification of the reaction and chosen fractions from the size exclusion chromatography, were analyzed via SDS-PAGE (**Figure 3.12**). Fractions that contained polyUb securin were concentrated and measured protein concentration was 0.6 mg/mL ( $\epsilon^{1\%}(\text{securin}) = 3.68$ ). Since ubiquitin protein does not contain any aromatic amino acid residues, the measured protein concentration reflects the concentration of securin.

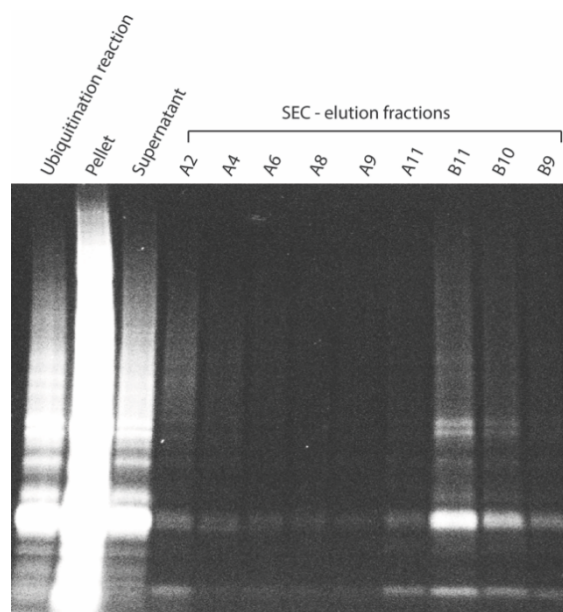


**Figure 3.12. Analysis of individual steps during the generation of polyUb securin via SDS-PAGE.**

The substrate molecules were detected by imaging of fluorescence of the fluorescein label. Fractions showing the fluorescence (A11, B11, B10) contain polyUb securin.

#### 3.4.2. *In vitro* degradation of polyUb securin

The ability of purified proteasome complexes to unfold, deubiquitinate and degrade a protein substrate was tested *in vitro* using the generated and purified fluorescently labeled polyUb securin and was monitored by SDS-PAGE and imaging of fluorescence where the disappearance of fluorescence indicates the degradation of the substrate.

The *in vitro* degradation assay with proteasome complexes purified from bovine testes shows that the substrate is efficiently degraded already after 1 hour (**Figure 3.13**). To distinguish different steps during substrate degradation two additional reactions were set with Rpn11 inhibitor capzimin that impairs the deubiquitination activity and thus the degradation,

and with MG132, the proteasome inhibitor that inhibits only the degradation of the substrate, but not the deubiquitination.

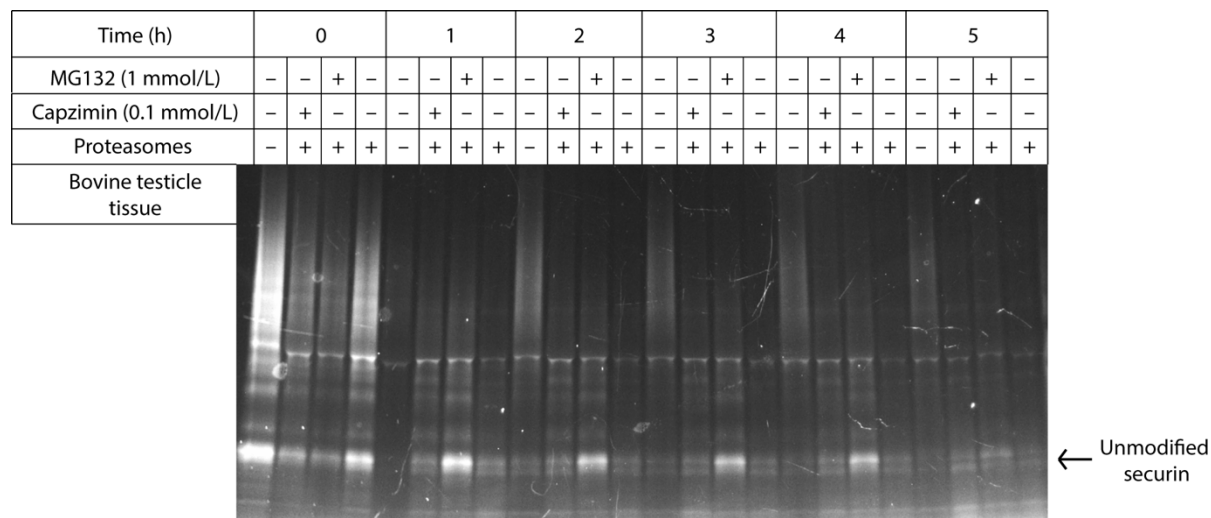


**Figure 3.13.** *In vitro* degradation assay with proteasome complexes purified from bovine testes. The assay was performed with three different reactions: the reaction with only proteasomes, with proteasomes and 0.1 mmol/L capzimin, Rpn11 inhibitor and with proteasomes and 1 mmol/L MG132, inhibitor of proteolytic activity of 20S CP; the reaction with only the substrate was used as a control (first lane); time-aliquots were taken at times indicated. On the right, the unmodified securin is marked.

In the reaction with only proteasomes, the fluorescence from the polyUb securin disappears and the fluorescent signal from unmodified securin remains constant over the time-course of reaction, which indicates that the substrate is deubiquitinated and degraded. Meanwhile, in the reaction with the proteasome inhibitor MG132 the fluorescent signal from unmodified full-length securin increased in intensity which indicates that polyUb securin is deubiquitinated but not degraded. In the reaction where capzimin was present, due to the inhibition of Rpn11 DUB activity, the degradation was slightly delayed, but still present because the shuttle DUBs, UCHL5 and USP14, are copurified with proteasome complexes and deubiquitinate substrate which allows its degradation.

The activity of proteasome complexes purified from IFN- $\gamma$  treated and untreated RKO cells was verified using the same *in vitro* degradation assay (**Figure 3.14**)

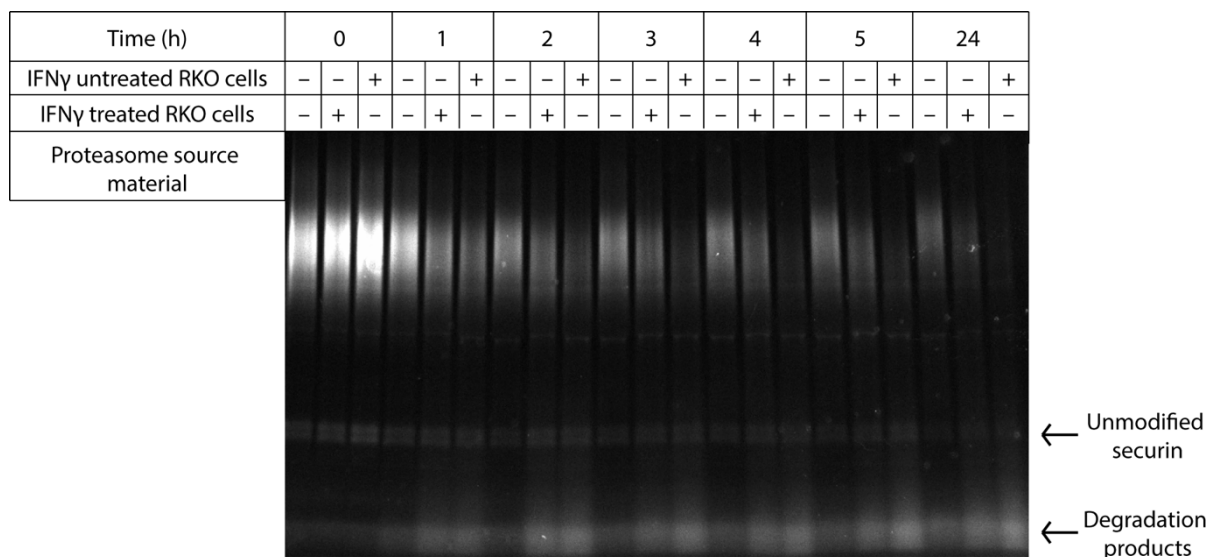


**Figure 3.14.** *In vitro* degradation assay with proteasome complexes purified from IFN- $\gamma$  treated and untreated RKO cells. The reaction with only the substrate was used as a control (first lane); time-aliquots were taken at times indicated. On the right, the unmodified securin and degradation products are marked.

Proteasome complexes from both, IFN- $\gamma$  treated and untreated RKO cells, are active and degrade the polyUb securin. However, the degradation was more efficient in the reaction with proteasome complexes from untreated RKO cells.

### 3.4.3. Analysis of peptides generated during proteasomal degradation of polyUb securin

#### 3.4.3.1. Peptide fragments after degradation by proteasome complexes purified from RKO cells

Apart from testing the activity, the degradation products from an *in vitro* degradation assay with proteasome complexes from IFN- $\gamma$  treated and untreated RKO cells were subjected to analysis by mass spectrometry. The goal was to see whether the IFN- $\gamma$  induction of the inducible  $\beta$ 2i and  $\beta$ 5i subunits or the induction of PA28 $\alpha\beta$  would result in different cleavage specificities or have an impact on the several other parameters: the peptide pattern, the number of different peptides and/or the mean peptide length. Detected peptide fragments (**Table S3**, **Table S4**) are shown in **Figure 3.15**.



**Figure 3.15.** Different peptides generated from securin by proteasome complexes purified from RKO cells. The pink lines mark the peptides generated by proteasome complexes from both, IFN- $\gamma$  treated and untreated RKO cells; the purple lines mark the peptides generated by proteasome complexes from IFN- $\gamma$  treated RKO cells; the green lines mark the peptides generated by proteasome complexes from untreated RKO cells. Bold letters mark the N terminal cutting site. The substrate sequence is shown from the N to C terminus.

Using the 50% (v/v) and 70% (v/v) ACN elution, the sequence coverage by the mass spectrometry for both reactions was around 45% (**Table S3**). Most of the generated peptide fragments were the same, however, several unique peptides were detected in reaction with proteasomes from IFN- $\gamma$  treated or untreated cells. However, only three of all unique peptides, regardless of the reaction, had a detection score that is reliable (best score > 200.0) – two from the degradation by proteasomes from IFN- $\gamma$  treated RKO cells (KGPLKQKQPSF and GPLKQKQPSF) and one from the degradation by proteasomes from untreated RKO cells (VELPPVAAD) (**Table 3.1**). The number of peptides and the mean size of the peptides were calculated and analysed using the t-Test Two-Sample Assuming Equal Variances (**Table S8**). The mean size of peptides did not change significantly in reaction with proteasomes from IFN- $\gamma$  treated RKO cells.

**Table 3.1.** Quantitative analysis of peptides generated from securin by proteasome complexes purified from RKO cells

Parameter	IFN- $\gamma$ treated RKO cells	IFN- $\gamma$ untreated RKO cells
<b>N (peptides)</b>	15	18
<b>Mean size (<math>\mu</math>) of peptides</b>	10.13 $\pm$ 1.33	9.83 $\pm$ 1.25
<b>N (unique peptides, best score &gt;200.0)</b>	2	1

To further analyze generated peptides, the cleavage pattern of securin was predicted using two different prediction softwares: NetChop, 20S 3.0 network (Nielsen, 2005) and PProC (Kuttler, 2000, Nussbaum, 2001) (**Figure S1**). PProC uses a method for predicting human and yeast proteasome cleavage sites based on the *in vitro* digestion data of enolase I. The quantitative effect of different residues on cleavage specificity is considered using the hill climbing algorithm. NetChop uses a method for predicting the constitutive or immunoproteasome cleavage sites on the basis of a multilayered artificial neural network. The method is based on the *in vitro* digestion data and sequence signal from the boundaries of naturally processed MHC class I ligands. The latter was included on the basis of an assumption that proteasome cleavage sites mostly lies at the C terminal of MHC class I ligands. The cleavage sites predicted by both softwares are shown in **Figure 3.16**.



**Figure 3.16. Prediction of the proteasome/immunoproteasome cleavage sites from the securin.** Amino acids indicated in purple represent the cleavage sites predicted only by the NetChop server; amino acids indicated in orange represent the cleavage sites predicted only by the PProC server; amino acids indicated in green are cleavage sites predicted by both servers. The marked amino acid is on the N terminus of cleavage site; a red asterisk indicates experimental and predicted N terminal cleavage site; a blue asterisk indicates only experimental N cleavage site; underlined amino acid represents compatible experimental and predicted N terminal cleavage site.

Combining these two softwares for the prediction of cleavage sites enabled the detection of potential N terminal cleavage sites that are specific for immunoproteasomes because NetChop detects proteasome and immunoproteasome cleavage sites whereas PProC detects only proteasome cleavage sites, thereby amino acids indicated in purple in **Figure 3.16** represent the potential immunoproteasome N terminal cleavage sites. Two of those sites (Ala20 and Lys161) were compatible with experimental data, that is those cleavage sites were present only in peptides generated by the IFN- $\gamma$  treated RKO cells. The majority of experimental cleavage sites (13/17) were predicted by one of the servers and most of them (11/13) were compatible with the proteasome/immunoproteasome differences in cleavage sites.

3.4.3.2. Peptide fragments after degradation by the 26S proteasome in the presence or absence of 11S activators.

An *in vitro* degradation assay with polyUb securin was performed with the 26S proteasome in the presence or absence of 11S regulators to investigate whether the formation of the hybrid complexes might affect the peptide pattern, promote the generation of certain peptides or alter the mean size or the number of peptides generated only by the 26S proteasome.

After the degradation and subsequent elution of peptides from the Sep Pak C18 columns with 30% (v/v) and 40% (v/v) ACN, peptide analysis resulted with a high sequence coverage, around 90% (**Table S5**). Among all detected peptides (**Table S7**) only peptides with best score >200.0 are considered reliable and were used for quantitative analysis shown in **Table 3.2**.

**Table 3.4. Quantitative analysis of peptides generated from securin by proteasome complexes purified from bovine heart in the presence or absence of different 11S regulators.**

Parameter	26S	26S + PA28 $\alpha\beta$	26S + PA28 $\gamma$
N (peptides; best score >200.0)	120	180	189
Mean size of peptides (best score >200.0)	11.10 $\pm$ 2.91	12.12 $\pm$ 2.92	12.02 $\pm$ 2.94
N (unique peptides; best score >200.0)	0	27	2
	<b>26S + PA28<math>\alpha\beta/\gamma</math></b>		
N (unique peptides; best score >200.0)	36		

The number of detected peptides in individual reaction shows that due to the presence of either the PA28 $\alpha\beta$  or PA28 $\gamma$ , the number of different peptides was increased and the t-Test Two-Sample Assuming Equal Variances indicates that the mean size of generated peptides increased significantly (**Table S9**). Looking at peptide sequences, all peptides found in the reaction with 26S proteasomes were also present in the reaction with PA28 $\alpha\beta$  or PA28 $\gamma$ , respectively. However, the degradation of securin by the 26S proteasome in the presence of PA28 $\alpha\beta$  resulted in the generation of 27 peptides with unique sequences, and only two in the presence of PA28 $\gamma$  (**Table S6**). Additionally, 32 peptides were common between reactions with either PA28 $\alpha\beta$  or PA28 $\gamma$  and were not present in reaction with only 26S proteasomes. In **Figure 3.17** the position of every unique individual peptide within a securin sequence is marked.



**Figure 3.17.** Different peptides generated from securin by proteasome complexes purified from bovine heart in the presence of PA28 $\alpha\beta$  and/or PA28 $\gamma$ . The purple lines mark the unique peptides generated by proteasome complexes in the presence of only PA28 $\alpha\beta$ ; the green lines mark the unique peptides generated by proteasome complexes in the presence of only PA28 $\gamma$ ; pink lines mark the peptides generated by proteasome complexes in the presence of either the PA28 $\alpha\beta$  or PA28 $\gamma$ . The three dots indicate that the sequence is continued in the next line. Bold letters mark the N terminal cutting site. The substrate sequence is shown from the N to C terminus.

Interestingly, most of the identified unique peptides are located in the first half of a protein substrate: 25 out of 27 from a reaction with PA28 $\alpha\beta$ , 28 out of 36 shared unique peptides from reactions with 11S regulators and all unique peptides detected in a reaction with PA28 $\gamma$ .

### 3.5. Analysis of purified proteasome complexes by negative stain TEM

The purity and composition of individual proteasome fractions after density gradient ultracentrifugation were verified using the negative-stain TEM. Micrographs in **Figure 3.17** show clear proteasome complexes with good contrast. The distribution of proteasome subcomplexes and complexes was inspected visually of every second gradient fraction. Free 19S and 20S CP were mostly in fractions ranging from 10-12, the 26S and hybrid proteasome complexes were mainly seen in fractions 13 to 16, while 30S proteasome complexes were usually in last few fractions, from fraction 17 to 19.

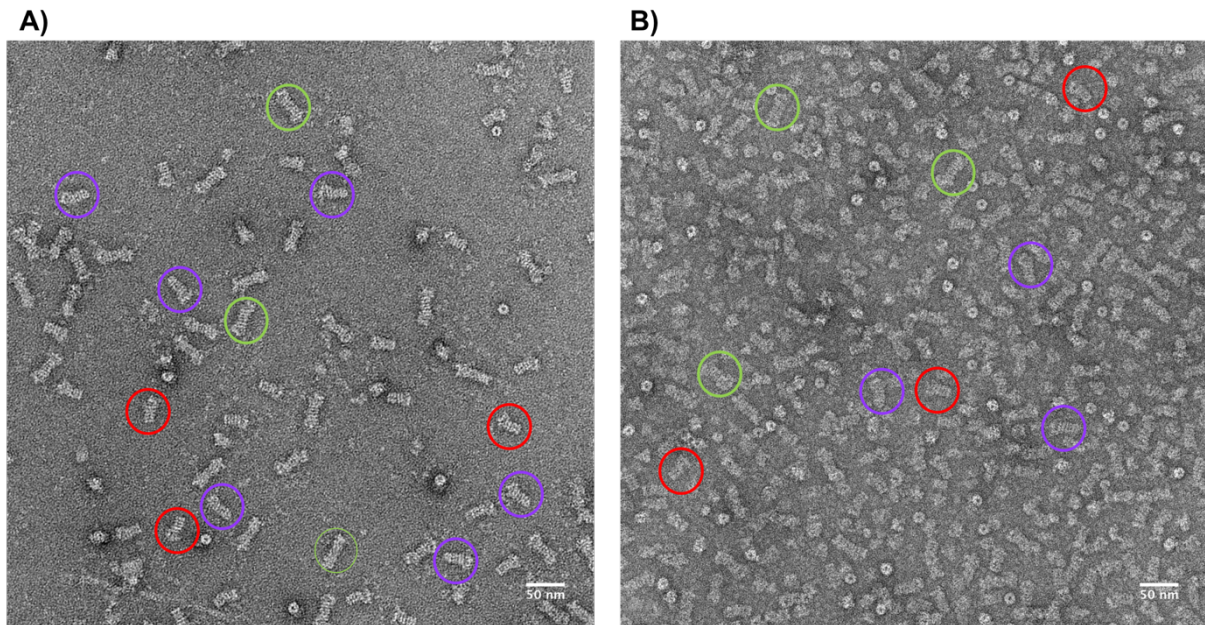


**Figure 3.17.** Negative stain micrographs of proteasome complexes imaged with a Tecnai G<sup>2</sup> 20 microscope equipped with an Eagle 4k HS camera.

Proteasome complexes purified from **A)** IFN- $\gamma$  treated RKO cells, **B)** bovine testes. Red circles show 26S proteasomes, green circles show 30S proteasome and purple circles show hybrid proteasomes.

The negative-stain EM grids of gradient fractions from IFN- $\gamma$  treated RKO cells and bovine testes that contained the majority of hybrid proteasome complexes were used to collect the negative-stain dataset. The collected dataset of the proteasome sample from IFN- $\gamma$  treated RKO cells was obtained at 0° and 30° stage tilt and 2133 raw micrographs were recorded whereas the dataset proteasomes from bovine testes was obtained at only 0° stage tilt and 700 micrographs were recorded. Negative datasets were processed in order to obtain 2D class averages (**Figure 13.8**).



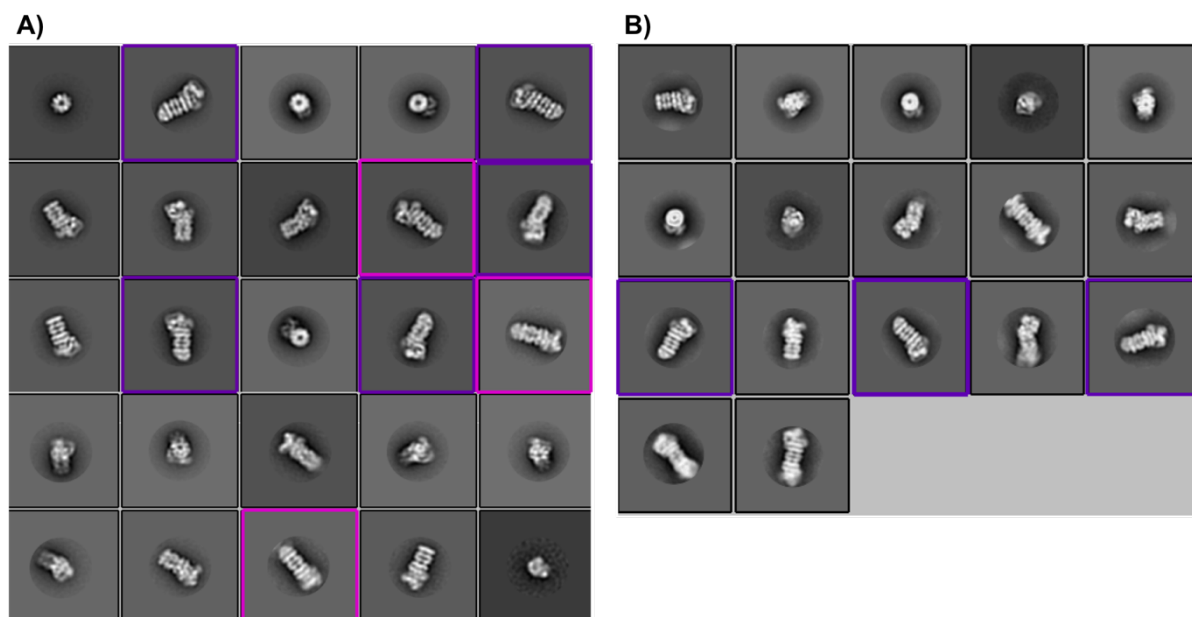


**Figure 3.18.** 2D class averages clearly showing proteasome complexes computed using the software RELION.

A) 2D class averages of proteasome complexes from IFN- $\gamma$  treated RKO cells. The number of picked particles was 133 718; the number of particles belonging to showed 2D class averages was 24 878; the number of particles belonging to 2D class averages in boxed squares was 1 719. B) 2D class averages of proteasome complexes from bovine testes. The number of picked particles was 211 766; the number of particles belonging to showed 2D class averages was 19 182; the number of particles belonging to 2D class averages in boxed squares was 248. The pink squares show 2D class averages of the hybrid proteasome containing PA28 $\alpha\beta$  or PA28 $\gamma$  and purple squares show 2D class averages of the hybrid proteasome containing PA200 proteasome activator.

The number of particles belonging to 2D class averages which clearly showed the hybrid proteasome complex (“side views” of particles) comprised only 6.9% and 1.3% of the total number of particles belonging to 2D class averages in **Figure 3.18** in case of the sample from IFN- $\gamma$  treated RKO cells and bovine testes, respectively.

### 3.6. Structural analysis of the hybrid proteasome by single-particle cryo-EM.

Prior to the preparation of cryo-grids, proteasome samples were subjected to a buffer exchange to remove sucrose that would hinder a cryo-EM analysis. Cryo-grids were prepared from the proteasome sample from IFN- $\gamma$  treated RKO cells and bovine testes, and cryo-EM micrographs were collected (**Figure 3.19**).

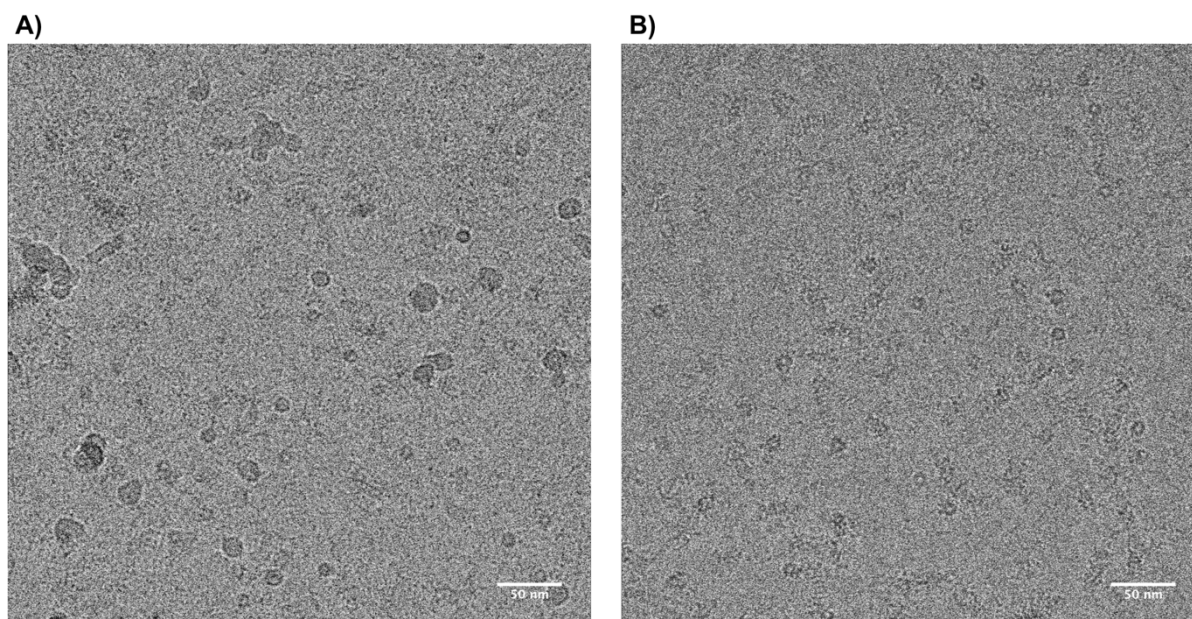


**Figure 3.19.** Cryo-EM micrographs of proteasome complexes imaged with a Titan Krios microscope equipped with a Falcon III direct detector camera.

Proteasome complexes purified from A) IFN- $\gamma$  treated RKO cells and B) bovine testes.

Only micrographs that show good contrast and the particles are recognizable were used for particle picking. Picked particles were subjected to reference-free 2D classification to clean the particle stacks and remove junk particles (**Figure 3.20**).

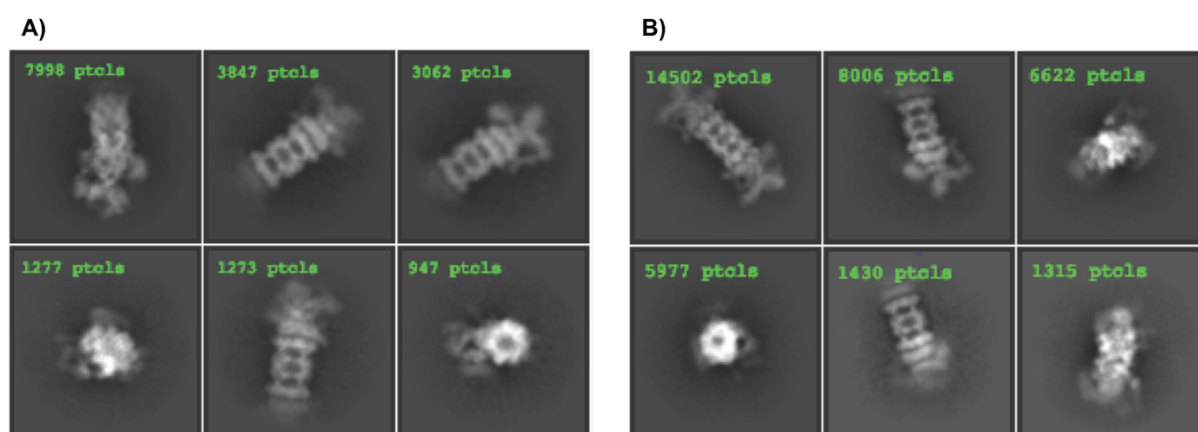


**Figure 3.20.** 2D class averages of proteasome complexes computed using the CryoSPARC software.

Examples of good 2D class averages of proteasome complexes from A) IFN- $\gamma$  treated RKO cells and B) bovine testes that were used for further analysis.

Only particles belonging to 2D class averages that showed clear proteasomal density were subjected to 3D analysis. The individual steps of the 3D analysis of particles are shown in **Figure 3.21** for IFN- $\gamma$  treated RKO cells and in **Figure 3.22** for bovine testes datasets, respectively.

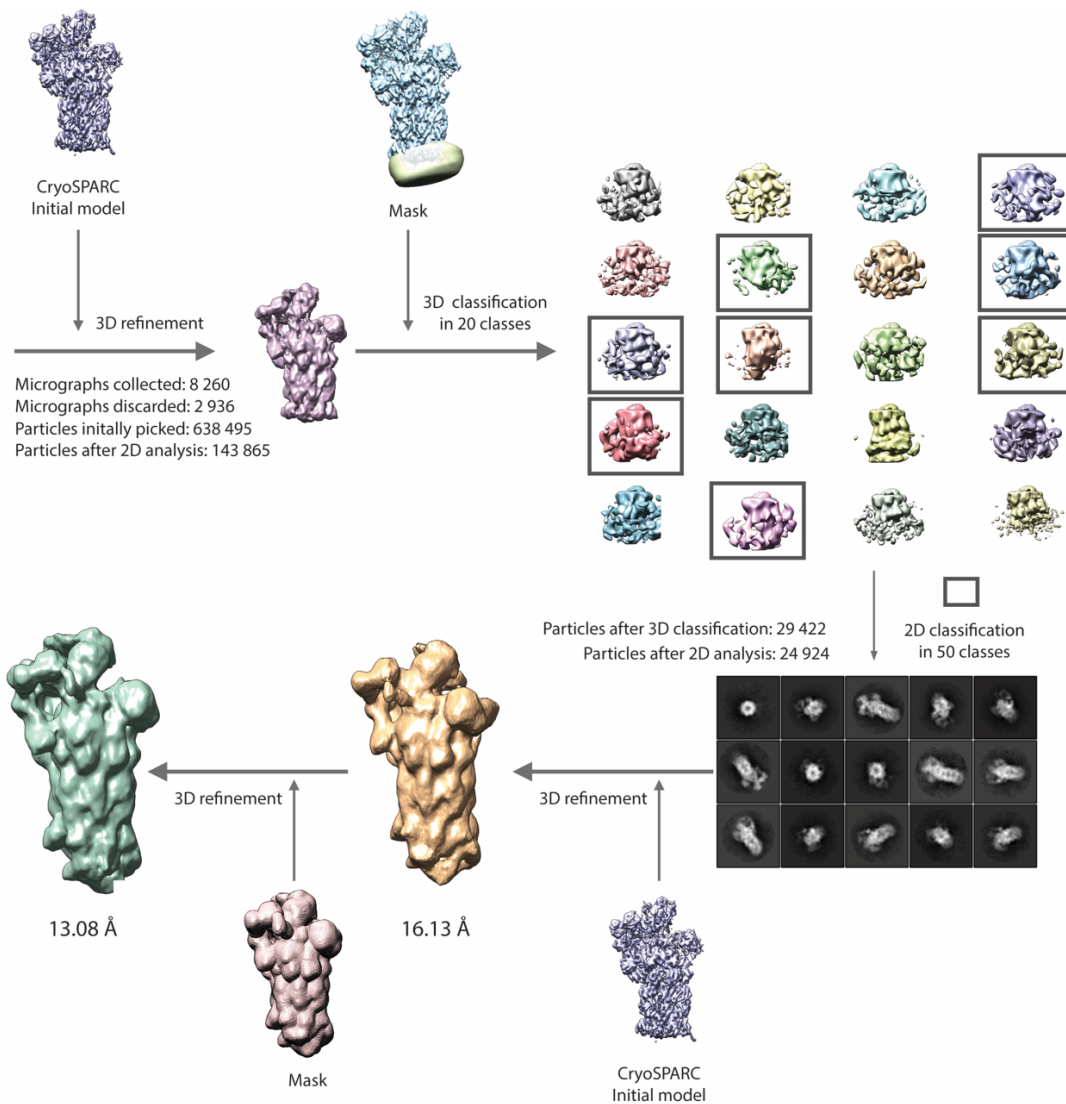


**Figure 3.21. Schematics of the particle sorting scheme for the dataset collected from IFN- $\gamma$  treated RKO cells.**

An initial model was generated from the best 2D class averages using CryoSPARC. With this, all particles were aligned by refinement in RELION. The refined particles were 3D classified in 20 classes by using a hybrid mask. All classes were visually inspected in UCSF Chimera. Particles belonging to 3D classes that showed a density different from the 19S RP density were subjected to 2D classification. 2D class averages showing clear densities of hybrid proteasome complexes were subjected to 3D refinement with an initial model as a reference and without using a mask. Afterward, a mask for the whole hybrid proteasome complex was applied and the structure was re-refined to a 13.08 Å structure.

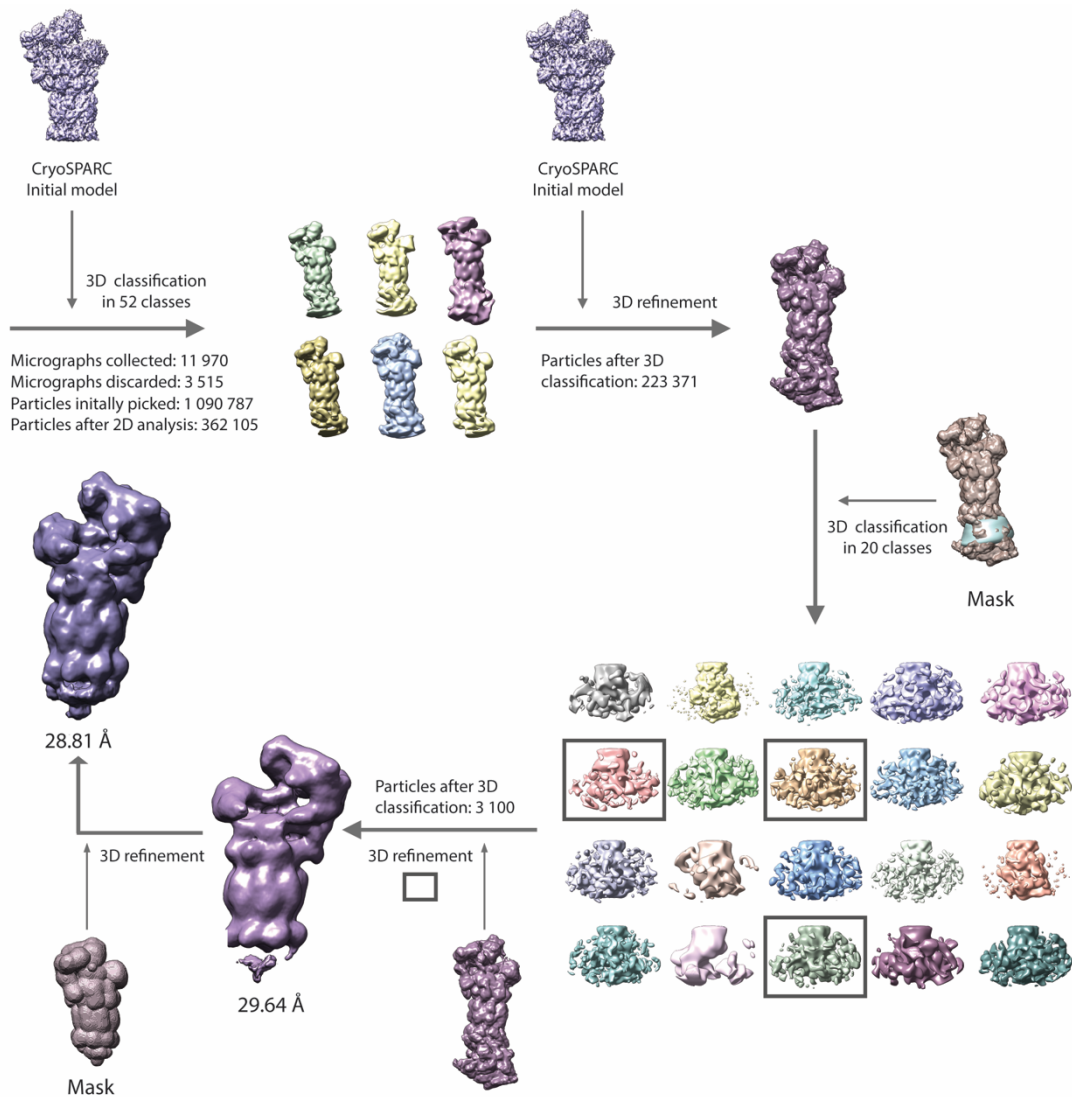


**Figure 3.22.** Schematics of the particle sorting scheme for the dataset collected from proteasomes from bovine testes.

An initial model was generated from the best 2D class averages using CryoSPARC. With this, all particles were 3D classified in packages of 90 526 in 13 classes each. All classes were visually inspected in UCSF Chimera (shown are only good 3D class averages). After the visual inspection, all particles belonging to good 3D class averages were refined without using a mask. The refined particles were 3D classified in 20 classes by using a hybrid mask. All 3D class averages were also visually inspected in UCSF Chimera. Particles belonging to 3D classes that showed a density different from the 19S RP density were refined without using a mask. Afterward, a mask for the whole hybrid proteasome complex was applied and the structure was re-refined to a 26.81 Å structure.

A very small number of particles belonged to 3D class averages that contained densities indicative of the hybrid proteasome after applying the mask on the 11S/PA200 area – only 3100 particles in case of bovine testes and 24 924 in case of IFN- $\gamma$  treated RKO cells. However, that was still enough to obtain one final structure from each dataset (**Figure 3.23**).

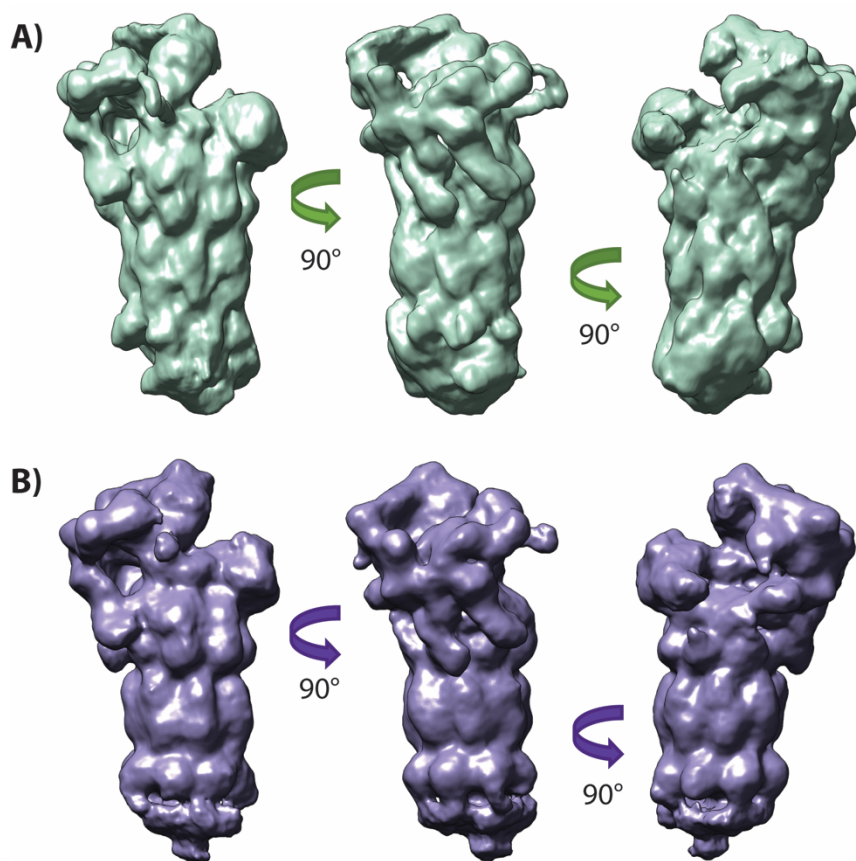


**Figure 3.23. 3D models of hybrid proteasomes.**

The 3D surface representation of a hybrid proteasome structure from A) IFN- $\gamma$  treated RKO cells and B) bovine testes is shown from different sides. The three different subcomplexes of the hybrid proteasome can be identified: the 20S CP, the 19S RP on the top and the PA200 on the bottom of the 20S core particle. However, all parts show smeared and blurred densities, especially in A).

Despite smeared features of the final structure, the general appearance of the hybrid proteasome can be recognized. The structures of PA28 $\alpha\beta$  and PA200 proteasome activators have been solved (Huber & Groll, 2017, Sadre-Bazzaz et al. 2010), and by comparing the density present in the bottom part of a structure shown in **Figure 3.23. A and B** with those structures, the obtained final structures from both data sets show hybrid proteasome complex with PA200 on one side and 19S RP on the opposite side of the 20S CP.

Furthermore, the angular distribution of the final models was determined (**Figure 3.23**). To do so, the equidistant projections are first generated from the model that covers the entire Euler sphere. Entire particle data set is then cross-correlated to each reference projection. A correlation coefficient is generated between each experimental particle and reference projection. Each experimental particle is matched to the reference projection that gave the highest correlation coefficient. Therefore, it is assumed that this particle matches the Euler angles (theta ( $\theta$ ), phi ( $\varphi$ ) and psi ( $\psi$ )) of the reference projection.

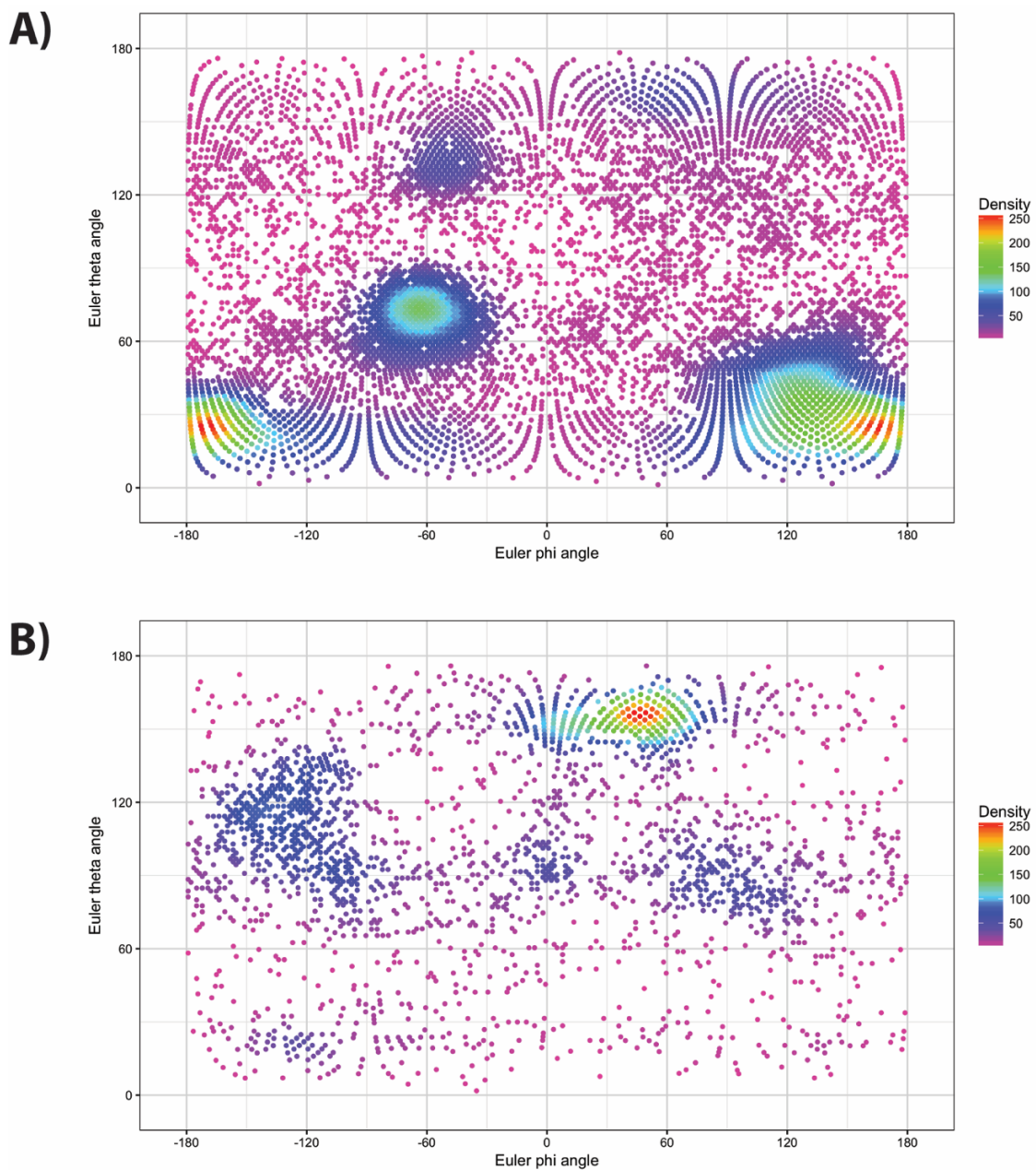


**Figure 3.23. The angular distribution of the final structures.**

**A) The Euler angle distribution of the final 13.08 Å structure from IFN- $\gamma$  treated RKO cells and B) the Euler angle distribution of the final 26.81 Å structure from bovine testes showing the spread of particles in angular space around the reference model. The  $\theta$  and  $\phi$  axes are indicated. Each dot inside the plot indicates the position of a matched projection.**

Ideally, one would want the distribution plot to be completely filled or have at least a tomographic series, indicating that all possible views of the specimen have been imaged. Unfortunately, that's not the case in **Figure 3.23 A and B**. Clearly, the angular distribution of

each model shows that a remarkable amount of certain particle views is absent which is reasonable if the number of particles is too low.

The final processing step was the resolution estimation and the final resolution of obtained structures was estimated by Fourier shell correlation. In the case of hybrid proteasome structure from IFN- $\gamma$  treated RKO cells, a resolution of 13.08 Å was determined and in the case of hybrid proteasome structure from bovine testes, a resolution of 26.81 Å was determined (Figure 3.25).

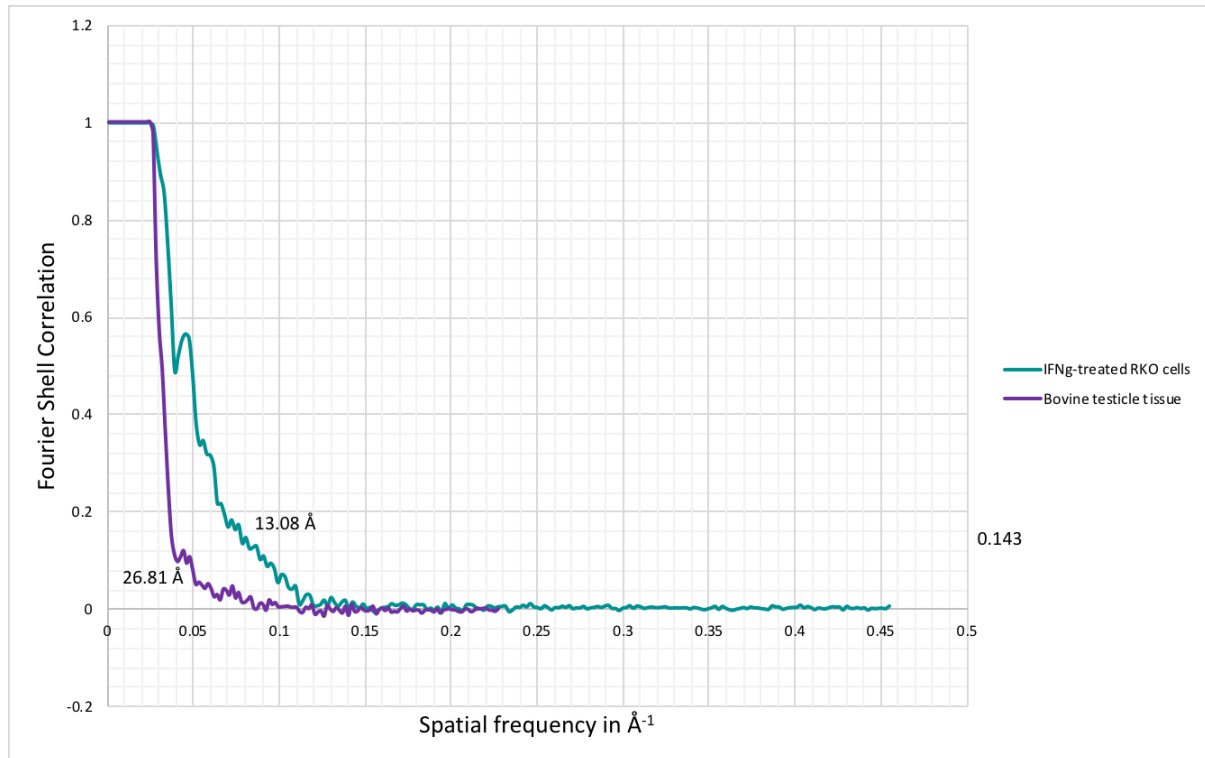


**Figure 3.25. FSC curve for the 3D volume.**

**The estimated resolution by FSC for the hybrid proteasome structure from IFN- $\gamma$  treated RKO cells is approximately 13.08 Å and 26.81 Å for a hybrid proteasome structure from bovine testes.**

## 4. Discussion

Proteasomes perform the majority of proteolysis that occurs in the cytosol and nucleus of eukaryotic cells, and thereby, perform crucial roles in cellular regulation and homeostasis. The catalytic heart of proteasome complexes is the 20S core particle that possesses three distinct proteolytic active sites with different specificities. Because the catalytic sites are sequestered inside the 20S CP, the activity of the 20S CP is primarily regulated through association with proteasome activator complexes that facilitate substrate access (Rechsteiner & Hill, 2005). The most broadly conserved proteasome activator is the 19S regulatory particle. The other two activator families are the 11S complexes (PA28 $\alpha\beta$  and PA28 $\gamma$ ) and PA200 (Stadtmueller & Hill, 2011). However, the understanding of the regulation of proteasome activity is mixed. On the one hand, it is clear that 19S RP, as part of the 26S proteasome, mediates degradation of polyUb proteins and that this activity has a major impact on a broad range of biological processes. On the other hand, whereas the biochemical basis for stimulation of peptidase 20S CP activity by 11S complexes and PA200 are relatively well characterized, the biological role of these proteasome activator families is only incompletely understood. Furthermore, it was found by co-immunoprecipitation and subsequently confirmed by electron microscopy analysis, that 11S/PA200 activators and the 19S RP can simultaneously bind on the opposite ends of the same 20S CP (Hendil et al., 1998, Kopp et al., 2001). This complex has been named the ‘hybrid proteasome.’ To date, it is plausible that the 26S proteasome and hybrid complexes both contribute to the ATP- and ubiquitin-dependent proteolytic pathway in mammalian cells (Tanahashi et al., 2000), but only the 26S proteasome is extensively described in a vast number of publications (Chen et al., 2016, Haselbach et al., 2017, Schweitzer, et al., 2016, Wehmer et al., 2017, Zhu et al., 2018). Hence, this thesis aimed to investigate and characterize the functional and structural properties of hybrid proteasome complexes.

### 4.1. Affinity purification of proteasome complexes using an ubiquitin-like domain

Purification of hybrid proteasome complexes was usually very difficult due to their extreme lability (e.g., they do not withstand standard chromatographic methods or exposure to high ionic strength buffers). However, not so long-ago a method for the affinity purification of mammalian proteasome complexes that uses the proteasome’s intrinsic affinity for the UBL domain of a human Rad23B (Besche & Goldberg, 2012) was shown to preserve labile protein-protein interactions and thus present an appropriate purification method for this type of



proteasome complexes. Hence, a large amount of the bait protein GST-UBL was successfully purified.

The cell extracts prepared from bovine organs (pancreas, liver, spleen, brain, testicle, and heart) were used to screen for 11S regulators/PA200 and establish which of the organs mentioned above have them expressed and in what amounts. Additionally, cell extracts of IFN- $\gamma$  treated RKO cells were used as source of hybrid proteasome complexes since it was shown that IFN- $\gamma$ , apart from the induction of  $\beta$ i immunoproteasome subunits (Huber et al., 2012), induces the expression of PA28 $\alpha\beta$  and consequently increases the number of hybrid proteasome complexes (Tanahashi et al., 2000).

Proteasome purification was successful from every bovine organ with only one exception; the amount purified from the bovine spleen was lower in comparison to other organs. The lower amount from the bovine spleen is most probably due to the less efficient tissue homogenization and hence less concentrated extract. Likewise, the purification of proteasome complexes from RKO cells was also successful and comparable in amounts of purified complexes between IFN- $\gamma$  treated and untreated RKO cells.

However, since GST-UBL was used in large excess, the GST-UBL was still present in high amounts in the sample after the elution. To get rid of the excess GST-UBL, a density gradient ultracentrifugation using the 10-30% sucrose gradient was performed. Most of the GST-UBL (~38 kDa) was neatly separated from proteasomes and kept in the first few fractions of a sucrose gradient while whole proteasome complexes or their subcomplexes traveled much further according to their differences in molecular mass (11S/PA200 complexes (200 kDa), free 20S CP and 19S RP (700 kDa), the 26S and 30S proteasome complexes (1.4 and 2.1 MDa). Hybrid proteasome complexes have a molecular mass of approximately 1.6 MDa. Realistically, it was not expected to obtain a fraction containing only hybrid proteasome complexes, but rather a fraction with 26S proteasomes enriched with hybrid proteasome complexes due to a relatively small difference in their molecular masses and a small number of hybrid proteasome complexes that is generally present in cells (Pickering & Davies, 2012). In future, a protocol should be developed that would aim for the isolation of hybrid proteasome complexes only and result in more concentrated hybrid proteasome samples.

## **4.2. Semiquantitative mass spectrometry as a screening tool for 11S and PA200 proteasome activators**

Several reports exist about the expression profiles of 11S and PA200 proteasome activators in mammals, mainly from rat, mouse and bovine tissues (Noda et al., 2000, Soza et al., 1997, Ustrell et al., 2002). Unambiguously, according to those studies, the PA200 is highly abundant in bovine testes. Meanwhile, reports about PA28 expression profiles and abundance are slightly contrary. Soza et al. (1997) showed that PA28 proteasome activators are highly expressed in liver, lungs, and kidneys and have low expression in brain, thymus and spleen. Similarly, a study performed by Noda et al. (2000) showed high protein abundance of all three PA28 isoforms in liver and lungs but also in spleen and low abundance in the brain. However, the expression and even translation of 11S/PA200 proteasome activators alone do not tell much about the amount of those activators in specific tissues that are part of the hybrid proteasome complexes. That information could have been obtained in this thesis since the method for proteasome purification involved pulling on the Rpn10 subunit of the 19S RP with a bait protein GST-UBL, hence, all 11S and PA200 proteasome activators that are co-purified, are the ones forming the hybrid proteasome complexes.

As described in the previous section (see section 4.1.), proteasome complexes were purified from six different bovine organs in order to perform screening for the 11S and PA200 proteasome activators in organ extracts and accompanying elutions by mass spectrometry. To semi-quantify results, the relative amount of each regulator per proteasome complex in the individual sample was determined using the detected normalized area. Unfortunately, such analysis does not provide a quantitative comparison between different organs, or even between extracts and elutions from the same organ; only relative amounts of proteasome activators normalized to the same value for the  $\alpha 1$  (e.g., all proteasome activators in extract from bovine spleen or all proteasome activators in elution from bovine brain) could be compared.

In general, all three 11S and PA200 proteasome activators were found in all bovine organs, except heart. Interestingly, the relative amounts of individual proteasome activators in specific organ extracts show a clear bias towards the higher abundance of PA28 $\alpha\beta$  complexes over the PA28 $\gamma$  and PA200 proteasome activators, whereas in elutions the amounts are comparable with the only exception being the relative amounts of PA28 $\alpha$  and PA28 $\beta$  in elution from bovine spleen. This indicates that approximately the same amount of either the PA28 $\alpha\beta$ , PA28 $\gamma$  or PA200 proteasome activator can be found in hybrid proteasome complexes within

the same organ, apart from the much higher amount of the PA28 $\alpha\beta$  hybrid complexes found in spleen.

The relatively high abundance of the PA28 $\alpha\beta$  proteasome activator and PA28 $\alpha\beta$  hybrid complexes in spleen, an immune system organ, is in accordance with indications for the involvement of the PA28 $\alpha\beta$  and PA28 $\alpha\beta$  hybrid complexes in MHC class I antigen presentation (Yang et al., 1995, Rechsteiner & Hill, 2005). However, their presence in immune privileged organs like brain and testes indicate that PA28 $\alpha\beta$  containing proteasome complexes play a role in other biological processes as well, e.g., the degradation of oxidized and misfolded proteins (Jiang et al., 2018). Surprisingly, in bovine testes, the relative amount of PA200 was the lowest even though it was reported to have a very high abundance in testes (Ustrell et al., 2002). Nevertheless, for further analysis of native hybrid proteasome complexes, the bovine testes were chosen as a source material due to the presence of all three proteasome activators in elutions and the fact that purity and yield from this organ were among the highest.

The same semiquantitative approach was used for the analysis of a relative abundance of 11S/PA200 proteasome activators and inducible  $\beta$ i immunoproteasome subunits in IFN- $\gamma$  treated and untreated RKO cells. The observed difference in the pattern of relative amounts of distinct proteasome activators in cell extracts is most likely due to the IFN- $\gamma$  induced expression of PA28 $\alpha$  and PA28 $\beta$  whereas PA28 $\gamma$  and PA200 are not responsive to IFN- $\gamma$  treatment (Tanahashi et al., 1997). Despite IFN- $\gamma$  treatment, the relative amount of PA28 $\alpha\beta$  was comparable to the relative amount of PA28 $\gamma$  and PA200 that is involved in the formation of hybrid proteasome complexes since their relative amounts in elutions do not differ dramatically as in extracts between treated and untreated RKO cells. The concentration-dependent formation of PA28 $\alpha\beta$  hybrid complexes that was observed in the case of IFN- $\gamma$  treatment of HeLa cells wasn't reproduced with RKO cells (Tanahashi et al., 2000).

The analysis of relative amounts of inducible  $\beta$ i immunoproteasome subunits showed that RKO cells constitutively express low and comparable amounts of  $\beta$ 2i and  $\beta$ 5i, whereas  $\beta$ 1i was not detected. It is well known that IFN- $\gamma$  induces the expression of all three inducible  $\beta$ i immunoproteasome subunits (Vigneron & Van den Eynde, 2014). However, the cell line used in this thesis was shown to have slightly impaired IFN- $\gamma$  signaling (Heink et al., 2006). In RKO cells, upon IFN- $\gamma$  treatment, only the  $\beta$ 2i subunit is expressed and adequately preprocessed via autocatalytic cleavage, which is a prerequisite for its incorporation into the 20S iCP. However, the  $\beta$ 1i subunit, even though expressed, has an impaired autocatalytic

cleavage and almost no mature  $\beta 1i$  subunit can be found in RKO cells upon IFN- $\gamma$  treatment (Heink et al., 2006). Since only mature  $\beta 1i$  can be incorporated into the 20S iCP it's logical that the  $\beta 1i$  subunit wasn't detected in proteasome sample from IFN- $\gamma$  treated RKO cells. The  $\beta 5i$  subunit was shown to have a more complicated expression profile in IFN- $\gamma$  treated RKO cells because IFN- $\gamma$  induces expression of a non-functional isoform  $\beta 5iE1$  whereas in normal IFN- $\gamma$  response, an isoform  $\beta 5iE2$  is expressed. The  $\beta 5iE1$  is incorporated into the 20S iCP with remarkably lower efficiency than  $\beta 5iE2$  due to the impaired interaction with a chaperone involved in the maturation of 20S iCP (Heink et al., 2006). Such response to IFN- $\gamma$  treatment explains why only a low amount of  $\beta 5i$  subunit was detected in comparison to a much higher relative amount of  $\beta 2i$ .

Nevertheless, there are no existing reports about altered PA28 $\alpha\beta$  induction in RKO cell line. Hence this cell line should still be usable for obtaining the PA28 $\alpha\beta$  hybrid complexes. The possible reason for the absence of increased formation of PA28 $\alpha\beta$  hybrid complexes in RKO cells upon IFN- $\gamma$  treatment could be that PA28 $\alpha\beta$  complex preferably forms hybrid proteasome complexes with 20S iCP, for which RKO cells are deficient, and in much smaller extent with cCP. The former would be an indirect indication that PA28 $\alpha\beta$  hybrid complexes formed with 20S iCP have an important role in MHC class I antigen production (Yang et al., 1995) and not only 26S immunoproteasomes and/or PA28 $\alpha\beta$  in complex with the 20S iCP. To test whether PA28 $\alpha\beta$  indeed prefers the 26S iCP complex in order to form a hybrid proteasome one should obtain pure 26S proteasome samples containing only cCPs or iCPs and measure binding affinities.

### **4.3. Generation of polyUb proteasome substrate and functional assays**

For performing activity assays with purified proteasome complexes, the polyUb substrate was produced. Human securin (~23 kDa) was chosen as a model proteasome substrate. *In vivo*, securin is the target of an APC/C mediated ubiquitination (Hagting et al., 2002), hence APC/C was used to produce polyUb securin in amounts sufficient for various *in vitro* degradation assays. The additional purification steps were performed after the ubiquitination, including the acidification of a sample and size exclusion chromatography. These additional steps ensured that purified polyUb securin was separated from all other components of the ubiquitination reaction so that their presence does not affect the degradation by proteasome complexes. The *in vitro* degradation assay performed with purified polyUb securin was designed to investigate the activity of purified proteasome complexes, the

difference in cleavage specificities of proteasomes purified from IFN- $\gamma$  treated RKO cells in comparison with the ones from untreated cells as well as the difference in cleavage specificities of different hybrid proteasome complexes using the *in vitro* reconstitution approach from purified components.

An *in vitro* degradation of polyUb securin by proteasome complexes purified from bovine testes showed that even in 100x molar excess of substrate, the degradation is almost complete after only one hour which means that there is a multiple turnover by a single 26S proteasome. Additional reactions with recently discovered Rpn11 inhibitor, capzimin (Li et al., 2017) and inhibitor of all three proteolytic activities of the 20S CP, MG132, resulted in an apparent impairment of deubiquitination and degradation activities of proteasome complexes. Slightly delayed deubiquitination, and hence, the degradation of substrate molecules in the reaction with capzimin indicate that Rpn11 activity is indeed inhibited by capzimin. However, the presence of deubiquitination activity can be attributed to co-purified DUBs, USP14 and UCHL5. Meanwhile, due to the inhibition of proteolytic activity by MG132, proteasome complexes efficiently deubiquitinate but do not degrade the substrate. This deubiquitination leads to the accumulation of deubiquitinated substrate. However, after 24 hours, even in the reaction with MG132, the degradation took place, since MG132 does not occupy all active sites at once and some degradation might still be possible (Shibatani et al., 2006).

An *in vitro* degradation of polyUb securin by proteasome complexes from IFN- $\gamma$  treated and untreated RKO cells also showed that the substrate is efficiently bound, deubiquitinated and degraded. However, even after 24 hours, a small amount of polyUb securin was still present in both reactions even though the concentration of proteasome complexes was the same as in the previous assay. One possible explanation for that could be the higher amount of GST-UBL still present in the proteasome sample. The GST-UBL competes with polyUb securin for the binding site on Rpn10, thus most probably interferes with the initial, substrate binding step.

#### **4.4. Analysis of the generated pattern of peptide fragments by different proteasome complexes**

After confirmation that purified proteasome complexes are indeed active and degrade produced polyUb securin, the investigation of cleavage specificities of purified proteasome complexes followed. For that purpose, an *in vitro* degradation assay and subsequent analysis of the generated pattern of peptide fragments were used and adapted from Cascio & Goldberg

(2005). To minimize the possibility of reentry and repeated cleavage of peptides already released by the proteasome, it was important to perform an *in vitro* assay in the presence of an initial large molar excess of the substrate over the enzyme and to ensure that the fraction of substrate consumed is never 100%. Previous, similar studies were performed, however, only with the PA28 $\alpha\beta$  and 26S proteasome mixtures and with partially denatured, non-ubiquitinated proteins as substrates (Cascio & Goldberg, 2005). Here, the same approach was used, but with a polyUb substrate, to investigate the effect of IFN- $\gamma$  induction of PA28 $\alpha\beta$  and  $\beta$ i subunits, mostly  $\beta$ 2i, on proteasome cleavage pattern. Likewise, the cleavage pattern of the 26S proteasome in the presence or absence of the PA28 $\alpha\beta$  or PA28 $\gamma$  complex was investigated.

According to the results obtained by an *in vitro* degradation of polyUb securin by proteasomes from IFN- $\gamma$  treated and untreated RKO cells, the same 24-hour assay was performed for analysis of peptide pattern since the degradation was not complete even after 24 hours. Unfortunately, the sequence coverage for both reactions did not exceed 47%, and less than a half of all detected peptides had a detection score above the significant value of 200.0. Thus, the information obtained was reasonably insufficient to draw any reliable conclusions.

Moreover, servers for prediction of cleavage sites generated a much higher number of different peptides (around 80) as well as much shorter peptides (four amino acids on average) than obtained experimentally. Such a difference between the predicted and experimentally obtained number of cleavages and peptide lengths indicate that either the peptide purification went wrong and smaller peptides most likely just went through the column and did not bind or detection was not sensitive enough to detect all, especially smaller peptides.

Nevertheless, the IFN- $\gamma$  induction of PA28 $\alpha\beta$  and/or  $\beta$ 2i did not affect the total number of different peptides generated and the mean peptide length, respectively. Although few unique peptides were detected in each reaction, only three of them had a significant score. This result contradicts previous degradation assays with PA28 $\alpha\beta$  enriched proteasome samples where the number of unique peptides increased significantly (Cascio & Goldberg, 2005, Raule et al., 2014). One explanation could be that due to the very low sequence coverage and/or detection of only longer peptides the possible unique peptides were not detected. Another possibility is that the relative amount of PA28 $\alpha\beta$  was not high enough to reproduce the result. Most probably, the majority of PA28 $\alpha\beta$  was not bound in hybrid proteasome complexes and was still in the extract after proteasome purification.

The impaired IFN- $\gamma$  induction of immunoproteasome complexes in RKO cells is the most probable explanation why there were not so many matches with predicted immunoproteasome potential cleavage sites. Only two potential iCP cleavage sites were identified, Ala20 and Leu161 followed by Gly162, that are consistent with a preference of immunoproteasomes for hydrophobic amino acids at the P1 position and Gly at P1' position (Toes et al., 2001).

For the investigation of different hybrid proteasome complexes on the pattern of peptides generated after degradation of polyUb substrate, a method developed by Cascio et al. (2002) and Kopp et al. (2001) for *in vitro* reconstitution of hybrid complexes from purified components was used. At the time, only PA28 $\alpha\beta$  and PA28 $\gamma$  complexes were available for this type of assay. Since proteasome samples from bovine heart did not contain 11S and PA200 proteasome activators, but only pure 26S proteasome subunits, they were most adequate for *in vitro* reconstitution with PA28 complexes and the following degradation of polyUb securin.

In this experiment the sequence coverage was much higher (around 90%) than with RKO cells and consequently so was the number of peptides detected with a score above 200.0. The size distribution of the products of the 26S proteasome was affected by the formation of the hybrid complexes that is in the presence of PA28 $\alpha\beta$  or PA28 longer peptides were produced. Moreover, the number of different peptides increased in both *in vitro* reactions. This indicates that both PA28 proteasome activators broaden the spectrum of degradation products by expanding the number of peptide bonds susceptible to hydrolysis once the substrate enters the 20S CP. It is possible that this increase in the peptide bonds susceptible to hydrolysis occurs due to the allosteric regulation of specificity pockets (Sn – Sn') of the 20S CP by the PA28 proteasome activators.

These changes in peptide production were additionally confirmed by mass spectrometry sequencing, which showed that while many peptides were generated both by 26S proteasomes and hybrid proteasome complexes (19S-20S-PA28 $\alpha\beta$  and 19S-20S-PA28 $\gamma$ ) several were generated only if PA28 $\alpha\beta$  or PA28 $\gamma$ , or both were present. Much higher percentage of peptides generated only in the presence of PA28 $\alpha\beta$ , and not PA28 $\gamma$  suggests non-equivalent allosteric regulation of active sites in hybrid proteasome complexes by the PA28 $\alpha\beta$  and PA28 $\gamma$ . This finding could be explained by the observations made by Li & Rechsteiner (2001) that binding of PA28 $\gamma$  to only 20S CP results in a selective allosteric stimulation of only the trypsin-like activity and the chymotrypsin-like and PGPH-like activities

are suppressed while PA28 $\alpha\beta$  stimulates all three proteolytic activities and presumably have a much more complex allosteric effect on the 20S CP.

Specifically, most of the unique peptides generated in the presence of PA28 $\alpha\beta$  and/or PA28 $\gamma$  are positioned in the N terminal part of securin, an observation similar to the one made by Cascio et. al., (2002) with IGF-1 degradation in the presence of PA28 $\alpha\beta$ . The interpretation that this is due to the prevention of the complete degradation of this region to di/tripeptides would suggest that the 11S regulators might indeed serve as some sort of a smart sieve allowing the passage of only certain peptides while the main route of product exit would be through 19S RP. At the same time, these results strongly oppose the role of 11S regulators in hybrid proteasomes as simple-gate openers for accelerated product release because in that case, one would expect the same set of products in the presence or absence of 11S regulators; but the products would appear sooner. Moreover, the observation that the rate of protein hydrolysis does not change in the presence of PA28 $\alpha\beta$  strongly opposed this role as well (Cascio et al., 2002).

Since it seems that the formation of hybrid proteasome indeed changes the cleavage specificities of the 26S proteasome, a much deeper peptide sequence analysis not covered in this thesis should be done, e.g., the amino acid composition of unique peptides. Likewise, this effect should preferably be investigated on a variety of different polyUb substrates with different biological contexts to see whether this is substrate dependent and to what extent and what would be the biological implication of having different set of peptides.

Also, a screening for more possible conditions under which hybrid proteasomes form, e.g., increase in overall substrate concentration, increase of a certain substrate/s concentration, presence of different PIPs, postranslation modifications etc., could also help in shedding more light on what would be the biological function of these complexes.

#### **4.5. Inspection of purified proteasome complexes by negative stain TEM and structural analysis of the hybrid proteasome by single-particle cryo-EM**

Proteasome complexes purified from bovine testes and IFN- $\gamma$  treated RKO cells were used for structural analysis of hybrid proteasome complexes. The negative stain TEM analysis of purified proteasomes complexes showed uniformly distributed particles over the carbon film, in amounts scarcely sufficient for further analysis. Moreover, completely pure fractions, i.e. fractions containing only one type of proteasome complex, could not be obtained, and most of the fractions contained all proteasome complexes in different amounts. Hybrid proteasome



complexes were mainly seen in fractions 14 and 15 together with 26S proteasomes and smaller portion of 30S proteasome complexes and their amount did not exceed more than a few percents.

The approximate percentage of hybrid proteasome complexes was calculated by collecting a negative stain dataset and subsequent processing of micrographs to obtain 2D class averages. Only particles belonging to 2D class averages showing (tilted) side views of the complex can be unambiguously assigned to the hybrid proteasome complex, while the top and the bottom views could easily be mistaken for the 26S proteasome. The relatively low amounts of the hybrid particles seen in negative stain electron micrographs, 6.9% and 1.3% in the sample from IFN- $\gamma$  treated RKO cells and bovine testes, respectively, probably underestimates their actual abundance in solution. The low amount could be either due to the centrifugal force of 100 000 $\times$ g and large dilution of the sample during density gradient ultracentrifugation which might cause the dissociation of 11S/PA200 proteasome activators or relatively harsh procedures (e.g., staining, blotting) during the preparation of negative stain EM grids.

Distinct proteasome activators were assigned to certain 2D class averages of hybrid proteasome complexes based on the previously published electron micrographs of the 20S CP bound PA28 and PA200 proteasome activators (**Figure 4.1**) (Jiang et al., 2018). The presence of only PA200 containing hybrid proteasome complexes in 2D class averages from bovine testes is not surprising since, as already mentioned, this proteasome activator is highly abundant in testes (Rechsteiner & Hill, 2005).

Meanwhile, the amount of PA28 $\alpha\beta$  hybrid proteasome complexes from RKO cells was meager, despite the IFN- $\gamma$  induction of the PA28 $\alpha\beta$ . The reason could be that the induction was not as effective as in other cases (Tanahashi et al., 2000) due to a different cell line and/or PA28 complexes are much more susceptible to dissociation upon sample preparation conditions mentioned above or during the proteasome purification steps. The latter would also explain the lack of hybrid proteasomes with PA28 activators in the sample from bovine testes.

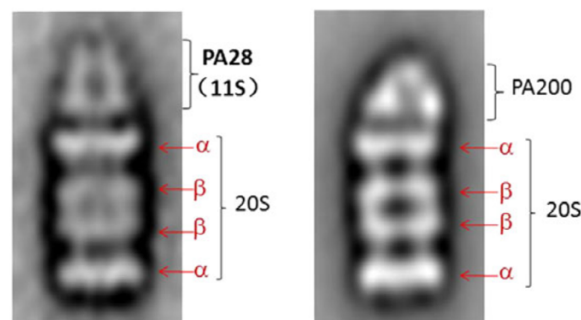


**Figure 4.1.** Electron micrographs of two different singly-capped forms of proteasomes.

**A) PA28-proteasomes include the PA28 $\alpha\beta$ -proteasome and the PA28 $\gamma$ -proteasome. B) The PA200-proteasome complex. Taken from (Jiang et al., 2018).**

Despite a small percentage of hybrid proteasomes seen in negative stain micrographs, cryo-grids of corresponding gradient fractions were prepared and datasets collected for the sample from bovine testicles and IFN- $\gamma$  treated RKO cells. During most steps of the micrograph processing (e.g., manual particle picking, reference-free 2D classification, and an initial model building) particles of hybrid proteasomes were not clearly and undoubtedly visible due to their low share in the overall number of picked particles. Only after applying a mask on the region where 11S or PA200 regulators are positioned in the hybrid proteasome complex, 3D class-averages were detected with densities different from densities that correspond to the 19S RP in the 30S proteasome complex. Particles belonging to those 3D class averages were extracted and in case of the bovine testes upon two rounds of refinement, a cryo-EM 3D reconstruction of the hybrid proteasome complex was obtained to a resolution of 26.81 Å. Meanwhile, the same situation was not for particles extracted from IFN- $\gamma$  treated RKO cells. Those particles had to be subjected to one more round of reference-free 2D-classification to remove junk particles and only after the particle-stack cleaning the subsequent two rounds of refinement resulted in a cryo-EM 3D reconstruction resembling the hybrid proteasome complex obtained to a resolution of 13.08 Å. However certain features of final models, especially the one obtained from IFN- $\gamma$  treated RKO cells, are smeared. The smeared features could be explained either because certain missing views of the complex or because some views of the complex are more presented than the others. The resolution limit in each case can be explained with the deficient number of high-quality particle images and the coinciding missing angles of the particle views.

Undoubtedly, the amount of hybrid proteasome complexes that can be obtained from cell extracts is insufficient for obtaining a high-resolution structures and, as already mentioned, a procedure for obtaining a sample should be adjusted to result in a more pure and concentrated hybrid proteasome sample. For this one could use an already described *in vitro* reconstitution approach and further more try to optimize the conditions of reconstitution that would favour a more efficient complex formation. Once obtained, the high-resolution structures of hybrid proteasome complexes could be compared with the already existing high-resolution structures of the 26S proteasome. Such comparison could potentially reveal structural features that would explain different cleavage patterns described in this thesis. More deeper structural characterization and comparison could give insights whether formation of these hybrid complexes perhaps changes the dynamic of entire complex.

## 5. Conclusions

- Affinity purification of mammalian proteasomes using the GST-tagged ubiquitin-like domain from a human Rad23B as a bait protein proved to be a sufficiently sensitive and effective method for the isolation of hybrid proteasomes without much impact on the integrity of the complex.
- The protein identification by mass spectrometry showed that PA28 $\alpha\beta$ , PA28 $\gamma$  and PA200 proteasome activators are constitutively expressed in bovine brain, liver, spleen, pancreas and testes, but their presence was not detected in bovine heart.
- The relative amount of PA28 $\alpha\beta$ , PA28 $\gamma$  or PA200 within the hybrid proteasome complex was comparable between different proteasome activators in every bovine organ, except spleen, where more PA28 $\alpha\beta$  was involved in the formation of hybrid proteasomes than PA28 $\gamma$  and PA200.
- RKO cells constitutively express PA28 $\alpha\beta$ , PA28 $\gamma$  and PA200 proteasome activators and inducible  $\beta$ 2i and  $\beta$ 5i subunits. Upon IFN- $\gamma$  treatment, the relative amount of PA28 $\alpha\beta$  and of inducible  $\beta$ 2i subunit increased.
- The relative amount of PA28 $\alpha\beta$  within the hybrid proteasomes in RKO cells hasn't significantly changed after the IFN- $\gamma$  treatment which contradicts previous observations stated in the literature. Since RKO cells are deficient in the formation of iCPs, the low levels of PA28 $\alpha\beta$  hybrid proteasomes despite the induction of PA28 $\alpha\beta$  by IFN- $\gamma$  indicates a possible preference of PA28 $\alpha\beta$  to form a hybrid proteasome with the iCP rather than with the cCP.
- IFN- $\gamma$  induction of PA28 $\alpha\beta$  and  $\beta$ 2i/ $\beta$ 5i subunits had no significant influence on cleavage specificities of proteasome complexes. The lack of a large-scale effect on the 26S proteasome cleavage specificities highlights the deficiency in the formation of iCPs.
- In the presence of *in vitro* reconstituted hybrid proteasome complexes the cleavage specificities of the 26S proteasome are changed; the number of different peptides is greater and peptides with unique sequences are generated, and the mean peptide size is slightly increased. The observed change in the peptide pattern was more significant in the presence of PA28 $\alpha\beta$  hybrid proteasomes than PA28 $\gamma$  hybrid proteasomes. These results imply that PA28 proteasome activators in hybrid proteasome complexes do not play just a simple role in opening the 20S CP gate for the release of degradation products, but also affect the

cleavage specificities of 20S CP, the extent of which is much higher by the PA28 $\alpha\beta$  than PA28 $\gamma$ .

- The majority of the negative stain 2D class averages and the obtained cryo-EM 3D reconstructions represent the PA200 hybrid proteasome complex. This indicates that this hybrid proteasome complex is either the most abundant, the most stable hybrid proteasome complex, or both, in bovine testes and IFN- $\gamma$  treated RKO cells, respectively.
- Very low amounts of hybrid proteasome complexes that had been obtained directly from organ or cell extracts were insufficient for detailed structural analysis by single-particle cryo-EM. Moreover, the cryo-grid preparing conditions such as blotting, might also have a negative influence on the final amount of complexes in collected micrographs and additionally decrease the number of hybrid proteasome particles. However, rather than collecting much bigger datasets, a strategy for obtaining samples enriched with hybrid proteasome complexes is of great interest for further studies of their structural characteristics as well as for conducting a more sophisticated functional assays.

## 6. Literature

1. Agard, D., Cheng, Y., Glaeser, R. M., & Subramaniam, S. (2014). Single-particle cryo-electron microscopy (cryo-EM): Progress, challenges, and perspectives for further improvement. In P. Hawkes (Ed.), *Advances in Imaging and Electron Physics* (1<sup>st</sup> edition, Vol. 185, pp. 113–137). Elsevier.
2. Bai, X. chen, McMullan, G., & Scheres, S. H. W. (2015). How cryo-EM is revolutionizing structural biology. *Trends in Biochemical Sciences*, 40(1), 49–57.
3. Bajorek, M., & Glickman, M. H. (2004). Ubiquitin-proteasome system. *Cellular and Molecular Life Sciences*, 61(13), 1579–1588.
4. Bard, J. A. M., Goodall, E. A., Greene, E. R., Jonsson, E., Dong, K. C., & Martin, A. (2018). Structure and Function of the 26S Proteasome. *Annual Review of Biochemistry*, 87, 697–724.
5. Besche, H. C., & Goldberg, A. L. (2012). Affinity Purification of Mammalian 26S Proteasomes Using an Ubiquitin-Like Domain. In R. J. Dohmen & M. Scheffner (Ed.), *Ubiquitin Family Modifiers and the Proteasome* (Vol. 832, pp. 423–432). Springer Science+Business Media, LCC.
6. Brown, N. G., VanderLinden, R., Watson, E. R., Weissmann, F., Ordureau, A., Wu, K. P., Zhang, W., Yu, S., Mercredi, P. Y., Harrison, J. S., Davidson, I. F., Qiao, R., Lu, Y., Dube, P., Brunner, M. R., Grace, C. R. R., Miller, D. J., Haselbach, D., Jarvis, M. A., Yamaguchi, M., Yanishevski, D., Petzold, G., Sidhu, S. S., Kuhlman, B., Kirschner, M. W., Wade Harper, J., Peters, J. M., Stark, H., & Schulman, B. A. (2016). Dual RING E3 architectures regulate multiubiquitination and ubiquitin chain elongation by APC/C. *Cell*, 165(6), 1440–1453.
7. Cascio, P. (2014). PA28 $\alpha\beta$ : The enigmatic magic ring of the proteasome? *Biomolecules*, 4(2), 566–584.
8. Cascio, P., Call, M., Petre, B. M., Walz, T., & Goldberg, A. L. (2002). Properties of the hybrid form of the 26S proteasome containing both 19S and PA28 complexes. *EMBO Journal*, 21(11), 2636–2645.
9. Cascio, P., & Goldberg, A. L. (2005). Preparation of hybrid (19S-20S-PA28) proteasome complexes and analysis of peptides generated during protein degradation. *Methods in Enzymology*, 398(1999), 336–352.
10. Chen, S., Wu, J., Lu, Y., Ma, Y.-B., Lee, B.-H., Yu, Z., Ouyang, Q., Finley, D. J., Kirschner, M. W., & Mao, Y. (2016). Structural basis for dynamic regulation of the

- human 26S proteasome. *Proceedings of the National Academy of Sciences*, 113(46), 12991–12996.
11. Chen, X., Barton, L. F., Chi, Y., Clurman, B. E., & Roberts, J. M. (2007). Ubiquitin-Independent Degradation of Cell-Cycle Inhibitors by the REG $\gamma$  Proteasome. *Molecular Cell*, 26(6), 843–852.
  12. Ciechanover, A., & Brundin, P. (2003). The ubiquitin proteasome system in neurodegenerative diseases: sometimes the chicken, sometimes the egg. *Neuron*, 40(2), 427–446.
  13. Coux, O., Tanaka, K., & Goldberg, A. L. (1996). Structure and Functions of the 20S and 26S Proteasomes. *Annual Review of Biochemistry*, 65(1), 801–847.
  14. Dahlmann, B. (2016). Mammalian proteasome subtypes: Their diversity in structure and function. *Archives of Biochemistry and Biophysics*, 591, 132–140.
  15. de la Pena, A. H., P., Goodall, E. A., Gates, S. N., Lander, G. C., & Martin, A. (2018). Structures of the substrate-engaged 26S proteasome reveal the mechanisms for ATP hydrolysis-driven translocation. **bioRxiv preprint first posted online Aug. 16, 2018.**
  16. DeMartino, G. N., & Slaughter, C. A. (1999). The proteasome, a novel protease regulated by multiple mechanisms. *The Journal of Biological Chemistry*, 274(20), 22123–22126.
  17. Fabre, B., Lambour, T., Delobel, J., Amalric, F., Monsarrat, B., Burlet-Schiltz, O., & Bousquet-Dubouch, M. P. (2013). Subcellular Distribution and Dynamics of Active Proteasome Complexes Unraveled by a Workflow Combining in Vivo Complex Cross-Linking and Quantitative Proteomics. *Molecular & Cellular Proteomics*, 12(3), 687–699.
  18. Ferrell, K., Wilkinson, C. R. ., Dubiel, W., & Gordon, C. (2000). Regulatory subunit interactions of the 26S proteasome, a complex problem. *Trends in Biochemical Sciences*, 25(2), 83–88.
  19. Finley, D., Chen, X., & Walters, K. J. (2016). Gates, Channels, and Switches: Elements of the Proteasome Machine. *Trends in Biochemical Sciences*, 41(1), 77–93.
  20. Frank, J. (2002). Single-Particle Imaging of Macromolecules by Cryo-Electron Microscopy. *Annual Review of Biophysics and Biomolecular Structure*, 31(1), 303–319.
  21. Gasteiger, E., Hoogland, C., Gattiker, A., Duvaud, S., Wilkins, M. R., Appel, R. D., & Bairoch, A. (2005). Protein Identification and Analysis Tools on the ExPASy Server. *The Proteomics Protocols Handbook*, 571–607.

22. Glickman, M. H., Rubin, D. M., Fried, V. A., & Finley, D. (1998). The Regulatory Particle of the *Saccharomyces cerevisiae* Proteasome. *Molecular and Cellular Biology*, 18(6), 3149–3162.
23. Groll, M., Bajorek, M., Köhler, A., Moroder, L., Rubin, D. M., Huber, R., Glickman, M. H., & Finley, D. (2000). A gated channel into the proteasome core particle. *Nature Structural Biology*, 7(11), 1062–1067.
24. Groll, M., Ditzel, L., Löwe, J., Stock, D., Bochtler, M., Bartunik, H. D., & Huber, R. (1997). Structure of 20S proteasome from yeast at 2.4 Å resolution. *Nature*, 386(3), 463-771.
25. Groll, M., & Huber, R. (2003). Substrate access and processing by the 20S proteasome core particle. *International Journal of Biochemistry and Cell Biology*, 35(5), 606–616.
26. Groll, M., & Huber, R. (2004). Inhibitors of the eukaryotic 20S proteasome core particle: A structural approach. *Biochimica et Biophysica Acta - Molecular Cell Research*, 1695(1–3), 33–44.
27. Hagemann, C., Patel, R., & Blank, J. L. (2003). MEKK3 interacts with the PA28gamma regulatory subunit of the proteasome. *The Biochemical Journal*, 373(1), 71–79.
28. Hagting, A., Den Elzen, N., Vodermaier, H. C., Waizenegger, I. C., Peters, J. M., & Pines, J. (2002). Human securin proteolysis is controlled by the spindle checkpoint and reveals when the APC/C switches from activation by Cdc20 to Cdh1. *Journal of Cell Biology*, 157(7), 1125–1137.
29. Harauz, G., & van Heel, M. (1986). Exact filters for general geometry three dimensional reconstruction. *Optik*, 73, 146-156.
30. Harshbarger, W., Miller, C., Diedrich, C., & Sacchettini, J. (2015). Crystal structure of the human 20S proteasome in complex with carfilzomib. *Structure*, 23(2), 418–424.
31. Haselbach, D., Schrader, J., Lambrecht, F., Henneberg, F., Chari, A., & Stark, H. (2017). Long-range allosteric regulation of the human 26S proteasome by 20S proteasome-targeting cancer drugs. *Nature Communications*, 8, 15578.
32. He, J., Kulkarni, K., Da Fonseca, P. C. A., Krutauz, D., Glickman, M. H., Barford, D., & Morris, E. P. (2012). The structure of the 26S proteasome subunit Rpn2 reveals its PC repeat domain as a closed toroid of two concentric  $\alpha$ -helical rings. *Structure*, 20(3), 513–521.
33. Heink, S., Fricke, B., Ludwig, D., Kloetzel, P. M., & Krüger, E. (2006). Tumor cell lines expressing the proteasome subunit isoform LMP7E1 exhibit immunoproteasome deficiency. *Cancer Research*, 66(2), 649–652.

34. Hendil, K. B. (1998). Simultaneous binding of PA28 and PA700 activators to 20 S proteasomes. *The Biochemical Journal*, 332(3), 749–754.
35. Hershko, A., & Ciechanover, A. (1998). The Ubiquitin System. *Annual Review of Biochemistry*, 67, 425-479.
36. Hoffman, L., Pratt, G., & Rechsteiner, M. (1992). Multiple Forms of the 20-S Multicatalytic and the 26-S Ubiquitin/ATP-Dependent Proteases from Rabbit Reticulocyte Lysate. *Journal of Biological Chemistry*, 267(31), 22362–22368.
37. Huang, L., Haratake, K., Miyahara, H., & Chiba, T. (2016). Proteasome activators, PA28 $\gamma$  and PA200, play indispensable roles in male fertility. *Scientific Reports*, 6(March), 2–10.
38. Huber, E. M., Basler, M., Schwab, R., Heinemeyer, W., Kirk, C. J., Groettrup, M., & Groll, M. (2012). Immuno- and constitutive proteasome crystal structures reveal differences in substrate and inhibitor specificity. *Cell*, 148(4), 727–738.
39. Huber, E. M., & Groll, M. (2017). The Mammalian Proteasome Activator PA28 Forms an Asymmetric  $\alpha_4\beta_3$  Complex. *Structure*, 25(10), 1473–1480.
40. Iwanczyk, J., Sadre-Bazzaz, K., Ferrell, K., Kondrashkina E., Formosa, T., Hill, C. P., & Ortega, J. (2006). Structure of the Blm10-20S Proteasome Complex by Cryo-electron Microscopy. Insights into the Mechanism of Activation of Mature Yeast Proteasomes. *Journal of Molecular Biology*, 363(3), 648-659.
41. Jiang, T. X., Zhao, M., & Qiu, X. B. (2018). Substrate receptors of proteasomes. *Biological Reviews*, 8, 000-000.
42. Jin, L., Williamson, A., Banerjee, S., Philipp, I., & Rape, M. (2008). Mechanism of Ubiquitin-Chain Formation by the Human Anaphase-Promoting Complex. *Cell*, 133(4), 653–665.
43. Khor, B., Bredemeyer, A. L., Huang, C.-Y., Turnbull, I. R., Evans, R., Maggi, L. B., White, J. M., Walker, L. M., Carnes, K., Hess, R. A., & Sleckman, B. P. (2006). Proteasome activator PA200 is required for normal spermatogenesis. *Molecular and Cellular Biology*, 26(8), 2999–3007.
44. Kish-Trier, E., & Hill, C. P. (2013). Structural Biology of the Proteasome. *Annual Review of Biophysics*, 42(1), 29–49.
45. Kopp, F., Dahlmann, B., & Kuehn, L. (2001). Reconstitution of hybrid proteasomes from purified PA700-20 S complexes and PA28 $\alpha\beta$  activator: Ultrastructure and peptidase activities. *Journal of Molecular Biology*, 313(3), 465–471.



46. Kuttler, C., Nussbaum, A.K., Dick, T.P., Rammensee, H. G., Schild, H., & Haderler, K.P. (2000). An algorithm for the prediction of proteasomal cleavages. *Journal of Molecular Biology*, 298, 417-429
47. Lander, G. C., Estrin, E., Matyskiela, M. E., Bashore, C., Nogales, E., & Martin, A. (2012). Complete subunit architecture of the proteasome regulatory particle. *Nature*, 482(7384), 186–191.
48. Li, J., Gao, X., Joss, L., & Rechsteiner, M. (2000). The proteasome activator 11 S REG or PA28: Chimeras implicate carboxyl-terminal sequences in oligomerization and proteasome binding but not in the activation of specific proteasome catalytic subunits. *Journal of Molecular Biology*, 299(3), 641–654.
49. Li, J., & Rechsteiner, M. (2001). Molecular dissection of the 11S REG (PA28) proteasome activators. *Biochimie*, 83(3–4), 373–383.
50. Li, J., Yakushi, T., Parlati, F., MacKinnon, A. L., Perez, C., Ma, Y., Carter, K. P., Colayco, S., Magnuson, G., Brown, B., Nguyen, K., Vasile, S., Suyama, E., Smith, L. H., Sergienko, E., Pinkerton, A. B., Chung, T. D. Y., Palmer, A. E., Pass, I., Hess, S., Cohen, S. M., & Deshaies, R. J. (2017). Capzimin is a potent and specific inhibitor of proteasome isopeptidase Rpn11. *Nature Chemical Biology*, 13(5), 486–493.
51. Li, X., Amazit, L., Long, W., Lonard, D. M., Monaco, J. J., & O'Malley, B. W. (2007). Ubiquitin- and ATP-Independent Proteolytic Turnover of p21 by the REG $\gamma$ -Proteasome Pathway. *Molecular Cell*, 26(6), 831–842.
52. Li, X., Lonard, D. M., Jung, S. Y., Malovannaya, A., Feng, Q., Qin, J., Tsai, S. Y., Tsai, M., & O'Malley, B. W. (2006). The SRC-3/AIB1 coactivator is degraded in a ubiquitin- and ATP-independent manner by the REG $\gamma$  proteasome. *Cell*, 124(2), 381–392.
53. Löwe, J., Stock, D., Jap, B., Zwickl, P., Baumeister, W., & Huber, R. (1995). Crystal Structure of the 20S proteasome from the Archaeon *T. acidophilum* at 3.4 Å Resolution. *Science*, 268, 533–539.
54. Mao, I., Liu, J., Li, X., & Luo, H. (2008). REG $\gamma$ , a proteasome activator and beyond? *Cellular and Molecular Life Sciences*, 65(24), 3971–3980.
55. Marques, A. J., Palanimurugan, R., Matias, A. C., Ramos, P. C., & Dohmen, R. J. (2009). Catalytic Mechanism and Assembly of the Proteasome Catalytic Mechanism and Assembly of the Proteasome. *Chemical Reviews*, 109, 1509–1536.
56. Mastronarde, D. N. (2005). Automated electron microscope tomography using robust prediction of specimen movements. *Journal of Structural Biology*, 152(1), 36–51.
57. Matthews, W., Driscoll, J., Tanaka, K., Ichihara, A., & Goldberg, A. L. (1989). Involvement of the proteasome in various degradative processes in mammalian cells.

- Proceedings of the National Academy of Sciences of the United States of America, 86(8), 2597–2601.
58. Moriishi, K., Okabayashi, T., Nakai, K., Moriya, K., Koike, K., Murata, S., Chiba, T., Tanaka, K., Suzuki, R., Suzuki, T., Miyamura, T., & Matsuura, Y. (2003). Proteasome activator PA28 $\gamma$ -dependent nuclear retention and degradation of hepatitis C virus core protein. *Journal of Virology*, 77(19), 10237–10249.
  59. Murata, S., Kawahara, H., Tohma, S., Yamamoto, K., Kasahara, M., Nabeshima, Y. I., Tanaka, K., & Chiba, T. (1999). Growth retardation in mice lacking the proteasome activator PA28 $\gamma$ . *Journal of Biological Chemistry*, 274(53), 38211–38215.
  60. Nie, J., Wu, M., Wang, J., Xing, G., He, F., & Zhang, L. (2010). REG $\gamma$  proteasome mediates degradation of the ubiquitin ligase Smurf1. *FEBS Letters*, 584(14), 3021–3027.
  61. Nielsen, M., Lundegaard, C., Lund, O., & Kesmir, C. (2005). The role of the proteasome in generating cytotoxic T cell epitopes: Insights obtained from improved predictions of proteasomal cleavage. *Immunogenetics*, 57(1-2), 33-41.
  62. Noda, C., Tanahashi, N., Shimbara, N., Hendil, K. B., & Tanaka, K. (2000). Tissue distribution of constitutive proteasomes, immunoproteasomes, and PA28 in rats. *Biochemical and Biophysical Research Communications*, 277(2), 348–354.
  63. Nussbaum, A. K., Dick, T. P., Keilholz, W., Schirle, M., Stevanovic, S., Dietz, K., Heinemeyer, W., Groll, M., Wolf, D. H., Huber, R., Rammensee, H. G., & Schild, H. (1998). Cleavage motifs of the yeast 20S proteasome subunits deduced from digests of enolase 1. *Proceedings of the National Academy of Sciences*, 95(21), 12504–12509.
  64. Nussbaum, A.K., Kuttler, C., Haderl, K.P., Rammensee, H. G., Schild, H. (2001). PProC: A Prediction Algorithm for Proteasomal Cleavages. *Immunogenetics*, 53, 87-94.
  65. Ohi, M., Li, Y., Cheng, Y., & Waiz, T. (2004). Negative Staining and Image Classification – Powerful Tools in Modern Electron microscopy. *Biological Procedures Online*, 6(1), 23-24.
  66. Opoku-Nsiah, K. A., & Gestwicki, J. E. (2018). Aim for the core: suitability of the ubiquitin-independent 20S proteasome as a drug target in neurodegeneration. *Translational Research*, 1–10.
  67. Orlova, E. V., & Saibil, H. R. (2011). Structural analysis of macromolecular assemblies by electron microscopy. *Chem Rev*, 111(12), 7710–7748.

68. Ortega, J., Heymann, J. B., Kajava, A. V., Ustrell, V., Rechsteiner, M., & Steven, A. C. (2005). The axial channel of the 20 S proteasome opens upon binding of the PA200 activator. *Journal of Molecular Biology*, 346(5), 1221–1227.
69. Pettersen, E. F., Goddard, T. D., Huang, C. C., Couch, G. S., Greenblatt, D. M., Meng, E. C., & Ferrin, T. E. (2004). UCSF Chimera - A visualization system for exploratory research and analysis. *Journal of Computational Chemistry*, 25(13), 1605–1612.
70. Pickering, A. M., & Davies, K. J. A. (2012). Differential roles of proteasome and immunoproteasome regulators Pa28 $\alpha\beta$ , Pa28 $\gamma$  and Pa200 in the degradation of oxidized proteins. *Archives of Biochemistry and Biophysics*, 523(2), 181–190.
71. Prakash, S., Tian, L., Ratliff, K. S., Lehotzky, R. E., & Matouschek, A. (2004). An unstructured initiation site is required for efficient proteasome-mediated degradation. *Nature Structural and Molecular Biology*, 11(9), 830–837.
72. Punjani, A., Rubinstein, J. L., Fleet, D. J., & Brubaker, M. A. (2017). CryoSPARC: Algorithms for rapid unsupervised cryo-EM structure determination. *Nature Methods*, 14(3), 290–296.
73. Qian, M. X., Pang, Y., Liu, C. H., Haratake, K., Du, B. Y., Ji, D. Y., Wang, G. F., Zhu, Q., Q., Song, W., Yu, Y., Zhang, X. X., Huang, H. T., Miao, S., Chen, L. B., Zhang, Z. H., Liang, Y. N., Liu, S., Cha, H., Yang, D., Zhai, Y., Komatsu, T., Tsuruta, F., Li, H., Cao, C., Li, W., Li, G. H., Cheng, Y., Chiba, T., Wang, L., Goldberg, A. L., Shen, Y., & Qiu, X. B. (2013). Acetylation-mediated proteasomal degradation of core histones during DNA repair and spermatogenesis. *Cell*, 153(5).
74. Raule, M., Cerruti, F., Benaroudj, N., Migotti, R., Kikuchi, J., Bachi, A., Navon, A., Dittmar, G., & Cascio, P. (2014). PA28 $\alpha\beta$  reduces size and increases hydrophilicity of 20S immunoproteasome peptide products. *Chemistry and Biology*, 21(4), 470–480.
75. Rechsteiner, M., & Hill, C. P. (2005). Mobilizing the proteolytic machine: Cell biological roles of proteasome activators and inhibitors. *Trends in Cell Biology*, 15(1), 27–33.
76. Rosenzweig, R., & Glickman, M. H. (2008). Chaperone-driven proteasome assembly. *Biochemical Society Transactions*, 36(5), 807–812.
77. Sadre-Bazzaz, K., Whitby, F. G., Robinson, H., Formosa, T., & Hill, C. P. (2010). Structure of a Blm10 Complex Reveals Common Mechanisms for Proteasome Binding and Gate Opening. *Molecular Cell*, 37(5), 728–735.
78. Scheffner, M., Nuber, U., & Huibregtse, J. M. (1995). Protein ubiquitination involving an E1–E2–E3 enzyme ubiquitin thioester cascade. *Nature*. 373, 81–83.

79. Schmeisser, M., Heisen, B. C., Luettich, M., Busche, B., Hauer, F., Koske, T., Knauber, K. H., & Stark, H. (2009). Parallel, distributed and GPU computing technologies in single-particle electron microscopy. *Acta Crystallographica Section D: Biological Crystallography*, 65(7), 659–671.
80. Schmidt, M., & Finley, D. (2014). Regulation of proteasome activity in health and disease. *Biochimica et Biophysica Acta - Molecular Cell Research*, 1843(1), 13–25.
81. Schmidt, M., Hanna, J., Elsasser, S., & Finley, D. (2005). Proteasome-associated proteins: Regulation of a proteolytic machine. *Biological Chemistry*, 386(8), 725–737.
82. Schweitzer, A., Aufderheide, A., Rudack, T., Beck, F., Pfeifer, G., Plitzko, J. M., Sakata, E., Schulten, K., Förster, F., & Baumeister, W. (2016). Structure of the human 26S proteasome at a resolution of 3.9 Å. *Proceedings of the National Academy of Sciences*, 113(28), 7816–7821.
83. Shibatani, T., Carlson, E. J., Larabee, F., McCormack, A. L., Früh, K., & Skach, W. R. (2006). Global organization and Function of Mammalian Cytosolic Proteasome Pools: Implications for PA28 and 19S Regulatory complexes. *Molecular Biology of the Cell*, 17, 4962-4971.
84. Soza, A., Knuehl, C., Groettrup, M., Henklein, P., Tanaka, K., & Kloetzel, P. M. (1997). Expression and subcellular localization of mouse 20S proteasome activator complex PA28. *FEBS Letters*, 413, 27-34.
85. Stadtmueller, B. M., & Hill, C. P. (2011). Proteasome Activators. *Molecular Cell*, 41, 8-19.
86. Suzuki, R., Moriishi, K., Fukuda, K., Shirakura, M., Ishii, K., Shoji, I., Wakita, T., Miyamura, T., Matsuura, Y., & Suzuki, T. (2009). Proteasomal turnover of hepatitis C virus core protein is regulated by two distinct mechanisms: a ubiquitin-dependent mechanism and a ubiquitin-independent but PA28gamma-dependent mechanism. *Journal of Virology*, 83(5), 2389–2392.
87. Tanahashi, N., Murakami, Y., Minami, Y., Shimbara, N., Hendil, K. B., & Tanaka, K. (2000). Hybrid Proteasomes. Induction by Interferon- $\gamma$  and Contribution to ATP-dependent Proteolysis. *Biochemistry*, 275(19), 14336–14345.
88. Tanahashi, N., Yokota, K. Y., Ahn, J. Y., Chung, C. H., Fujiwara, T., Takahashi, E. I., DeMartino, G. N., Slaughter, C. A., Toyonaga, T., Yamamura, K., Shimbara, N., & Tanaka, K. (1997). Molecular properties of the proteasome activator PA28 family proteins and  $\gamma$ -interferon regulation. *Genes to Cells*, 2(3), 195–211.
89. Tanaka, K. (2009). The proteasome : Overview of structure and functions. *Proceedings of the Japan Academy*, 85, 12–36.

90. Tang, G., Peng, L., Baldwin, P. R., Mann, D. S., Jiang, W., Rees, I., & Ludtke, S. J. (2007). EMAN2: An extensible image processing suite for electron microscopy. *Journal of Structural Biology*, 157(1), 38–46.
91. Toes, R. E. M., Nussbaum, A. K., Degermann, S., Schirle, M., Emmerich, N. P. N., Kraft, M., Laplace, C., Zwinderman, A., Dick, T. P., Müller, J., Schönfish, B., Schmid, C., Fehlinf, H. J., Stevanovic, S., Rammensee, H. G., & Schild, H. (2001). Discrete cleavage motifs of constitutive and immunoproteasomes revealed by quantitative analysis of cleavage products. *The Journal of Experimental Medicine*, 194(1), 1–12.
92. Tomko, R. J., & Hochstrasser, M. (2013). Molecular Architecture and Assembly of the Eukaryotic Proteasome. *Annual Review of Biochemistry*, 82(1), 415–445.
93. Unno, M., Mizushima, T., Morimoto, Y., Tomisugi, Y., Tanaka, K., Yasuoka, N., & Tsukihara, T. (2002). The structure of the mammalian 20S proteasome at 2.75 Å resolution. *Structure*, 10(5), 609–618.
94. Ustrell, V., Hoffman, L., Pratt, G., & Rechsteiner, M. (2002). Pa200, a nuclear proteasome activator involved in DNA repair. *EMBO Journal*, 21(13), 3516–3525.
95. Vigneron, N., & Van den Eynde, B. J. (2014). Proteasome subtypes and regulators in the processing of antigenic peptides presented by class I molecules of the major histocompatibility complex. *Biomolecules*, 4(4), 994–1025.
96. Wade, R. A. (1992). A brief look at imaging and contrast transfer. *Ultramicroscopy*, 46(1-4), 145-156
97. Wang, X., Cimermancic, P., Yu, C., Schweitzer, A., Chopra, N., Engel, J. L., Greenberg, C., Huszagh, A. S., Beck, F., Sakata, E., Yang, Y., Novitsky, E. J., Leitner, A., Nanni, P., Kahraman, A., Guo, X., Dixon, J. E., Rychnovsky, S. D., Aebersold, R., Baumeister, W., Sali, A., & Huang, L. (2017). Molecular Details Underlying Structures and Regulation of the human 26S Proteasome.
98. Wehmer, M., Rudack, T., Beck, F., Aufderheide, A., Pfeifer, G., Plitzko, J. M., Förster, F., Schulten, K., Baumeister, W., & Sakata, E. (2017). Structural insights into the functional cycle of the ATPase module of the 26S proteasome. *Proceedings of the National Academy of Sciences*, 114(6), 1305–1310.
99. Welk, V., Coux, O., Kleene, V., Abeza, C., Trumbach, D., Eickelberg, O., & Meiners, S. (2016). Inhibition of proteasome activity induces formation of alternative proteasome complexes. *Journal of Biological Chemistry*, 291(25), 13147–13159.
100. Whitby, F. G., Masters, E. I., Kramer, L., Knowlton, J. R., Yao, Y., Wang, C. C., & Hill, C. P. (2000). Structural basis for the activation of 20S proteasomes by 11S regulators. *Nature*, 408(6808), 115–120.

101. Wolf, D. H., & Hilt, W. (2004). The proteasome: A proteolytic nanomachine of cell regulation and waste disposal. *Biochimica et Biophysica Acta - Molecular Cell Research*, 1695(1–3), 19–31.
102. Worden, E. J., Dong, K. C., & Martin, A. (2017). An AAA Motor-Driven Mechanical Switch in Rpn11 Controls Deubiquitination at the 26S Proteasome. *Molecular Cell*, 67(5), 799–811.
103. Yang, Y., Fruh, K., Ahn, K., & Peterson, P. A. (1995). In vivo assembly of the proteasomal complexes, implications for antigen processing. *Journal of Biological Chemistry*, 270(46), 27687–27694.
104. Zhang, K. (2016). Gctf: Real-time CTF determination and correction. *Journal of Structural Biology*, 193(1), 1–12.
105. Zheng, S. Q., Palovcak, E., Armache, J. P., Verba, K. A., Cheng, Y., & Agard, D. A. (2017). MotionCor2: Anisotropic correction of beam-induced motion for improved cryo-electron microscopy. *Nature Methods*, 14(4), 331–332.
106. Zhu, Y., Wang, W. L., Yu, D., Ouyang, Q., Lu, Y., & Mao, Y. (2018). Structural mechanism for nucleotide-driven remodeling of the AAA-ATPase unfoldase in the activated human 26S proteasome. *Nature Communications*, 9(1), 1–12.
107. Zivanov, J., Nakane, T., Forsberg, B., Kimanius, D., Hagen, W. J. H., Lindahl, E., & Scheres, S. H.W. (2018). RELION-3: new tool for automated high-resolution cryo-EM structure determination. *bioRxiv*, 2018.

## 7. Supplement informations

**Figure S1. Prediction of cleavage sites for securin by constitutive proteasomes and immunoproteasomes.**

**Table S1. Protein identification by mass spectrometry.**

**Table S2. Semiquantitative analysis of 11S/PA200 proteasome activators and  $\beta$ i subunits.**

**Table S3. Coverage details for the *in vitro* degradation of human securin by proteasome complexes from IFN- $\gamma$  treated and untreated RKO cells.**

**Table S4. Peptide details for the *in vitro* degradation of human securin by proteasome complexes from IFN- $\gamma$  treated and untreated RKO cells.**

**Table S5. Coverage details for the *in vitro* degradation of human securin by proteasome complexes from bovine heart in the presence or absence of PA28 proteasome activators.**

**Table S6. Peptide details for the *in vitro* degradation of human securin by proteasome complexes from bovine heart in the presence or absence of PA28 proteasome activators.**

**Table S7. Peptide details for the *in vitro* degradation of human securin by proteasome complexes from bovine heart in presence or absence of PA28 proteasome activators.**

**Table S8. t-Test Two-Sample Assuming Equal Variances of the peptide lengths generated from securin by proteasome complexes from RKO cells.**

**Table S9. -Test Two-Sample Assuming Equal Variances of the peptide lengths generated from securin by the 26S proteasome in the presence or absence of PA28 $\alpha\beta$  or PA28 $\gamma$ .**

**A)** PAPAroC predicts the following (82) proteasomal cleavages (made by human proteasome type III) in securin (212 amino acids):

1	MATLIY   VD   KE   NGEPTGRVV   A
21	KDGL   K   L   GSGPSIKAL   DG   RSQ
41	V   STPRFG   KTF   D   AP   PAL   P   KAT
61	RKA   LGT   V   NRATEKS   V   KTKGP
81	LK   Q   K   QP   SF   SA   K   K   MTEKT   V   KA
101	KSS   VP   ASD   D   A   YPEIEK   F   F   PF
121	NP   LDPE   S   F   DL   PEEH   Q   I   AHL   P
141	LSG   VPLMI   LD   E   EREL   EK   L   F   Q
161	L   GP   PSPVK   M   P   SP   PWES   N   LL   Q
181	S   PSSI   L   ST   L   D   V   ELP   PVA   A   D   I
201	D   IGG   C   G   HHHHHH

**B)** NetChop 3.0 predictions using version 20S. Threshold 0.500000

```

212 Sequence
MATLIYVDKENGEPGTRVVAKDGLKLGSGPSIKALDGRSQVSTPRFGKTFDAPPALPKATRKALGTVNRATEKSVKTKGP
SS.SSS.S.S.....S..S...S.S....S.SS..S..S.....SS.SS.....S.SS.S..S..S.S.S...
LKQKQPSFSAKKMTKTKVAKSSVPASDDAYPEIEKFFPNPLDFESFDLPEEHQIAHLPLSGVPLMILDEERELEKLFQ
..S.....S.S.....S.....SS.....S.SS.....SS.S.S.....S.S.S.....SS.S.SSSSSS..S.SSS
LGPPSPVKMPPWESNLLQSPSSILSTLDVELPPVAADIDIGGCGHHHHHH
S.....S.....SS.....SSSSSS.S...SS.S...SS.SS..
-----
Number of cleavage sites 77. Number of amino acids 212. Protein name Sequence

```

**Figure S1. Prediction of cleavage sites for securin by constitutive proteasomes and immunoproteasomes.**

**A)** PAPAroC prediction of cleavage sites. The output shows the predicted cleavage site indicated with red vertical bar and the number of predicted cleavage sites. The amino acid on the left side of a red vertical bar is the N terminal cutting site. **A)**NetChop prediction of cleavage sites. The output shows the predicted cleavage site indicated with symbol S and the number of predicted cleavage sites. The predicted cleavage site is after the assigned ‘S’ i.e. the peptide-bond on the C terminal side of an amino acid with an assigned ‘S’ is cleaved.

**Table S1. Protein identification by mass spectrometry.**

Gene	Description	Extract Norm. area.	Elution Norm. area.
<b>Bovine brain</b>			
PSMD11	26S proteasome non-ATPase regulatory subunit 11	2.70E+07	1.80E+09
PSMD13	26S proteasome non-ATPase regulatory subunit 13	2.46E+07	1.50E+09
PSMD3	26S proteasome non-ATPase regulatory subunit 3	8.76E+06	1.49E+09
PSMC6	26S proteasome regulatory subunit 10B	1.10E+07	1.38E+09
PSMC5	26S proteasome regulatory subunit 8	2.52E+07	1.37E+09
PSMC2	26S proteasome regulatory subunit 7	1.21E+07	1.24E+09
PSMA5	Proteasome subunit alpha type-5	1.30E+08	1.22E+09
PSMD4	26S proteasome non-ATPase regulatory subunit 4	1.61E+07	1.21E+09
RAD23B	UV excision repair protein RAD23 homolog B	4.12E+07	1.15E+09
PSMC4	26S proteasome regulatory subunit 6B	1.65E+07	1.14E+09
USP14	Ubiquitin carboxyl-terminal hydrolase 14	5.97E+07	1.10E+09
PSMD7	26S proteasome non-ATPase regulatory subunit 7	1.69E+07	1.09E+09
PSMD6	26S proteasome non-ATPase regulatory subunit 6	1.96E+07	1.04E+09
PSMD2	26S proteasome non-ATPase regulatory subunit 2	1.64E+07	1.03E+09
PSMA7	Proteasome subunit alpha type-7 OS=Bos taurus	1.01E+08	8.35E+08
PSMD8	26S proteasome non-ATPase regulatory subunit 8	1.69E+07	7.97E+08
PSMD12	26S proteasome non-ATPase regulatory subunit 12	7.00E+06	7.76E+08
PSMA3	Proteasome subunit alpha type-3	1.01E+08	6.79E+08
PSMA6	Proteasome subunit alpha type-6	6.36E+07	6.31E+08



PSMA2	Proteasome subunit alpha type-2	6.34E+07	5.97E+08
PSMB1	Proteasome subunit beta type-1	9.97E+07	5.96E+08
PSMA1	Proteasome subunit alpha type-1	6.96E+07	5.54E+08
PSMB2	Proteasome subunit beta type-2	6.03E+07	5.45E+08
PSMB6	Proteasome subunit beta type-6	6.40E+07	4.83E+08
PSMB3	Proteasome subunit beta type-3	7.25E+07	4.27E+08
PSMB4	Proteasome subunit beta type-4	6.32E+07	3.68E+08
PSMA4	Proteasome subunit alpha type-4	8.53E+07	3.61E+08
PSMB7	Proteasome subunit beta type-7	3.29E+07	2.38E+08
PSMB5	Proteasome subunit beta type-5	3.30E+07	2.22E+08
ADRM1	Proteasomal ubiquitin receptor ADRM1	5.18E+06	2.00E+08
UCHL5	Ubiquitin carboxyl-terminal hydrolase isozyme L5	3.86E+06	1.05E+08
PSMD9	26S proteasome non-ATPase regulatory subunit 9	1.41E+07	1.00E+08
PAAF1	Proteasomal ATPase-associated factor 1	4.39E+05	3.56E+07
PSMB9	Proteasome subunit beta type-9	2.12E+07	2.59E+07
PSMB10	Proteasome subunit beta type-10	8.57E+05	1.74E+07
PSMB8	Proteasome subunit beta type-8	4.09E+06	1.60E+07
PSMF1	Proteasome inhibitor PI31 subunit	1.19E+07	1.50E+07
RAD23A	UV excision repair protein RAD23 homolog A	1.06E+07	1.02E+07
PSME2	Proteasome activator complex subunit 2	1.14E+07	8.79E+06
PSME1	Proteasome activator complex subunit 1	3.51E+07	4.70E+06
PSME4	Proteasome activator complex subunit 4	1.62E+06	1.41E+06
PSMG2	Proteasome assembly chaperone 2	1.82E+06	9.44E+05
PSMG3	Proteasome assembly chaperone 3	8.64E+04	5.37E+05
UBXN1	UBX domain-containing protein 1	1.92E+06	3.52E+05
PSME3	Proteasome activator subunit 3	3.73E+06	5.09E+05
HUWE1	HECT, UBA and WWE domain containing 1, E3 ubiquitin protein ligase	4.85E+06	1.50E+08

#### Bovine liver

RAD23B	UV excision repair protein RAD23 homolog B	6.36E+07	1.19E+09
PSMD3	26S proteasome non-ATPase regulatory subunit 3	2.03E+07	9.11E+08
PSMC2	26S proteasome regulatory subunit 7	2.39E+07	8.80E+08
PSMA5	Proteasome subunit alpha type-5	1.59E+08	8.62E+08
PSMD11	26S proteasome non-ATPase regulatory subunit 11	3.61E+07	8.25E+08
PSMC5	26S proteasome regulatory subunit 8	3.97E+07	7.31E+08
PSMD13	26S proteasome non-ATPase regulatory subunit 13	3.97E+07	7.06E+08
PSMA6	Proteasome subunit alpha type-6	1.61E+08	7.06E+08
USP14	Ubiquitin carboxyl-terminal hydrolase 14	2.03E+07	7.04E+08
PSMD2	26S proteasome non-ATPase regulatory subunit 2	2.80E+07	7.03E+08
PSMC4	26S proteasome regulatory subunit 6B	2.44E+07	6.61E+08
PSMD4	26S proteasome non-ATPase regulatory subunit 4	4.14E+07	6.57E+08
PSMA7	Proteasome subunit alpha type-7	1.38E+08	6.34E+08
PSMD7	26S proteasome non-ATPase regulatory subunit 7	4.02E+07	5.22E+08
PSMC6	26S proteasome regulatory subunit 10B	2.80E+07	5.07E+08
PSMA3	Proteasome subunit alpha type-3	1.04E+08	4.95E+08
PSMB1	Proteasome subunit beta type-1	1.02E+08	4.59E+08
PSMD6	26S proteasome non-ATPase regulatory subunit 6	4.25E+07	4.57E+08
PSMB2	Proteasome subunit beta type-2	7.34E+07	4.08E+08
PSMA2	Proteasome subunit alpha type-2	8.66E+07	3.92E+08
PSMB6	Proteasome subunit beta type-6	6.47E+07	3.78E+08
PSMD8	26S proteasome non-ATPase regulatory subunit 8	3.62E+07	3.60E+08
PSMA1	Proteasome subunit alpha type-1	8.75E+07	3.52E+08
PSMD12	26S proteasome non-ATPase regulatory subunit 12	2.16E+07	3.40E+08
PSMB4	Proteasome subunit beta type-4	7.80E+07	3.28E+08
PSMA4	Proteasome subunit alpha type-4	8.80E+07	2.96E+08
PSMB3	Proteasome subunit beta type-3	5.45E+07	2.69E+08
PSMB7	Proteasome subunit beta type-7	4.15E+07	2.27E+08
PSMB5	Proteasome subunit beta type-5	3.55E+07	1.21E+08

PSMD9	26S proteasome non-ATPase regulatory subunit 9	1.59E+07	7.77E+07
PAAF1	Proteasomal ATPase-associated factor 1	3.70E+06	6.56E+07
PSMB9	Proteasome subunit beta type-9	3.80E+06	5.13E+07
PSMB10	Proteasome subunit beta type-10	4.41E+06	3.03E+07
PSMB8	Proteasome subunit beta type-8	4.12E+06	3.02E+07
ADRM1	Proteasomal ubiquitin receptor ADRM1	5.39E+06	2.32E+07
PSME1	Proteasome activator complex subunit 1	3.34E+08	2.23E+07
PSME2	Proteasome activator complex subunit 2	1.36E+08	1.47E+07
UCHL5	Ubiquitin carboxyl-terminal hydrolase isozyme L5	2.89E+06	9.21E+06
PSMF1	Proteasome inhibitor PI31 subunit	1.27E+07	6.47E+06
RAD23A	UV excision repair protein RAD23 homolog A	4.63E+06	5.28E+06
PSME4	Proteasome activator complex subunit 4	2.28E+06	3.05E+06
UBXN1	UBX domain-containing protein 1	6.37E+07	5.74E+05
PSMG3	Proteasome assembly chaperone 3	1.62E+05	6.68E+04
PSMG2	Proteasome assembly chaperone 2	1.08E+06	6.19E+04
PSME3	Proteasome activator subunit 3	3.68E+06	5.37E+05
HUWE1	HECT, UBA and WWE domain containing 1, E3 ubiquitin protein ligase	3.98E+06	3.12E+07

#### Bovine spleen

PSMD4	26S proteasome non-ATPase regulatory subunit 4	4.89E+07	6.56E+08
RAD23B	UV excision repair protein RAD23 homolog B	2.25E+07	5.88E+08
PSMA7	Proteasome subunit alpha type-7	2.02E+08	3.02E+08
PSMA5	Proteasome subunit alpha type-5	1.93E+08	2.83E+08
PSMC4	26S proteasome regulatory subunit 6B	2.28E+07	2.25E+08
PSMA1	Proteasome subunit alpha type-1	1.03E+08	1.81E+08
PSMC6	26S proteasome regulatory subunit 10B	2.34E+07	1.79E+08
PSMA2	Proteasome subunit alpha type-2	1.03E+08	1.61E+08
PSMC2	26S proteasome regulatory subunit 7	2.25E+07	1.51E+08
PSMD11	26S proteasome non-ATPase regulatory subunit 11	3.93E+07	1.49E+08
PSMC5	26S proteasome regulatory subunit 8	7.60E+07	1.43E+08
PSMB1	Proteasome subunit beta type-1	1.18E+08	1.41E+08
PSMD7	26S proteasome non-ATPase regulatory subunit 7	2.41E+07	1.10E+08
PSMB2	Proteasome subunit beta type-2	7.56E+07	1.04E+08
PSMD2	26S proteasome non-ATPase regulatory subunit 2	2.78E+07	1.03E+08
PSMD6	26S proteasome non-ATPase regulatory subunit 6	2.11E+07	1.03E+08
USP14	Ubiquitin carboxyl-terminal hydrolase 14	2.84E+07	8.72E+07
PSMA6	Proteasome subunit alpha type-6	7.71E+07	8.71E+07
PSMD3	26S proteasome non-ATPase regulatory subunit 3	1.96E+07	7.98E+07
PSMD12	26S proteasome non-ATPase regulatory subunit 12	1.79E+07	7.89E+07
PSMA3	Proteasome subunit alpha type-3	1.27E+08	7.86E+07
PSMB8	Proteasome subunit beta type-8	4.38E+07	5.95E+07
PSMD13	26S proteasome non-ATPase regulatory subunit 13	3.64E+07	5.87E+07
PSMD8	26S proteasome non-ATPase regulatory subunit 8	2.27E+07	5.70E+07
PSMB6	Proteasome subunit beta type-6	1.59E+07	5.67E+07
PSMA4	Proteasome subunit alpha type-4	1.01E+08	5.44E+07
PSMB3	Proteasome subunit beta type-3	8.58E+07	5.42E+07
PSMB4	Proteasome subunit beta type-4	8.85E+07	4.93E+07
PSMB7	Proteasome subunit beta type-7	2.00E+07	4.92E+07
PSMB9	Proteasome subunit beta type-9	1.60E+08	4.21E+07
PSME1	Proteasome activator complex subunit 1	5.72E+08	3.88E+07
PSMB10	Proteasome subunit beta type-10	4.11E+07	3.88E+07
PSME2	Proteasome activator complex subunit 2	2.17E+08	1.41E+07
PAAF1	Proteasomal ATPase-associated factor 1	1.97E+06	1.16E+07
RAD23A	UV excision repair protein RAD23 homolog A	9.62E+06	1.02E+07
PSME4	Proteasome activator complex subunit 4	7.64E+05	7.59E+06
ADRM1	Proteasomal ubiquitin receptor ADRM1	5.46E+06	7.49E+06
PSMD9	26S proteasome non-ATPase regulatory subunit 9	1.63E+07	5.06E+06
PSMB5	Proteasome subunit beta type-5	3.65E+06	4.64E+06

UCHL5	Ubiquitin carboxyl-terminal hydrolase isozyme L5	4.78E+06	2.24E+05
PSMF1	Proteasome inhibitor PI31 subunit	9.11E+06	4.79E+04
UBXN1	UBX domain-containing protein 1	4.04E+06	4.79E+04
PSMG3	Proteasome assembly chaperone 3	1.00E+05	4.79E+04
PSMG2	Proteasome assembly chaperone 2	2.07E+06	4.79E+04
PSME3	Proteasome activator subunit 3	5.85E+06	9.37E+05
HUWE1	HECT, UBA and WWE domain containing 1, E3 ubiquitin protein ligase	2.21E+06	5.29E+06

### Bovine pancreas

PSMA5	Proteasome subunit alpha type-5	2.96E+08	2.02E+09
PSMD11	26S proteasome non-ATPase regulatory subunit 11	6.55E+07	1.97E+09
PSMC6	26S proteasome regulatory subunit 10B	4.55E+07	1.74E+09
PSMD13	26S proteasome non-ATPase regulatory subunit 13	6.36E+07	1.65E+09
RAD23B	UV excision repair protein RAD23 homolog B	4.97E+07	1.62E+09
PSMC4	26S proteasome regulatory subunit 6B	4.11E+07	1.47E+09
PSMD4	26S proteasome non-ATPase regulatory subunit 4	2.97E+07	1.45E+09
PSMC2	26S proteasome regulatory subunit 7	5.72E+07	1.42E+09
PSMC5	26S proteasome regulatory subunit 8	6.40E+07	1.31E+09
PSMA6	Proteasome subunit alpha type-6	1.36E+08	1.25E+09
USP14	Ubiquitin carboxyl-terminal hydrolase 14	2.89E+07	1.12E+09
PSMD6	26S proteasome non-ATPase regulatory subunit 6	3.51E+07	1.10E+09
PSMD2	26S proteasome non-ATPase regulatory subunit 2	3.81E+07	1.10E+09
PSMD7	26S proteasome non-ATPase regulatory subunit 7	4.81E+07	1.07E+09
PSMA7	Proteasome subunit alpha type-7	2.39E+08	1.02E+09
PSMB1	Proteasome subunit beta type-1	1.68E+08	9.38E+08
PSMB2	Proteasome subunit beta type-2	1.03E+08	9.37E+08
PSMA3	Proteasome subunit alpha type-3	1.88E+08	9.11E+08
PSMA2	Proteasome subunit alpha type-2	1.55E+08	8.84E+08
PSMD12	26S proteasome non-ATPase regulatory subunit 12	3.65E+07	8.59E+08
PSMD3	26S proteasome non-ATPase regulatory subunit 3	2.73E+07	8.26E+08
PSMD8	26S proteasome non-ATPase regulatory subunit 8	4.10E+07	7.50E+08
PSMB9	Proteasome subunit beta type-9	1.62E+08	7.49E+08
PSMA1	Proteasome subunit alpha type-1	1.51E+08	7.37E+08
PSMB4	Proteasome subunit beta type-4	1.27E+08	5.60E+08
PSMA4	Proteasome subunit alpha type-4	1.52E+08	5.21E+08
PSMB3	Proteasome subunit beta type-3	1.22E+08	5.03E+08
PSMB7	Proteasome subunit beta type-7	2.14E+07	4.40E+08
PSMB6	Proteasome subunit beta type-6	2.17E+07	2.75E+08
PSMD9	26S proteasome non-ATPase regulatory subunit 9	3.29E+07	1.93E+08
PSMB8	Proteasome subunit beta type-8	5.26E+07	1.68E+08
UCHL5	Ubiquitin carboxyl-terminal hydrolase isozyme L5	1.10E+07	1.27E+08
ADRM1	Proteasomal ubiquitin receptor ADRM1	1.39E+07	1.25E+08
PSMB10	Proteasome subunit beta type-10	5.87E+07	1.21E+08
PSMB5	Proteasome subunit beta type-5	1.81E+06	1.13E+08
PAAF1	Proteasomal ATPase-associated factor 1	1.17E+06	2.73E+07
PSME1	Proteasome activator complex subunit 1	5.31E+08	1.17E+07
PSME2	Proteasome activator complex subunit 2	2.02E+08	1.14E+07
PSME4	Proteasome activator complex subunit 4	3.12E+05	1.07E+07
RAD23A	UV excision repair protein RAD23 homolog A	1.94E+07	7.88E+06
PSMF1	Proteasome inhibitor PI31 subunit	1.31E+07	3.12E+06
UBXN1	UBX domain-containing protein 1	1.93E+07	1.95E+06
PSMG2	Proteasome assembly chaperone 2	8.33E+06	1.57E+06
PSMG3	Proteasome assembly chaperone 3	2.38E+06	6.23E+04
PSME3	Proteasome activator subunit 3	2.31E+07	1.49E+06
HUWE1	HECT, UBA and WWE domain containing 1, E3 ubiquitin protein ligase	5.28E+06	1.94E+07

### Bovine testicle

PSMC2	26S proteasome regulatory subunit 7	1.61E+08	4.34E+09
PSMD4	26S proteasome non-ATPase regulatory subunit 4	8.20E+07	4.21E+09
PSMC4	26S proteasome regulatory subunit 6B	1.07E+08	3.61E+09
PSMD11	26S proteasome non-ATPase regulatory subunit 11	1.66E+08	3.46E+09
PSMC6	26S proteasome regulatory subunit 10B	1.19E+08	3.25E+09
PSMD6	26S proteasome non-ATPase regulatory subunit 6	9.05E+07	3.24E+09
PSMD7	26S proteasome non-ATPase regulatory subunit 7	8.82E+07	3.09E+09
PSMC5	26S proteasome regulatory subunit 8	1.70E+08	2.93E+09
PSMA7	Proteasome subunit alpha type-7	2.75E+08	2.47E+09
PSMD2	26S proteasome non-ATPase regulatory subunit 2	1.02E+08	2.41E+09
PSMA5	Proteasome subunit alpha type-5	5.01E+08	2.27E+09
USP14	Ubiquitin carboxyl-terminal hydrolase 14	6.46E+07	2.24E+09
PSMD12	26S proteasome non-ATPase regulatory subunit 12	6.82E+07	2.20E+09
PSMD3	26S proteasome non-ATPase regulatory subunit 3	6.70E+07	1.94E+09
RAD23B	UV excision repair protein RAD23 homolog B	5.22E+07	1.70E+09
PSMA1	Proteasome subunit alpha type-1	2.33E+08	1.50E+09
PSMD8	26S proteasome non-ATPase regulatory subunit 8	1.02E+08	1.37E+09
PSMD13	26S proteasome non-ATPase regulatory subunit 13	1.41E+08	1.36E+09
PSMA2	Proteasome subunit alpha type-2	2.73E+08	1.16E+09
PSMD9	26S proteasome non-ATPase regulatory subunit 9	9.10E+07	1.12E+09
PSMB1	Proteasome subunit beta type-1	2.86E+08	7.58E+08
ADRM1	Proteasomal ubiquitin receptor ADRM1	3.55E+07	7.02E+08
PSMB8	Proteasome subunit beta type-8	3.18E+07	5.74E+08
PSMB2	Proteasome subunit beta type-2	1.90E+08	5.43E+08
PSMA3	Proteasome subunit alpha type-3	3.31E+08	5.23E+08
PSMA4	Proteasome subunit alpha type-4	2.31E+08	4.34E+08
PSMA6	Proteasome subunit alpha type-6	2.62E+08	3.93E+08
PSMB3	Proteasome subunit beta type-3	1.76E+08	3.92E+08
PSMB4	Proteasome subunit beta type-4	1.90E+08	3.51E+08
PSMB9	Proteasome subunit beta type-9	1.06E+08	3.33E+08
PSMB10	Proteasome subunit beta type-10	2.21E+07	2.01E+08
PSMB6	Proteasome subunit beta type-6	9.68E+07	1.61E+08
PSMB7	Proteasome subunit beta type-7	1.08E+08	1.06E+08
UCHL5	Ubiquitin carboxyl-terminal hydrolase isozyme L5	4.77E+07	9.59E+07
PSME1	Proteasome activator complex subunit 1	3.60E+08	4.69E+07
RAD23A	UV excision repair protein RAD23 homolog A	2.67E+07	1.62E+07
PSMG2	Proteasome assembly chaperone 2	3.80E+07	8.41E+06
PSMB5	Proteasome subunit beta type-5	6.26E+07	7.91E+06
PAAF1	Proteasomal ATPase-associated factor 1	1.06E+07	5.56E+06
PSME2	Proteasome activator complex subunit 2	1.66E+08	4.29E+06
UBXN1	UBX domain-containing protein 1	2.69E+07	3.06E+06
PSMF1	Proteasome inhibitor PI31 subunit	2.13E+07	1.32E+06
PSME4	Proteasome activator complex subunit 4	1.75E+07	7.00E+05
PSMG3	Proteasome assembly chaperone 3	9.99E+06	5.58E+04
PSME3	Proteasome activator subunit 3	2.24E+07	3.57E+06
HUWE1	HECT, UBA and WWE domain containing 1, E3 ubiquitin protein ligase	1.28E+07	1.67E+08

### Bovine heart

RAD23B	UV excision repair protein RAD23 homolog B		1.13E+10
PSMC2	26S proteasome regulatory subunit 7		4.44E+08
PSMC5	26S proteasome regulatory subunit 8		3.57E+08
PSMD4	26S proteasome non-ATPase regulatory subunit 4		3.29E+08
PSMC4	26S proteasome regulatory subunit 6B		2.69E+08
PSMC6	26S proteasome regulatory subunit 10B		2.59E+08
PSMD3	26S proteasome non-ATPase regulatory subunit 3		2.33E+08

PSMD6	26S proteasome non-ATPase regulatory subunit 6	1.83E+08
PSMD7	26S proteasome non-ATPase regulatory subunit 7	1.77E+08
PSMD2	26S proteasome non-ATPase regulatory subunit 2	1.75E+08
PSMD12	26S proteasome non-ATPase regulatory subunit 12	1.70E+08
PSMD11	26S proteasome non-ATPase regulatory subunit 11	1.47E+08
USP14	Ubiquitin carboxyl-terminal hydrolase 14	1.21E+08
PSMD13	26S proteasome non-ATPase regulatory subunit 13	1.01E+08
PSMA1	Proteasome subunit alpha type-1	8.21E+07
PSMD8	26S proteasome non-ATPase regulatory subunit 8	4.25E+07
PSMA7	Proteasome subunit alpha type-7	3.30E+07
PSMA6	Proteasome subunit alpha type-6	2.09E+07
PSMA2	Proteasome subunit alpha type-2	1.70E+07
PSMB1	Proteasome subunit beta type-1	1.63E+07
PSMA5	Proteasome subunit alpha type-5	1.51E+07
PSMB4	Proteasome subunit beta type-4	1.24E+07
ADRM1	Proteasomal ubiquitin receptor ADRM1	6.77E+06
PSMB5	Proteasome subunit beta type-5	5.86E+06
PSMA3	Proteasome subunit alpha type-3	5.57E+06
PSMD9	26S proteasome non-ATPase regulatory subunit 9	4.68E+06
PSMA4	Proteasome subunit alpha type-4	4.50E+06
PSMB6	Proteasome subunit beta type-6	4.27E+06
PSMB2	Proteasome subunit beta type-2	4.12E+06
PSMB3	Proteasome subunit beta type-3	2.36E+06
UCHL5	Ubiquitin carboxyl-terminal hydrolase isozyme L5	1.81E+06

#### IFN- $\gamma$ treated RKO cells

RAD23B	UV excision repair protein RAD23 homolog B	8.22E+07	1.72E+10
PSMD4	26S proteasome non-ATPase regulatory subunit 4	1.45E+08	1.95E+09
PSMC2	26S proteasome regulatory subunit 7	2.43E+08	1.82E+09
PSMC6	26S proteasome regulatory subunit 10B	2.09E+08	1.82E+09
PSMA7	Proteasome subunit alpha type-7	4.56E+08	1.71E+09
PSMA5	Proteasome subunit alpha type-5	9.98E+08	1.64E+09
PSMD7	26S proteasome non-ATPase regulatory subunit 7	1.72E+08	1.62E+09
VCP	Transitional endoplasmic reticulum ATPase	2.45E+08	1.45E+09
PSMA1	Proteasome subunit alpha type-1	2.51E+08	1.43E+09
PSMD2	26S proteasome non-ATPase regulatory subunit 2	3.04E+08	1.32E+09
PSMC3	26S proteasome regulatory subunit 6A	1.61E+08	1.21E+09
PSMD11	26S proteasome non-ATPase regulatory subunit 11	1.48E+08	1.10E+09
PSMD1	26S proteasome non-ATPase regulatory subunit 1	6.38E+07	9.65E+08
PSMC1	26S proteasome regulatory subunit 4	1.36E+08	9.58E+08
PSMC4	26S proteasome regulatory subunit 6B	1.10E+08	9.41E+08
PSMC5	26S proteasome regulatory subunit 8	8.10E+07	8.39E+08
PSMD6	26S proteasome non-ATPase regulatory subunit 6	8.37E+07	8.15E+08
PSMB2	Proteasome subunit beta type-2	2.07E+08	7.32E+08
PSMD3	26S proteasome non-ATPase regulatory subunit 3	9.01E+07	6.67E+08
PSMA6	Proteasome subunit alpha type-6	1.73E+08	5.95E+08
PSMA2	Proteasome subunit alpha type-2	2.21E+08	4.76E+08
USP14	Ubiquitin carboxyl-terminal hydrolase 14	1.54E+08	4.68E+08
PSMB5	Proteasome subunit beta type-5	1.12E+08	4.60E+08
PSMA3	Proteasome subunit alpha type-3	9.87E+07	4.54E+08
PSMB7	Proteasome subunit beta type-7	7.60E+07	4.07E+08
PSMA4	Proteasome subunit alpha type-4	1.05E+08	3.82E+08
PSMB1	Proteasome subunit beta type-1	5.25E+07	3.80E+08
PSMD12	26S proteasome non-ATPase regulatory subunit 12	7.50E+07	3.35E+08
PSMD8	26S proteasome non-ATPase regulatory subunit 8	5.81E+07	3.29E+08
ADRM1	Proteasomal ubiquitin receptor ADRM1	3.82E+07	3.24E+08
PSMD14	26S proteasome non-ATPase regulatory subunit 14	1.25E+07	3.14E+08
PSMB3	Proteasome subunit beta type-3	1.13E+08	2.67E+08
PSMB4	Proteasome subunit beta type-4	6.45E+07	2.59E+08

PSMD13	26S proteasome non-ATPase regulatory subunit 13	8.55E+07	2.52E+08
UHL5	Ubiquitin carboxyl-terminal hydrolase isozyme L5	3.68E+07	2.47E+08
PSMB6	Proteasome subunit beta type-6	4.84E+07	2.15E+08
PSMB9	Proteasome subunit beta type-9	3.18E+08	1.44E+08
PSMD5	26S proteasome non-ATPase regulatory subunit 5	1.27E+08	1.24E+08
UBE3A	Ubiquitin-protein ligase E3A	4.31E+06	9.89E+07
PSME1	Proteasome activator complex subunit 1	1.84E+09	7.95E+07
PSMB10	Proteasome subunit beta type-10	4.77E+07	7.51E+07
PSMD10	26S proteasome non-ATPase regulatory subunit 10	1.27E+08	5.59E+07
TXNL1	Thioredoxin-like protein 1	2.24E+08	4.07E+07
UBXN1	UBX domain-containing protein 1	6.40E+07	2.37E+07
HSPB1	Heat shock protein beta-1	1.74E+09	2.31E+07
PSME2	Proteasome activator complex subunit 2	5.82E+08	1.98E+07
PAAF1	Proteasomal ATPase-associated factor 1	1.75E+05	1.62E+07
PSME3	Proteasome activator complex subunit 3	2.46E+08	1.23E+07
PSME4	Proteasome activator complex subunit 4	3.04E+06	6.83E+06
UBQLN1	Ubiquilin-1	1.80E+08	1.81E+06
DNAJB2	DnaJ homolog subfamily B member 2	1.75E+05	1.81E+06
PSMF1	Proteasome inhibitor PI31 subunit	5.06E+07	1.31E+06
KIAA0368	Proteasome adapter and scaffold protein ECM29	4.05E+07	3.63E+05
RAD23A	UV excision repair protein RAD23 homolog A	2.70E+07	2.46E+05
UBE3C	Ubiquitin-protein ligase E3C	2.08E+06	1.06E+05
PSMG2	Proteasome assembly chaperone 2	1.12E+07	4.98E+04
UBQLN4	Ubiquilin-4	5.54E+06	4.98E+04
IDE	Insulin-degrading enzyme	5.08E+06	4.98E+04
UBR1	E3 ubiquitin-protein ligase UBR1	5.06E+05	1.81E+04

#### Untreated RKO cells

RAD23B	UV excision repair protein RAD23 homolog B	2.10E+08	1.20E+10
PSMD4	26S proteasome non-ATPase regulatory subunit 4	1.59E+08	1.99E+09
PSMA5	Proteasome subunit alpha type-5	9.19E+08	1.89E+09
PSMC2	26S proteasome regulatory subunit 7	3.25E+08	1.75E+09
PSMA7	Proteasome subunit alpha type-7	5.67E+08	1.73E+09
PSMA1	Proteasome subunit alpha type-1	3.50E+08	1.71E+09
PSMC6	26S proteasome regulatory subunit 10B	2.58E+08	1.66E+09
PSMD2	26S proteasome non-ATPase regulatory subunit 2	3.40E+08	1.35E+09
PSMD7	26S proteasome non-ATPase regulatory subunit 7	1.85E+08	1.30E+09
VCP	Transitional endoplasmic reticulum ATPase	3.09E+08	1.18E+09
PSMD1	26S proteasome non-ATPase regulatory subunit 1	9.50E+07	9.58E+08
PSMD11	26S proteasome non-ATPase regulatory subunit 11	2.44E+08	9.44E+08
PSMC3	26S proteasome regulatory subunit 6A	1.52E+08	9.28E+08
PSMC4	26S proteasome regulatory subunit 6B	1.15E+08	8.44E+08
PSMB2	Proteasome subunit beta type-2	2.87E+08	7.97E+08
PSMD6	26S proteasome non-ATPase regulatory subunit 6	5.97E+07	7.62E+08
PSMC1	26S proteasome regulatory subunit 4	1.37E+08	7.49E+08
PSMD3	26S proteasome non-ATPase regulatory subunit 3	1.22E+08	6.66E+08
PSMC5	26S proteasome regulatory subunit 8	1.09E+08	5.97E+08
PSMB7	Proteasome subunit beta type-7	1.41E+08	5.83E+08
PSMA3	Proteasome subunit alpha type-3	1.62E+08	5.66E+08
PSMA6	Proteasome subunit alpha type-6	1.89E+08	5.51E+08
PSMB5	Proteasome subunit beta type-5	1.34E+08	5.18E+08
USP14	Ubiquitin carboxyl-terminal hydrolase 14	2.07E+08	4.87E+08
PSMB6	Proteasome subunit beta type-6	6.29E+07	3.98E+08
PSMD8	26S proteasome non-ATPase regulatory subunit 8	6.00E+07	3.94E+08
PSMA4	Proteasome subunit alpha type-4	1.25E+08	3.58E+08
PSMA2	Proteasome subunit alpha type-2	1.64E+08	3.41E+08
PSMB1	Proteasome subunit beta type-1	1.33E+08	3.27E+08
ADRM1	Proteasomal ubiquitin receptor ADRM1	4.34E+07	2.93E+08
UHL5	Ubiquitin carboxyl-terminal hydrolase isozyme L5	3.60E+07	2.74E+08

PSMD14	26S proteasome non-ATPase regulatory subunit 14	1.43E+07	2.47E+08
PSMD12	26S proteasome non-ATPase regulatory subunit 12	1.10E+08	2.37E+08
PSMD13	26S proteasome non-ATPase regulatory subunit 13	9.90E+07	2.26E+08
PSMB3	Proteasome subunit beta type-3	1.36E+08	1.96E+08
PSMB4	Proteasome subunit beta type-4	1.26E+08	1.87E+08
PSMD5	26S proteasome non-ATPase regulatory subunit 5	1.28E+08	8.77E+07
UBE3A	Ubiquitin-protein ligase E3A	9.83E+06	6.60E+07
TXNL1	Thioredoxin-like protein 1	2.09E+08	4.58E+07
PSMD10	26S proteasome non-ATPase regulatory subunit 10	8.47E+07	3.73E+07
PSME1	Proteasome activator complex subunit 1	5.42E+08	1.79E+07
HSPB1	Heat shock protein beta-1	1.87E+09	1.68E+07
PAAF1	Proteasomal ATPase-associated factor 1	1.89E+05	1.37E+07
UBXN1	UBX domain-containing protein 1	5.19E+07	8.21E+06
PSME3	Proteasome activator complex subunit 3	2.98E+08	3.09E+06
PSME4	Proteasome activator complex subunit 4	7.43E+06	2.90E+06
DNAJB2	DnaJ homolog subfamily B member 2	1.89E+05	1.40E+06
UBQLN1	Ubiquilin-1	1.28E+08	1.21E+06
PSME2	Proteasome activator complex subunit 2	1.23E+08	2.85E+05
PSMB9	Proteasome subunit beta type-9	7.07E+06	3.58E+04
PSMB10	Proteasome subunit beta type-10	1.89E+05	3.58E+04
PSMF1	Proteasome inhibitor PI31 subunit	6.11E+07	3.58E+04
KIAA0368	Proteasome adapter and scaffold protein ECM29	3.99E+07	3.58E+04
RAD23A	UV excision repair protein RAD23 homolog A	2.41E+07	3.58E+04
PSMG2	Proteasome assembly chaperone 2	1.78E+07	3.58E+04
UBQLN4	Ubiquilin-4	5.34E+06	3.58E+04
IDE	Insulin-degrading enzyme	7.06E+06	3.58E+04
UBR1	E3 ubiquitin-protein ligase UBR1	5.01E+05	3.58E+04
UBE3C	Ubiquitin-protein ligase E3C	3.15E+06	2.04E+04

**NOTE: Norm. area. stands for normalized area and represents the relative abundance of the protein in the sample**

**Table S2. Semiquantitative analysis of 11S/PA200 proteasome activators and  $\beta$ i subunits.**

Gene	Description	Extract Norm. Area.	Elution Norm. Area.	Extract Norm. to PSMA1	Elution Norm. to PSMA1
<b>Bovine brain</b>					
PSMA1	Proteasome subunit alpha type-1	6.96E+07	5.54E+08	1.00E+00	1.00E+00
PSME2	Proteasome activator complex subunit 2	1.14E+07	8.79E+06	1.63E-01	1.59E-02
PSME1	Proteasome activator complex subunit 1	3.51E+07	4.70E+06	5.04E-01	8.47E-03
PSME4	Proteasome activator complex subunit 4	1.62E+06	1.41E+06	2.33E-02	2.54E-03
PSME3	Proteasome activator subunit 3	3.73E+06	5.09E+05	5.36E-02	9.19E-04
<b>Bovine liver</b>					
PSMA1	Proteasome subunit alpha type-1	3.52E+08	8.75E+07	1.00E+00	1.00E+00
PSME1	Proteasome activator complex subunit 1	2.23E+07	3.34E+08	6.34E-02	3.82E+00
PSME2	Proteasome activator complex subunit 2	1.47E+07	1.36E+08	4.16E-02	1.55E+00
PSME4	Proteasome activator complex subunit 4	3.05E+06	2.28E+06	8.65E-03	2.60E-02
PSME3	Proteasome activator subunit 3	5.37E+05	3.68E+06	1.52E-03	4.20E-02

<b>Bovine spleen</b>					
PSMA1	Proteasome subunit alpha type-1	1.81E+08	1.03E+08	1.00E+00	1.00E+00
PSME1	Proteasome activator complex subunit 1	3.88E+07	5.72E+08	2.15E-01	5.52E+00
PSME2	Proteasome activator complex subunit 2	1.41E+07	2.17E+08	7.82E-02	2.09E+00
PSME4	Proteasome activator complex subunit 4	7.59E+06	7.64E+05	4.20E-02	7.39E-03
PSME3	Proteasome activator subunit 3	9.37E+05	5.85E+06	5.19E-03	5.65E-02
<b>Bovine pancreas</b>					
PSMA1	Proteasome subunit alpha type-1	7.37E+08	1.51E+08	1.00E+00	1.00E+00
PSME1	Proteasome activator complex subunit 1	1.17E+07	5.31E+08	1.59E-02	3.52E+00
PSME2	Proteasome activator complex subunit 2	1.14E+07	2.02E+08	1.55E-02	1.34E+00
PSME4	Proteasome activator complex subunit 4	1.07E+07	3.12E+05	1.46E-02	2.07E-03
PSME3	Proteasome activator subunit 3	1.49E+06	2.31E+07	2.03E-03	1.53E-01
<b>Bovine testicle</b>					
PSMA1	Proteasome subunit alpha type-1	1.50E+09	2.33E+08	1.00E+00	1.00E+00
PSME1	Proteasome activator complex subunit 1	4.69E+07	3.60E+08	3.12E-02	1.55E+00
PSME2	Proteasome activator complex subunit 2	4.29E+06	1.66E+08	2.85E-03	7.10E-01
PSME3	Proteasome activator subunit 3	3.57E+06	2.24E+07	2.38E-03	9.61E-02
PSME4	Proteasome activator complex subunit 4	7.00E+05	1.75E+07	4.66E-04	7.52E-02
<b>IFN-γ treated RKO cells</b>					
PSMA1	Proteasome subunit alpha type-1	1.43E+09	2.51E+08	1.00E+00	1.00E+00
PSME1	Proteasome activator complex subunit 1	7.95E+07	1.84E+09	5.57E-02	7.33E+00
PSME2	Proteasome activator complex subunit 2	1.98E+07	5.82E+08	1.38E-02	2.32E+00
PSME3	Proteasome activator complex subunit 3	1.23E+07	2.46E+08	8.64E-03	9.80E-01
PSME4	Proteasome activator complex subunit 4	6.83E+06	3.04E+06	4.78E-03	1.21E-02
PSMB9	Proteasome subunit beta type-9	1.44E+08	3.18E+08	1.01E-01	1.27E+00
PSMB10	Proteasome subunit beta type-10	7.51E+07	4.77E+07	5.26E-02	1.90E-01
<b>Untreated RKO cells</b>					
PSMA1	Proteasome subunit alpha type-1	1.71E+09	3.50E+08	1.00E+00	1.00E+00



PSME1	Proteasome activator complex subunit 1	1.79E+07	5.42E+08	1.05E-02	1.55E+00
PSME3	Proteasome activator complex subunit 3	3.09E+06	2.98E+08	1.81E-03	8.53E-01
PSME4	Proteasome activator complex subunit 4	2.90E+06	7.43E+06	1.70E-03	2.13E-02
PSME2	Proteasome activator complex subunit 2	2.85E+05	1.23E+08	1.67E-04	3.50E-01
PSMB9	Proteasome subunit beta type-9	3.58E+04	7.07E+06	2.09E-05	2.02E-02
PSMB10	Proteasome subunit beta type-10	3.58E+04	1.89E+05	2.09E-05	5.41E-04

NOTE: PSMA1 -  $\alpha$ 1 proteasome subunit, PSME1 – PA28 $\alpha$ , PSME2 – PA28 $\beta$ , PSME3 – PA28 $\gamma$ , PSME4 – PA200, PSMB9 -  $\beta$ 2i, PSMB9 -  $\beta$ 5i. Norm. area. stands for normalized area and represents the relative abundance of the protein in the sample.

Table S3. Coverage details for the *in vitro* degradation of human securin by proteasome complexes from IFN- $\gamma$  treated and untreated RKO cells.

Proteasome source material	Coverage	Sequence
IFN- $\gamma$ treated RKO cells	43.4%	MATLIYVD <b>DKENGE</b> PGTRVVAKDGL <b>KLGS</b> GPSIKALDGRSQVSTPRFGKTFD <b>APPALPKATRKA</b> LGTVNRATEKSVKTK <b>GPLKQKQPSF</b> SAK <b>KMTEKTVKA</b> KSSVPASDD <b>DAYPEIEK</b> FFPNPLDFE SFDL <b>LPEEHQIAHL</b> PLSGVPLMILDEER <b>RELEKLFQLGPPSPVKM</b> PSPPWESNLLQSPSSILSTL DVEL <b>PPVAAD</b> IDIGGCGHHHHHH
Untreated RKO cells	46.7%	MATLIYVD <b>DKENGE</b> PGTRVVAKDGL <b>KLGS</b> GPSIKALDGRSQVSTPRFGKTFD <b>APPALPKATRKA</b> LGTVNRATEKSVKTK <b>GPLKQKQPSF</b> SAK <b>KMTEKTVKA</b> KSSVPASDD <b>DAYPEIEK</b> FFPNPLDFE SFDL <b>LPEEHQIAHL</b> PLSGVPLMILDEER <b>RELEKLFQLGPPSPVKM</b> PSPPWESNLLQSPSSILSTL DVEL <b>PPVAAD</b> IDIGGCGHHHHHH

NOTE: Only amino acids in bold contribute to coverage percentage. The sequence from human securin has a C terminal 6xHis tag. The color code corresponds to the peptide color code in Table S4.

Table S4. Peptide details for the *in vitro* degradation of human securin by proteasome complexes from IFN- $\gamma$  treated and untreated RKO cells.

Peptide sequence	Detected peptide		Best score
	IFN- $\gamma$ treated RKO cells	Untreated RKO cells	
<b>DAYPEIEKF</b>	X	X	191.3
<b>GPPSPVKM</b>	X	X	<b>237.4</b>
<b>LPEEHQIAHL</b>	X	X	<b>253.8</b>
<b>DKENGE</b> PGTRVVA	X		167.0
<b>KLGS</b> GPSIKAL	X	X	181.3
<b>APPALPKATRKA</b>	X	X	<b>263.2</b>
<b>DKENGE</b> PGTRVV	X	X	<b>240.1</b>
<b>GPLKQKQPSF</b>	X		<b>216.9</b>
<b>KLGS</b> GPSIK	X	X	<b>254.1</b>
<b>APPALPKATRKA</b>	X	X	<b>212.2</b>
<b>LPEEHQIA</b>	X	X	187.9
<b>RELEKLFQL</b>	X		175.5
<b>QLGPPSPVKM</b>	X	X	<b>254.2</b>
<b>GPLKQKQPSF</b>	X		<b>218.1</b>
<b>KMTEKTVKA</b>	X		160.4
<b>KENGE</b> PGTRVV		X	160.4
<b>ALDGRSQVST</b>		X	154.3
<b>STPRFGKTFD</b>		X	154.0
<b>APPALPKATR</b>		X	187.1
<b>APPALPKAT</b>		X	189.6

<u>APPALPKA</u>	X	156.8
<u>KQKQPSFSAK</u>	X	161.0
<u>VELPPVAAD</u>	X	208.8

NOTE: The symbol X marks the detected peptide in the sample. Best score represents the quantified detection reliability; the score above 200.0 is considered reliable. The color code corresponds to the peptide color code in Table S3.

Table S5. Coverage details for the *in vitro* degradation of human securin by proteasome complexes from bovine heart in the presence or absence of PA28 proteasome activators.

Sample	Coverage	Sequence
26S	91.51%	MATLIYVDKENGEPGTRVVAKDGLKLGSGPSIKALDGRSQVSTPRFGKTFDAP PALPKATRKALGTVNRATEKSVKTKGPLKQKQPSFSAKKMTEKTVKAKSSVPA SDDAYPEIEKFFPNPLDFESFDLPEEHQIAHLPLSGVPLMILDEERELEKLF QLGPPSPVKMPSPPWESNLLQSPSSILSTLDVELPPVAADIDIGCGHHHHHH
26S + PA28 $\alpha\beta$	87.26%	MA <b>TLIYVDKENGEPGTRVVAKDGLKLGSGPSIKALDGRSQVSTPRFGKTFDAP</b> PALPKATRK <b>ALGTVNRATEKSVKTKGPLKQKQPSFSAKKMTEKTVKAKSSVPA</b> <b>SD</b> DAYPEIEKFFPNPLDF <b>ESFDLPEEHQIAHLPLSGVPLMILDEERELEKLF</b> <b>QLGPPSPVKMPSPPWESNLLQSPSSILSTLDVELPPVAADIDIGCGHHHHHH</b>
26S + PA28 $\gamma$	95.75%	MATLIYVDKENGEPGTRVVAKD <b>GLKLGSGPSIKALDGRSQVSTPRFGKTFDAP</b> PALPKATRKALGTVNRATEKSVKTKGPLKQKQPSFSAKKMTEKTVKAKSSVPA SDDAYPEIEKFFPNPLDFESFDLPEEHQIAHLPLSGVPLMILDEERELEKLF QLGPPSPVKMPSPPWESNLLQSPSSILSTLDVELPPVAADIDIGCGHHHHHH

NOTE: Only colored amino acids contribute to coverage percentage. The sequence from human securin has a C terminal 6xHis tag. The color code corresponds to the peptide color code in Table S6 for unique peptides from PA28 $\alpha\beta$  and PA28 $\gamma$  reaction.

Table S6. Unique peptide details for the *in vitro* degradation of human securin by proteasome complexes from bovine heart in the presence of PA28 proteasome activators.

Unique peptide sequence	Best score	Unique peptide sequence	Best score
<b>26S + PA28<math>\alpha\beta</math></b>			
<b>GTVNRATEKSVKT</b>	218.5	<b>TLIYVDKENGEPGTRVVA</b>	333.4
<b>ALGTVNRATEKSVKT</b>	230.2	<b>VNRATEKSVKTKGPLKQ</b>	302.1
<b>KENGEPGTRVVAKDGL</b>	257.3	<b>LIYVDKENGEPGTRVVA</b>	234.5
<b>KLGSGPSIKALDGRSQV</b>	351.7	<b>IYVDKENGEPGTRVVAKD</b>	258.4
<b>VDKENGEPGTRVVAKD</b>	223.8	<b>YVDKENGEPGTRVVAKD</b>	318.4
<b>ESFDLPEEHQIAHL</b>	225.8	<b>TLIYVDKENGEPGTRVVAK</b>	377.7
<b>KLGSGPSIKALDG</b>	311.9	<b>KMTEKTVKA</b>	215.0
<b>RATEKSVKTKGPLKQ</b>	322.1	<b>GTVNRATEKSVKTK</b>	241.9
<b>TLIYVDKENGEPGTRVVAKD</b>	276.2	<b>TEKTVKAKSSVPAS</b>	260.3
<b>RVVAKDGL</b>	212.5	<b>LFQLGPPSPVKM</b>	237.3
<b>DKENGEPGTRVVAKDGLKL</b>	220.1	<b>KTGKPLKQKQPSFSAK</b>	276.8
<b>KTVKAKSSVPASD</b>	238.9	<b>DGLKLGSGPSIKAL</b>	229.8
<b>YVDKENGEPGTRVVA</b>	306.9	<b>DGLKLGSGPSIKA</b>	215.3
<b>GTVNRATEK</b>	212.3		
<b>26S + PA28<math>\gamma</math></b>			
<b>ALDGRSQV</b>	225.5	<b>GLKLGSGPSIKAL</b>	225.1
<b>26S + PA28<math>\alpha\beta</math>/PA28<math>\gamma</math></b>			
<b>AKDGLKLGSGPSI</b>	448.8	<b>KDGLKLGSGPSIKA</b>	270.6
<b>KLGSGPSIKALDGRSQVST</b>	448.4	<b>PLMILDEERE</b>	268.8
<b>KTFDAPPALPKATRK</b>	414.8	<b>IYVDKENGEPGTRVV</b>	268.4
<b>KGPLKQKQPSFSAKKM</b>	407.2	<b>PLSGVPLMI</b>	268.0
<b>ALGTVNRATEKSV</b>	352.5	<b>ATEKSVKTKGPLKQ</b>	256.9

<b>PASDDAYPEIEKF</b>	347.2	<b>ALGTVNRATEK</b>	256.6
<b>AKDGLKLGSGPSIKAL</b>	328.4	<b>KALDGRSQVST</b>	248.3
<b>DGRSQVSTPRFGKTFD</b>	325.0	<b>DDAYPEIEKF</b>	231.6
<b>GSGPSIKALDGRSQVST</b>	320.0	<b>KGPLKQKQPSFSA</b>	231.0
<b>DKENGEPTTRVVAKDGL</b>	312.9	<b>VAKDGLKL</b>	231.0
<b>PPSPVKMPSPPWE</b>	309.8	<b>APPALPKATRKALGTVN</b>	230.4
<b>GPPSPVKMPSPPWE</b>	309.6	<b>ALGTVNRATEKS</b>	229.6
<b>TEKTVKAKSSVPASD</b>	306.7	<b>LDEERELE</b>	225.8
<b>GPLKQKQPSFSAKMM</b>	305.0	<b>APPALPKATRKAL</b>	216.0
<b>QPSFSAKMMTE</b>	286.1	<b>GLKLGSGPSIKA</b>	212.7
<b>KDGLKLGSGPSIKAL</b>	283.7	<b>QPSFSAKMM</b>	205.4
<b>PLKQKQPSF</b>	278.8	<b>APPALPKATRKALG</b>	204.9
<b>PEEHQIAH</b>	271.5	<b>VKTGKPLKQ</b>	202.6

NOTE: Best score represents the quantified detection reliability; the score above 200.0 is considered reliable. The color code corresponds to the peptide color code in Table S5.

Table S7. Peptide details for the *in vitro* degradation of human securin by proteasome complexes from bovine heart in presence or absence of PA28 proteasome activators.

Peptide sequence	Detected peptide			Best score
	26S	26S + PA28 $\alpha\beta$	26S + PA28 $\gamma$	
AKDGLKLGSGPSI		X	X	448.8
KLGSGPSIKALDGRSQVST		X	X	448.4
FQLGPPSPVKM	X	X	X	443.2
KTFDAPPALPKATRKA	X	X	X	440.7
KLGSGPSIKALDGRSQ	X	X	X	428.5
QLGPPSPVKM	X	X	X	426.6
KTFDAPPALPKATRK		X	X	414.8
KQPSFSAKMM	X	X	X	411.3
KGPLKQKQPSFSAKMM		X	X	407.2
DKENGEPTTRVVAKD	X	X	X	405.8
VPLMILDEERE	X		X	404.4
KSVKTKGPLKQ	X	X	X	402.0
PLMILDEERE	X	X	X	401.5
KQPSFSAKMMTE	X	X	X	397.5
KDGLKLGSGPSI	X	X	X	395.6
KTFDAPPALPKATR	X	X	X	385.2
TEKSVKTKGPLKQ	X	X	X	383.9
YVDKENGEPTTRVV	X	X	X	381.5
PEEHQIAHL	X	X	X	379.8
LGPPSPVKM	X	X	X	378.5
TLIYVDKENGEPTTRVVAK		X		377.7
APPALPKATRKA	X	X	X	362.9
TLIYVDKENGEPTTRV	X	X	X	361.1
GSGPSIKALDGRSQ	X	X	X	359.1
AKDGLKLGSGPSIKA	X	X		358.1
KGPLKQKQPSFSAK	X	X	X	357.8
VDKENGEPTTRVV	X	X	X	353.8
ALGTVNRATEKSV		X	X	352.5
KLGSGPSIKALDGRSQV		X		351.7
LGTVNRATEKSV	X	X	X	350.8
PASDDAYPEIEKF		X	X	347.2
PPSPVKM	X	X	X	347.0
KQPSFSAKMMTE	X	X	X	340.6
KENGEPTTRVVAKD	X	X	X	338.1
TLIYVDKENGEPTTRVV	X	X	X	338.0
KTFDAPPALPKAT	X	X	X	334.5
TLIYVDKENGEPTTRVVA		X		333.4

GPLKQKQPSFSAK	X	X	X	332.0
ALGTVNRATE	X	X	X	331.8
APPALPKATRK	X	X	X	328.7
AKDGLKLGSGPSIKAL		X	X	328.4
VNRATEKSVKT	X	X	X	328.2
VDKENGE PGTRVVA	X	X	X	326.3
KLFQLGPPSPVKM	X	X	X	325.3
DGRSQVSTPRFGKTFD		X	X	325.0
LDEERELEKL	X	X	X	324.6
PSFSAKKMTE	X	X	X	324.3
SGPSIKALDGRSQ	X	X	X	324.0
RATEKSVKTKGPLKQ		X		322.1
GSGPSIKALDGRSQVST		X	X	320.0
LGTVNRATEK	X	X	X	318.5
YVDKENGE PGTRVVAKD		X		318.4
KGPLKQKQPSF	X	X	X	317.3
PSFSAKKMTE	X	X	X	316.4
GPPSPVKM	X	X	X	316.2
KLGGSPSIKAL	X	X	X	315.6
DKENGE PGTRVVAKDGL		X	X	312.9
KLGGSPSIKALDG		X		311.9
GPLKQKQPSFSAKKM		X		311.6
PPSPVKMPSPPWE		X	X	309.8
GPPSPVKMPSPPWE		X	X	309.6
YVDKENGE PGTRVVA		X		306.9
TEKTVKAKSSVPASD		X	X	306.7
QLGPPSPVKM	X	X	X	306.4
LGTVNRATE	X	X	X	305.3
GPLKQKQPSFSAKKM		X	X	305.0
APPALPKATRKALGT	X	X	X	305.0
KTKGPLKQKQPSF	X	X	X	303.5
DKENGE PGTRVV	X	X	X	303.2
GPLKQKQPSF	X	X	X	302.7
VNRATEKSVKTKGPLKQ		X		302.1
GPLKQKQPSFSA	X		X	300.2
YVDKENGE PGTRV	X	X	X	298.9
PSFSAKKM	X	X	X	294.3
KSSVPASDDAYPEIEKF	X	X	X	293.2
SVKTKGPLKQ	X	X	X	293.0
DGRSQVSTPRFGKTF	X	X	X	292.3
LIYVDKENGE PGTRVV	X	X	X	291.9
DKENGE PGTRVVA	X	X	X	291.7
KKMTEKTVKA		X		290.3
VELPPVAAD	X	X	X	290.2
APPALPKAT	X	X	X	288.2
QPSFSAKKMTE		X	X	286.1
KDGLKLGSGPSIKAL		X	X	283.7
DAPPALPKATRK	X	X	X	280.9
APPALPKATR	X	X	X	280.1
KLGGSPSIK	X	X	X	279.8
GTVNRATEKSV	X	X	X	279.2
PLKQKQPSF		X	X	278.8
KTKGPLKQKQPSFSAK		X		276.8
GSGPSIKALDGRSQV	X	X	X	276.5
TLIYVDKENGE PGTRVVAKD		X		276.2
KLGGPSIKA	X	X	X	272.7
KSSVPASDDAYPEIE	X	X	X	271.6
PEEHQIAH		X	X	271.5
ADIDIGGCGH	X	X	X	271.5
KDGLKLGSGPSIKA		X	X	270.6

LPEEHQIAH	X	X	X	269.6
PLMILDEERE		X	X	268.8
IYVDKENGEPGTRVV		X	X	268.4
PLSGVPLMI		X	X	268.0
YPEIEKF	X	X	X	267.8
LPEEHQIAHL	X	X	X	267.5
PPALPKAT	X	X	X	266.5
DAPPALPKATRKA	X	X	X	265.3
KENGEPTRV	X		X	264.3
GPPSPVKM	X	X	X	263.3
ALDGRSQVST	X	X	X	261.5
DAPPALPKATRKA	X	X	X	261.5
TEKTVKAKSSVPAS		X		260.3
KQPSFSAK	X	X	X	259.5
PPALPKATRKA	X	X	X	259.1
IYVDKENGEPGTRVVAKD		X		258.4
DLPEEHQIAHL	X	X	X	258.1
GLKLGSGPSI	X	X	X	257.9
KENGEPTRVVAKDGL		X		257.3
ATEKSVKTKGPLKQ		X	X	256.9
ALGTVNRATEK		X	X	256.6
KGPLKQKQPSFSAKMM		X		255.3
KLGSGPSIKALD	X	X	X	255.1
LGTVNRATEKSVKTK	X	X		252.1
QPSFSAKMMTE		X		251.9
LGTVNRATEKSVKTK	X	X	X	248.4
KALDGRSQVST		X	X	248.3
KQPSFSAKMM	X	X	X	247.0
QLGPPSPVKM	X	X	X	246.9
VSTPRFGKTFD	X	X	X	246.1
PASDDAYPEIE	X	X	X	244.7
PRFGKTFD	X	X	X	243.2
VPASDDAYPEIEKF	X	X		242.6
GTVNRATEKSVKTK		X		241.9
DKENGEPTRV	X	X	X	240.8
KTVKAKSSVPASD		X		238.9
KENGEPTRVV	X	X	X	238.2
LFQLGPPSPVKM		X		237.3
APPALPKA	X	X	X	237.2
PALPKATRKA	X	X	X	236.6
NGEPGTRVVAKD	X	X	X	235.4
QPSFSAKMM	X	X	X	234.9
AHLPLSGV	X	X	X	234.7
LIYVDKENGEPGTRVVA		X		234.5
VDKENGEPTRV	X		X	234.2
DLPEEHQIAH	X	X	X	233.7
PRFGKTF	X	X	X	232.6
DDAYPEIEKF		X	X	231.6
SGPSIKAL	X	X	X	231.5
KGPLKQKQPSFSA		X	X	231.0
VAKDGLKL		X	X	231.0
APPALPKATRKAALGTVN		X	X	230.4
ALGTVNRATEKSVKTK		X		230.2
DGLKLGSGPSIKAL		X		229.8
ALGTVNRATEKS		X	X	229.6
FESFDLPEEH	X	X		229.0
ESFDLPEEHQIAHL		X		225.8
LDEERELE		X	X	225.8
GLKLGSGPSIKAL			X	225.5
ALDGRSQV			X	225.1

GSGPSIKALD	X	X	X	224.8
VDKENGEPGTRVVAKD		X		223.8
FQLGPPSPVKM	X	X	X	223.0
GSGPSIKAL	X	X	X	221.5
VSTPRFGKTF	X	X	X	221.4
PPALPKATRK	X	X	X	220.3
DKENGEFGTRVVAKDGLKL		X		220.1
NGEPGTRVVA	X	X		219.6
GTVNRATEKSVKT		X		218.5
PSFSAKKM	X	X	X	218.1
GSGPSIKALDG	X	X	X	217.9
AKDGLKLG	X	X	X	217.6
PALPKATR	X	X	X	216.0
APPALPKATRKAL		X	X	216.0
DGLKLGSGPSIKA		X		215.3
KMTEKTVKA		X		215.0
LGTVNRATEKS	X	X	X	213.8
GLKLGSGPSIKA		X	X	212.7
RVVAKDGL		X		212.5
GTVNRATEK		X		212.3
KTKGPLKQ	X		X	210.4
QPSFSAKKMTE	X	X	X	210.0
TLIYVDKE	X	X		209.5
KENGEFGTRVVAK	X	X	X	209.3
KENGEFGTRVVA	X	X	X	208.5
DAYPEIEKF	X	X	X	207.6
QPSFSAKKM		X	X	205.4
APPALPKATRKALG		X	X	204.9
KSSVPASDDAY	X	X		204.6
VKTKGPLKQ		X	X	202.6
KQKQPSF	X		X	202.4
IDIGGCGH	X		X	200.9
SSVPASDDAYPEIEKF		X		199.1
NGEPGTRVVAKDGL		X		198.2
DLPEEHQIA	X	X	X	198.2
SGPSIKALDGRSQV		X		197.7
STPRFGKTFD	X	X	X	196.7
LDGRSQVST	X	X		196.2
KTFDAPPALPKA	X			196.1
KQPSFSA	X	X	X	196.0
QPSFSAKKM			X	194.8
SVKTKGPLKQK		X		194.6
TLIYVDKENGEFGT			X	194.6
DGRSQVSTPRF			X	193.5
LPEEHQIA	X	X	X	192.2
FSAKKMTE			X	191.7
GTVNRATEKSVKTKGPLKQ		X		190.2
DGRSQVSTPRFG	X	X	X	189.9
LGPPSPVKM	X	X	X	188.7
LIYVDKENGEFGT		X	X	188.6
KQPSFSAKKMTEKTVKA		X		188.5
ENGEFGTRVV	X			187.6
SGPSIKALD			X	187.4
PSSILSTLD	X		X	186.5
DAPPALPKATR		X	X	186.3
PALPKATRK	X	X	X	186.0
DAPPALPKAT	X	X	X	185.9
NGEPGTRVV	X	X	X	185.0
SAKKMTEKTVKA		X	X	184.9
KQPSFSAKKMTEKTVKA		X		184.7

KQKQPSFSAK	X		X	184.3
DGLKLGSGPSI	X			183.5
LIYVDKENGEPGTRVVAKD		X		182.6
ATLIYVDKE		X	X	182.5
TLIYVDKENG	X	X	X	181.7
PSPPWESN	X		X	181.6
ESFDLPEEHQI	X	X		181.3
YVDKENGEPGT			X	181.1
SAKKMTEKTVKA		X		178.3
LKLGSGPSI		X	X	176.6
PPALPKATR		X		175.0
ALGTVNRA	X	X	X	174.9
GEPGTRVVAKD		X	X	174.8
ESFDLPEEH			X	174.3
TLIYVDKENG	X	X	X	173.8
ESFDLPEEHQIAH			X	173.7
ATEKSVKTKGPLKQKQ		X		172.8
DAPPALPKA	X		X	170.9
STPRFGKTF		X	X	170.8
TLIYVDK	X		X	170.7
KMTEKTVKA		X		170.2
RELEKLF	X	X	X	168.5
KKMTEKTV		X		167.8
TLIYVDKEN			X	167.7
KENGEPGTRVVAKDGLKL		X		166.8
LDEERELEKLF			X	166.2
PSPPWES		X		166.1
IYVDKENGEPGT		X	X	166.1
PLSGVPLMILDEE		X		165.9
VPASDDAYPEIE		X		165.7
ADIDIGGCGHHH			X	163.2
LDEEREL	X	X	X	162.9
KFFPFNPLD			X	162.0
DKENGEPGTRVVAK	X			161.9
KALGTVNRA		X		161.8
KTKGPLKQKQ		X		161.4
VNRATEKSVKTK		X		160.3
AYPEIEKF		X	X	159.9
ERELEKL	X			159.8
GEPGTRVVA	X			158.7
RELEKLFQ	X	X	X	158.6
KKMTEKTVKA	X	X		158.4
FDAPPALPKAT		X		158.2
PLSGVPLMILDEE		X		157.6
KQPSFSAK			X	156.3
HQIAHLPLSGV		X		155.9
TFDAPPALPKAT		X		155.0
KTFDAPPAL			X	153.8
GPLKQKQPS		X		153.2
KSVKTKGPLKQK		X		152.8
EERELEKL		X		152.0
QPSFSAK	X			151.3
FDAPPALPKA			X	151.1
LDGRSQV			X	150.9
NGEPGTRVVAK		X		150.3

**NOTE: NOTE: The symbol X marks the detected peptide in the sample. Best score represents the quantified detection reliability; the score above 200.0 is considered reliable (in bold). The row marked in red represents the line between detected peptides with score > 200.0 that were used for semiquantitative and qualitative analysis from peptides with score < 200.0 that were discarded from analysis.**

**Table S8. t-Test Two-Sample Assuming Equal Variances of the peptide lengths generated from securin by proteasome complexes from RKO cells.**

Table gives t Stat value for the  $\alpha=0.05$  level of significance. If t Stat > t Critical one-tail (equality) ( $P(T \leq t)$  one-tail < 0.05), the null hypothesis ( $H_0: \mu_1 - \mu_2 = 0$ ) is rejected. Since this is not the case ( $0.62 < 1.69$ ), the observed difference between sample means of the peptide lengths is not significant.

Parameter	IFN $\gamma$ treated RKO cells	IFN $\gamma$ untreated RKO cells
Variance	2.26	1.55
Pooled Variance	1.87	
Hypothesized Mean Difference	0	
df	14	17
t Stat	0.62	
P(T $\leq t$ ) two-tail	0.26	
t Critical two-tail	1.69	

\*df: degrees of freedom.

**Table S9. -Test Two-Sample Assuming Equal Variances of the peptide lengths generated from securin by the 26S proteasome in the presence or absence of PA28 $\alpha\beta$  or PA28 $\gamma$ .**

The t-Test was performed separately for PA28 $\alpha\beta$  or PA28 $\gamma$  containing reactions to compare with the 26S proteasome containing sample. Table gives t Stat value for the  $\alpha=0.05$  level of significance. If t Stat > t Critical one-tail (equality) ( $P(T \leq t)$  one-tail < 0.05), the null hypothesis ( $H_0: \mu_1 - \mu_2 = 0$ ) is rejected. Since this is the case, the observed differences between sample means of the peptide lengths is significant.

Parameter	PA28 $\alpha\beta$	26S	PA28 $\gamma$	26S
Variance	8.62	5.76	8.64	5.76
Hypothesized Mean Difference	0		0	
df	298		307	
t Stat	3.14		2.83	
P(T $\leq t$ ) two-tail	0.0009		0.002	
t Critical two-tail	1.64		1.96	

\*df: degrees of freedom.



## 8. CURRICULUM VITAE

### Personal informations

Name: Katarina Belačić  
Email: katarina.belacic@gmail.com  
Date of birth: 03.11.1994.  
Nationality: Croatian  
Mother tongue: Croatian  
Other languages: English

### Education

2016 – 2018 Graduate programme of Molecular Biology, Division of Biology, Faculty of Science, University of Zagreb

2013 – 2016 Undergraduate programme of Molecular Biology, Division of Biology, Faculty of Science, University of Zagreb

2009 – 2013 High school education, Gymnasium, Daruvar

### Work experience

07/2017 – 01/2018 Part-time Pharmacovigilance and Regulatory Business Assistant

2014 – 2015 Student assistant in the zoology and botany laboratory practices

### Conferences

22.10.2016 3<sup>rd</sup> Chemistry student's symposium, Department of Chemistry, Faculty of Science, University of Zagreb

03./04.11.2016 Vienna Biocenter PhD syposium „Mind the App – Applications that Bridge Biology and Technology“, Vienna (Travel grant)

### Awards

2016 Rector's award for paper „Preparation of human seryl-tRNA-synthetase and tRNA<sup>Ser</sup> for mistranslation analysis of serine codons, Anja Kostelac i Katarina Belačić.